SANDIA REPORT
SAND2022-13822
Printed October 2022

Sandia National Laboratories

Optimal Electric Grid Black Start Restoration Subject to Intentional Threats

Kevin L. Stamber, Bryan Arguello, Richard A. Garrett, Walter E. Beyeler, Casey L. Doyle, David A. Schoenwald, Samuel T. Ojetola

Prepared by
Sandia National Laboratories
Albuquerque, New Mexico
87185 and Livermore,
California 94550

Issued by Sandia National Laboratories, operated for the United States Department of Energy by National Technology & Engineering Solutions of Sandia, LLC.

Available to DOE and DOE contractors from
U.S. Department of Energy
Office of Scientific and Technical Information
P.O. Box 62
Oak Ridge, TN 37831

Telephone: (865) 576-8401
Facsimile: (865) 576-5728
E-Mail: reports@osti.gov
Online ordering: http://www.osti.gov/scitech

Available to the public from
U.S. Department of Commerce
National Technical Information Service
5301 Shawnee Rd
Alexandria, VA 22312

Telephone: (800) 553-6847
Facsimile: (703) 605-6900
E-Mail: orders@ntis.gov
Online order: https://classic.ntis.gov/help/order-methods/

ABSTRACT

Efficient restoration of the electric grid from significant disruptions – both natural and manmade – that lead to the grid entering a failed state is essential to maintaining resilience under a wide range of threats. Restoration follows a set of black start plans, allowing operators to select among these plans to meet the constraints imposed on the system by the disruption. Restoration objectives aim to restore power to a maximum number of customers in the shortest time. Current state-of-the-art for restoration modeling breaks the problem into multiple parts, assuming a known network state and full observability and control by grid operators. These assumptions are not guaranteed under some threats.

This paper focuses on a novel integration of modeling and analysis capabilities to aid operators during restoration activities. A power flow-informed restoration framework, comprised of a restoration mixed-integer program informed by power flow models to identify restoration alternatives, interacts with a dynamic representation of the grid through a cognitive model of operator decision-making, to identify and prove an optimal restoration path. Application of this integrated approach is illustrated on exemplar systems. Validation of the restoration is performed for one of these exemplars using commercial solvers, and comparison is made between the steps and time involved in the commercial solver, and that required by the restoration optimization in and of itself, and by the operator model in acting on the restoration optimization output. Publications and proposals developed under this work, along with a path forward for additional expansion of the work, and summary of what was achieved, are also documented.

ACKNOWLEDGEMENTS

The authors would like to pass along their thanks to several of those whose work is cited here, especially Georgio Patsakis, Ignacio Aravena, and Shmuel Oren, University of California, Berkeley, for their willingness to discuss aspects of their work in detail. The authors also thank Bob Cummings, Senior Director of Engineering and Reliability Initiatives, North American Electric Reliability Corporation (retired), and Robert Abbott and Aaron Jones, Sandia National Laboratories, for their insight into the role of the operator in restoration and in development and review of the cognitive modeling and insight into operator decision making, respectively. Additional, and much needed thanks, for work in support of this effort as a graduate intern, to Will Linz, University of Illinois, Urbana-Champaign.

The authors also are grateful for the assistance of the Resilient Energy Systems Mission Campaign leadership and Sandia Financial Management staff, especially Mission Campaign Manager Craig Lawton, as well as Meghan Othart-Blaine and Karen Tafoya, who assisted in keeping this project on target, on budget, and on time.

Contents

LIST OF FIGURES

LIST OF TABLES

This page left blank

ACRONYMS AND TERMS

Acronym/Term	Definition
AC	Alternating Current
ACOPF	Alternating Current Optimal Power Flow
ACT-R	Adaptive Control of Thought-Rational
B&B	Branch-and-bound
DC	Direct Current
DCOPF	Direct Current Optimal Power Flow
DHS	US Department of Homeland Security
DoD	US Department of Defense
EMP	Electromagnetic pulse
GE	General Electric
IEEE	Institute of Electrical and Electronics Engineers
LDRD	Laboratory Directed Research & Development
LPAC	Linear Piecewise Alternating Current
MCM	Multiple Choice Model
MIP	Mixed-Integer Program
MW	megawatts
NDM	Network Dynamic Model
NERC	North American Electric Reliability Corporation
NNSA	National Nuclear Security Administration
PSLF	Positive Sequence Load Flow
RES	Resilient Energy Systems
RTS	Reliability Test System
WSCC	Western System Coordinating Council

This page left blank

1. GOALS

The purpose of this research document is to review efforts conducted under the Optimal Grid Restoration Subject to Intentional Threats Laboratory Directed Research & Development (LDRD) project. Within this document, the authors will summarize technical efforts in multiple areas of capability – optimization, dynamic simulation, and cognitive modeling. The authors will then review the steps necessary to integrate these efforts into a consistent framework, including case studies leveraging the integrated framework of models. Conclusions based on this effort will be discussed, and a future development path outlined.

The paper is summarized as follows: First, this section summarizes the research goals as originally proposed, along with a review of the literature associated with the state of the art in grid restoration. The subsequent section, Approach, covers not only the concepts of the technical efforts employed in this work, and their integration, but also covers the threat space faced by the grid, and the application of threats to the modeling framework. In Details on Research Performed, the methods leveraged based on those items described in Approach are described in specific detail. In Accomplishments, the paper reviews case studies and validation efforts completed leveraging the research as performed. The Impacts section outlines the impact of this research, in the form of papers and presentations made (both internally and externally), interactions with external entities to support the work, and proposals generated for future efforts leveraging this work. The Future Needs section identifies gaps, both in the combined capability, as well as in the individual elements as developed, for further exploration. Conclusions summarizes the work in a concise fashion. The Appendix captures inputs and outputs used and produced in optimization modeling conducted within the work.

1.1. Summary of Proposed Work

For the nation to be resilient, we must understand how intentional threats such as cyber and physical attacks will impact our power grid. Although significant research focus has been paid to outage extent subject to intentional threats, comparatively little work has been done to estimate the duration of these outages and to plan restoration actions. To improve and optimize grid resilience, we must understand how specific technologies – such as solid-state transformers or electromagnetic pulse (EMP) arrestors – can decrease outage duration, and understand how to restore service, especially for facilities critical to national security.

Existing methods such as static and dynamic alternating current (AC) power flow models (e.g., [51]) do not provide scalable, robust solutions when faced with severe contingencies of this nature. Restoration is accomplished by people making decisions with incomplete information under great stress. Although operational decision-making is key to effective restoration it has never been integrated into models of the restoration process. We propose an alternative formulation reflecting dynamic grid restoration from extreme outages based on a hybrid agent-based and system dynamics modeling approach. This approach to modeling restoration dynamics will be invaluable to programs within the US Department of Energy (DOE), the Department of Defense (DoD), the Department of Homeland Security (DHS), and the National Nuclear Security Administration (NNSA) who share the mission of improving our energy system's resilience to intentional threats.

We hypothesize that an alternative formulation with the following properties will be successful at simulating the dynamics of grid restoration subject to extreme events:

- Capturing the stability constraints of the power system
- Development of solutions that are robust to loss of many components
- Incorporation of operator decision-making in the restoration process

We will design, develop, and test a model representing restoration dynamics –starting black start-capable generators, cranking along a path to larger generation, prioritizing critical load restoration, and maintaining stability. The prospect of a model robust to multiple component failures necessitates a departure from highly parameterized models such as static or dynamic AC power flow. A promising alternative is the network diffusion formulation, implemented by Sandia with numerical solution algorithms in Beyeler et al [14], which has been employed to model disruptions to natural gas and petroleum fuels networks at the national scale. In this project, we will apply the network diffusion formulation as a surrogate to power grid physics. The primary relaxation stems from our state variables being the stable energization status of nodes in the network, instead of power flows or voltages.

To model restoration decisions by operators, we adopt a cognitive modeling system being applied to an analogous domain [1] coupled with the simulation. This work will build on extensive research at Sandia. Existing literature suggests efficient dispatch of repair resources in coordination with both steady-state and harmonic analysis of system conditions as two critical operations during restoration [21]. Validation of this formulation will be performed in multiple stages.

1.2. Background

There exists a long and well-documented history of substantial events impacting the performance of the electric grid in many locations around the world [6][12][44][46][73]. This literature indicates many identified causes for such disruptions [20][35], including damaging natural events, such as hurricanes [50] and manmade causes, such as cyber-attacks [64].

In the event of a complete disruption of a transmission and distribution area, as in the 1965 northeast blackout [49], there exists a need to have black start generators, ones that do not require connectivity to the rest of the grid (and corresponding support from the grid) in order to bring a generator back into service which, under normal conditions, would leverage power in the transmission system to assist in plant activation. A range of resources - diesel generators associated with a larger generator, hydroelectric generation facilities, and battery sets supporting gas turbines - all can be leveraged for the purpose of supporting black start operations [29].

Planning for restoration from a fully failed state involves the regional identification of black start resources. In many cases black start units are defined through commercial agreements or market structures [38]. Black start restoration, in turn, follows a defined process of energization and connection of black start units, so as to in turn energize busses and transmission lines and add loads, provided a range of performance parameters (voltage, phase angle, frequency) for components and the energized system are satisfied [31].

The ability to restore from a failed state (and to improve said restorations, so as to minimize the impact of disruptions) has long been a subject of research [48], including a variety of technologies within the grid considered for process improvement [28][30][60] and a range of techniques applied to the problem [47][48].

Optimization is a frequent method of choice for the development of black start restoration plans, and home to some of the most cutting-edge research on the problem [24][61]. These existing

techniques often work from an assumption of full observability and control of the grid on the part of the operator, implying the network is in a known state [10]. Under many of the causal circumstances described above, full observability cannot be assured. Similarly, and especially for cyber-based incidents, control of the grid on the part of the operator is not confirmable. Techniques are required to accommodate for these uncertainties in improving modeling of restoration of the grid from black start events.

This page left blank

2. APPROACH

This section summarizes the approach followed within the research, to include a discussion of the modeling techniques drawn into this research, the integration of these techniques, and a review of the threats facing the grid in implementation of the modeling structure.

2.1. Technical Efforts

The research, discussed in this section, builds on the concepts of the state of the art in optimization, creating a novel integration of restoration through static power flow models with network dynamics and cognitive modeling. It leverages an integration of a mixed inter linear programming model of restoration leveraged from work described in Aravena et al., [10] with power flow modeling from a range of sources, including Tan, Cai, and Lou [66]; Coffrin et al. [26]; and Aravena et al. [9] through a feasibility oracle as described in Aravena et al., [10] for the development of restoration plans. These are provided to an Operator Cognitive Model (OCM) developed in the Adaptive Control of Thought-Rational (ACT-R) framework [4] to work with both the optimized restoration plan and a Network Dynamic Model of the system (leveraging concepts from Corbet et al. [27]), monitoring the system to implement the schedule at the proper pace and adapting to any deviations from planned behavior. This chapter will describe each of these components in more detail.

2.1.1. Power Flow-Informed Restoration Model

A key goal of power flow-informed restoration models is to provide useable schedules for a utility operator to bring a power system back online after a full or partial blackout event. A candidate schedule should account for power flow physics during the restoration to ensure that, as components become energized, the system enters into a stable state. Linear steady-state power flow models are desirable for restoration because they are scalable for use in this application and these models have been well-studied [10][24][61]. This model benefits from recent advances in AC power flow models to provide enhanced realism over direct current (DC) models with respect to the steady state power physics during the restoration process and is solvable at scale. A summary of Aravena et. al., 2019 [10] is provided given that model's application in the next section. The reader is directed to their work for the formulation and a presentation of their notation (excluded here for brevity).

2.1.1.1. Restoration Model

A restoration model is used to determine the sequence of actions necessary to restore a power system [24]. The work by Aravena et al. [10] was selected as an appropriate modeling paradigm for the consideration of linearized AC power flows during blackout events. This model incorporated recent advances in restoration modeling that seemed pertinent for the use of simulating within an operator model environment. Here, we define these components as black start generators, non-black start generators, buses, and lines as a function of time. The model constrains the energization decisions for these components based on relationships between them and their place within the topology of the power system. These energization decisions reflect the temporal scale at which an operator would respond (e.g., minutes to hours). We define the optimal solution to this problem as a *restoration schedule*, comprised of the binary energization state of each component (e.g., energized or de-energized) at each time period in the time horizon.

2.1.1.2. Steady State Power Flow Models

This section provides an overview of the concepts for optimal steady state power flow modeling reviewed in this work for application to our problem, including benefits and detriments of the

various techniques. Power flow modeling of an electric power system is performed for a variety of reasons. The principal problems in grid resiliency addressed by power flow models in the literature are performance and reliability analysis [77], economic dispatch [57], and planning [22]; often these problems are solved with a common solution in mind. Optimal Power Flow modeling is essential to the reliable, efficient operation of the power grid.

Optimal Power Flow models usually consider an optimization function subject to a series of constraints drawing on the physical limitations of individual elements of the system, as well as on the connected nature of the system [57]. The objective function is typically a minimization, such as the minimization of power losses [66], of line losses, or of the cost of fuel or operations [23][25].

Power system restoration is an advanced application of power flow modeling. With prioritization and sequencing it can become a layered problem or can be presented as a mixed integer nonlinear program where the binary variables reflect the timing of restoration. This reflects an integration with the Restoration Model described above. Constraints are comprised of both equality and inequality constraints. The equality constraints capture power flow and power balance at each node in a network, following Ohm's and Kirchoff's laws. The inequality constraints capture the lower and upper bounds on each variable, respective of the physical constraints of the system, including:

- voltage magnitude of each bus;
- voltage angle difference between adjacent buses;
- active and reactive power output at each generator; and
- active and reactive power on each transmission line [25][55].

To the extent that the optimization function or the constraints contain nonlinearities, a range of approaches can be taken to simplify the nonlinearities, serving as relaxations or approximations of the problem. This can include:

- assuming a linearization of a nonlinear element [24];
- converting a nonlinearization into a series of piecewise linearities [24]; or
- decoupling of elements of the larger problem into subproblems [19].

For each problem, modeling of power flow is a simplification of the actual power flow, which contains numerous nonlinearities for which computational techniques are prone to issues in solution and convergence [37][54], especially for real-time calculations. Various techniques for dealing with these nonlinearities, including the simplification of nonlinearities into forms that are computationally tractable, and making assumptions on certain constraints, have been developed throughout the years [2][19].

2.1.1.2.1. DC Optimal Power Flow

The DC Optimal Power Flow (DCOPF) model is a linearized simplification of AC Optimal Power Flow (ACOPF) network model, with fixed voltage magnitudes (bus voltages equal to 1), resistance approximated to zero, and voltage angle differences between buses approximating zero [19]. As a consequence, reactive power variables are eliminated and inequality bounds are also typically removed [55]. Tan, Cai & Lou [66], as an example of a DCOPF model, leverages an optimization focused on the minimization of power losses during transmission over the network subject to the remaining bus and line constraints.

2.1.1.2.2. Linearized AC Optimal Power Flow

ACOPF models enforce the full extent of constraints on the objective function (including reactive power constraints and variables ignored by the DCOPF). The problem, with complete and accurate

constraints and an objective focused on minimizing costs, would meet multiple objectives, including minimization of losses and minimizing various operating costs in a single formulation [19]. There have been several approaches to examining the ACOPF problem with limited approximations. Two will be discussed here, which have been the focus of examination in this research: Coffrin and Van Henterwyck's Linear Piecewise Alternating Current (LPAC) Model [24][25][26] and the Multiple-Choice Model (MCM) of Aravena et al [9][10][61].

The LPAC Model makes a few linear programming approximations within the context of the AC power flow equations.

- First, the LPAC model linearly approximates the sine function, $\sin(x) \approx x$, since phase angle differences are close to zero in practice.
- Second, the LPAC model approximates the cosine function as a piecewise linear function [24]. The rationale for this approximation is that reactive power is highly dependent on phase angle differences and the cosine function is sensitive to perturbations away from zero.

For "hot-start" models, best used for stable network topologies, voltage magnitudes from a base-point solution are leveraged in the real and reactive power equations. A warm-start model leverages the "hot-start" concepts, further assuming that voltage magnitudes at generators are known, while those at other buses are dependent upon identifying the difference between the true voltage and an available target voltage. Finally, the cold start model, best for black-start restoration, merely assumes that voltage magnitudes are perturbed from one [24].

The works of Patsakis [61] and Aravena [9][10], as with our work, center around restoration of the grid, with a core dependency on power flow. In these works, the model represents the real and reactive power flow entering a branch (i, j) at bus i as functions of three variables: the voltage magnitude at bus i; the voltage magnitude at bus j; and the angle difference for branch (i, j). The three-dimensional domain captured by these variables is partitioned into cubes and the functions are each approximated with a hyperplane in each cube. The model then uses binary variables to pick a single cube and uses the linear hyperplane within that cube to approximate power flow. Much like the LPAC Model, this mixed-integer formulation utilizes curvature, but in three dimensions, to carefully partition their domains so that fine partitioning only occurs when there is significant curvature in the real or reactive power values.

2.1.1.3. Integration with a Feasibility Oracle

The goal of the restoration model is to obtain a restoration schedule that can be acted on by a power utility operator. We use steady state power flow calculations to help ensure islands generated by a schedule can attain a steady state. Towards this end, Aravena et al., 2019 [10] embed the restoration model in a decomposition algorithm with certain features akin to Benders decomposition. Specifically, their algorithm is similar in how a candidate solution is passed from a main problem to a subproblem to provide informative cuts to the branch-and-bound (B&B) tree [7][42]. However, the decomposition algorithm in Aravena [9] has significant tailored enhancements compared to a basic Benders decomposition.

The decomposition algorithm begins by solving the Master restoration problem in a mixed-integer program (MIP) B&B solver [72]. Any time an integer solution is found, a callback is used to extract the schedule and send it to the Feasibility Oracle. The Feasibility Oracle constructs and solves a sequence of increasingly rigorous subproblems to check for power flow feasibility in each island and

generates cuts for infeasible islands to prevent recurrence. As noted in their work, this decomposition algorithm allows for fast solution times at scale for specific use cases.

2.1.2. Network Dynamic Model

During implementation of a restoration plan, actual conditions on the system typically depart from the idealizations used to develop the plan. These deviations can delay or sometimes preclude restoration as envisioned in the plan, requiring operators to draw on heuristics, experience, and other sources of expert judgement. Our goal is to provide restoration plans that are robust considering all elements of the system (grid, operator, information flow, planning) and their interactions, as well as the pragmatics of implementation. To assess the interactions among a plan, the system, and the system operator, we require a "ground truth" simulator for the system that can present the kinds of problematic behaviors operators are likely to encounter. Such behaviors include power system dynamics, variability in load, and deviation of system conditions from those assumed in developing the plan.

Because the purpose of the ground truth simulator is to present the operator with a set of plausible unexpected conditions that might arise in the course of restart, the ability to efficiently create a set of alternative trajectories resulting from a diverse range of processes is essential. Simulating the behavior of a single fully specified system under ideal conditions is not the goal. To meet this distinct requirement, we have adapted a network simulation model originally developed to study disruptions on fluid transportation networks [27].

2.1.2.1. Background

The Network Dynamic Model (NDM) was originally developed under the aegis of the National Infrastructure Simulation and Analysis Center, a DHS program concerned with infrastructure function and disruption at national and regional scales, as NetFlow Dynamics. The NDM was designed to simulate the operation of fluid transmission pipeline networks under nominal and disrupted conditions, allowing decision-makers to rapidly delimit the degree and location of potential fuel supply shortfalls following large-scale insults to the system, such as production disruptions due to hurricanes. Existing models developed and used by industry were not designed to represent the system at this scale, or for this specific purpose. The model has been applied to petroleum and refined product networks in the US [14] and extended to petroleum [59] and natural gas [40] networks outside the US.

The model formulation [27] is based on assumptions appropriate for the scope and scale of the motivating problems: estimating consequences to consumers of the loss of supply or transmission capacity that persist over a day or days. Service constraints are assumed to arise from limits on transmission capacity across links in the network and on supply from external sources and potentially internal storage. The model represents flow along capacity-limited links and storage at capacity-constrained nodes. These properties, along with the structure of the network and the boundary conditions defined by potential supply and demand allow us to project the pattern of outflows the network will permit at various locations.

The system reaction also depends on the values of parameters that summarize the response of the operators of the various components of the system. Because the model is simple and runs quickly, it allows users to quickly explore a range of possible scenarios with respect to these essentially unknowable factors.

2.1.3. Operator Cognitive Model

As mentioned in the previous section, further complexity in modeling is required to increase simulation fidelity beyond idealized systems and accurately capture how events unfold during real-world failures. In addition to variability in load and system conditions, there is a strong human element controlling the overall behavior and recovery speed of the system. Decisions made by the grid operator when it is appropriate to connect generators, close lines, and introduce loads into the system all affect the state of the system moving forwards, and many of these decisions cannot be entirely automated or prescribed in detail via the restoration schedule. In addition, there are limits on the speed of task completion and parallelization that can be expected of a human operator that may conflict with the idealized situations assumed by an optimized schedule. Depending on the cause of the system disruption, the operator's information about the true condition of the system may be incomplete or corrupted, and their controls compromised. Having a more detailed understanding of the operator's decision making, activity delay, personal understanding of the state of the system can thus allow the model to be more accurate and feasible, as well as inform an expectation for the true duration of a recovery sequence.

2.1.3.1. Background

Our model includes a human OCM developed in the ACT-R framework [4], utilizing a tasking hierarchy developed at Sandia called CogTasks [1]. ACT-R is a cognitive modeling framework used to simulate the decision making and actions taken by a cognitive agent in response to varied stimuli; in this case we build our agent to read in restoration schedules and system state information from a console and make decisions about cranking generators, connecting them to the grid, and managing lines and loads in the system. ACT-R itself contains a deep development history that allows it to accurately capture the process and timing information involved in making decisions and taking the actions we prescribe.

The CogTasks library built on top of the ACT-R base is a recent development that specializes in hierarchical tasking information, built for the purpose of system reconstitution and troubleshooting. CogTasks takes the basic tasking framework that ACT-R provides and allows for the chaining of subtasks required to accurately model how a troubleshooting process takes place. For instance, if an operator reads in a schedule that they need to connect a generator, they need to understand and have the mental structure prepared to understand all the assumed preconditions that come with that, such as ensuring the generator frequency closely matches the system frequency. CogTasks provides the needed complexity to allow them to see the top-level task, then construct the 'stack' of needed subtasks, then work their way up the chain until they consider the top-level task complete and are ready to move to the next task. While seemingly simple, this is a complex process when working within the confines of human cognitive structures, and the library allows for this chaining to not only be done in a manner consistent with real-world cognition, but also wraps it into the overall ACT-R framework that allows for the timing to be accurately represented.

2.2. Integration of Modeling Techniques

This section reviews both integration of the models (e.g., how inputs and outputs are used) and application of the models performed to date.

2.2.1. Integration

Our model has three distinct pieces that operate in conjunction with each other: the power flow-informed restoration model leveraging the Feasibility Oracle; the NDM of the grid, and the OCM.

This combination, as applied to the system they are modeling, is shown in Figure 1. The three components work in conjunction to simulate a realistic grid restoration procedure, beginning with the restoration model which produces an optimal schedule for the system in question. This schedule is then passed to the OCM, which runs in conjunction with the dynamic grid model to attempt the implementation of the schedule. The NDM contains the information about what the system is expected to look like after the prescribed failure mode and is connected to the OCM via a virtual console through which it reports a variety of summary statistics including the voltage, angle, and frequency of the system. Further, the virtual console also contains hooks for the OCM to affect the system via actions such as cranking generators, energizing lines, connecting generators, and adding loads. These actions affect the dynamic grid model which is then reported back to the operator for further monitoring to ensure that the system is behaving as desired. The operator reads through the restoration script, attempting to implement the prescribed actions as appropriate for the system under question.

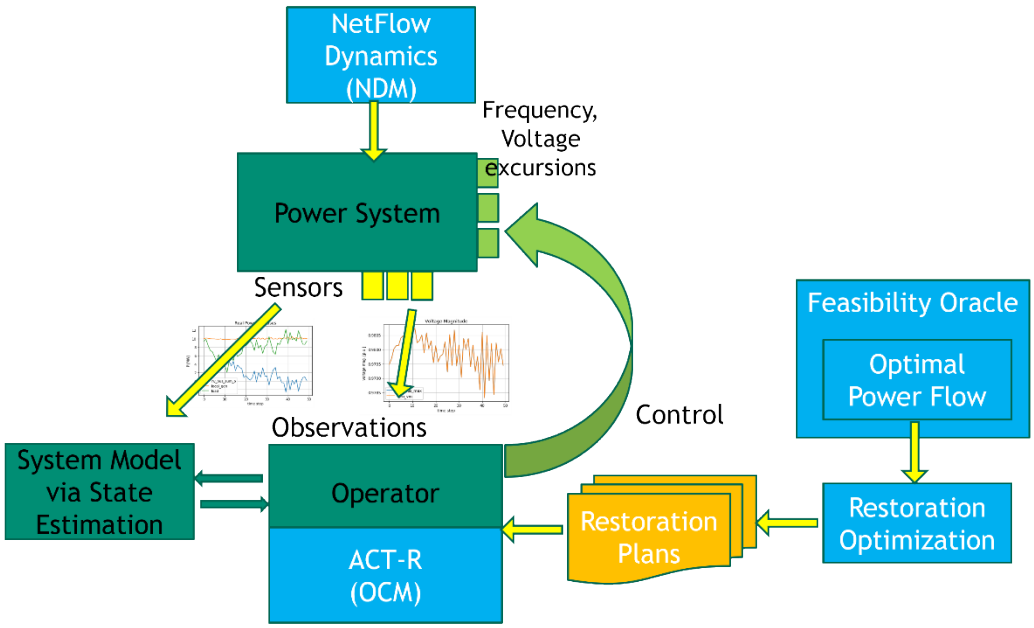

Figure 1. Model integration relative to interacting systems and information paths

2.2.2. Generalized Application

The analytic process, as shown in Figure 1, is performed as follows:

Initial focus of the effort was on development of restoration optimization plans relative to the Feasibility Oracle, leveraging an optimal power flow model (at right in Figure 1). Initial efforts in this space utilized concepts from the DCOPF model [66], with later efforts leveraging the MCM [10]. As discussed in Section 2.1.1, we are leveraging these static power flow models, that only find theoretical steady states, rather than full dynamic models that actually model how the grid behaves over time, as dynamic scheduling optimization models are almost surely intractable; in so doing we assume the grid is able to attain these theoretical steady states during operation.

The resultant restoration plans are used, in turn, by the ACT-R OCM, which assumes the system is in a stable state prior to the performance of any action. Actions are chosen based on the restoration plan (e.g., cranking generators, connecting generators, energizing lines, adding loads) and stability checks are performed using the NDM of the system, to check for any issues (e.g., voltage, phase

angle, frequency) affecting system stability resulting from the action chosen. If issues are found based on feedback provided from the NDM to the OCM, corrective actions can, in turn, be made, until stability is reached. At this point, the OCM can move on to the next step of the restoration plan; this process is repeated until the restoration plan is complete. The detail included in the OCM has gradually increased, with external subject matter experts providing guidance to the team on the ways in which system operators work with limited information to restore systems following significant disruptive events. Similarly, the NDM has been enhanced to capture departures from expected operation via tripping behaviors, which in turn provide feedback to the OCM for necessary corrective actions based on the operator's previous action.

Figure 2 shows an example of a restoration simulation using the integrated system. Generator reconnection at time 10 induces system transients, which the operator uses to assess the condition of the overall system, and to verify pre-conditions for the next restoration step, connecting load at time 140. Both time and frequency deviation are unitless in the NDM model. The time scale is set by generator inertia the fluid volume used to represent it at generating nodes. The relative variation in node potential from its equilibrium is interpreted as a relative variation in generator frequency.

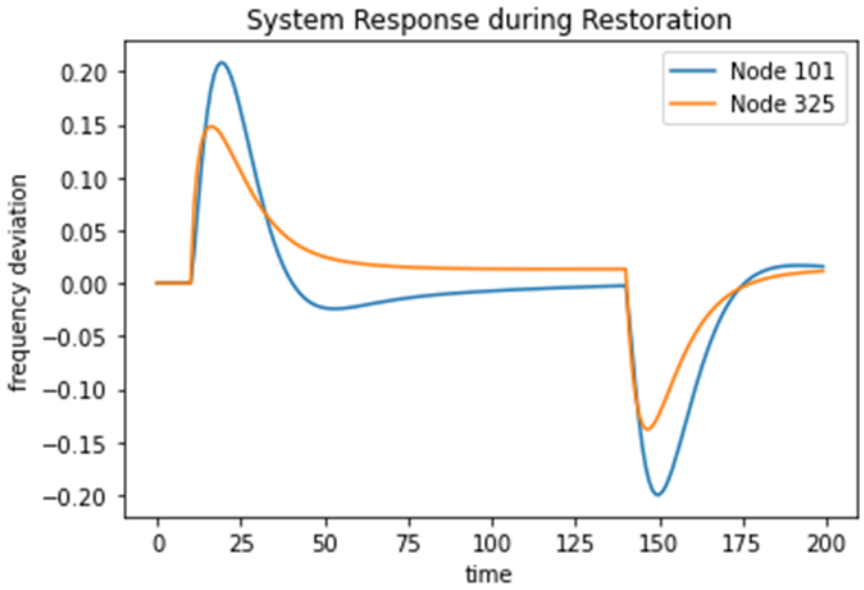

Figure 2. Frequency deviation as a function of time in restoration sequence at two network nodes of the RTS-96 system

2.3. Threats

There are several threat aspects of interest that can impact grid restoration. This section describes those in some detail, before advancing to a discussion on how threats and their aspects can impact our modeling paradigm, as described in Section 2.2 above.

2.3.1. Aspects of Threats

2.3.1.1. Threat Type

Threats to operation of the grid, as suggested in Section 1 above, come in two principal forms [71]. Naturally caused disruptions originate with a natural impact on grid performance. This mainly includes severe weather [58], such as hurricanes and severe storms, tornadoes, which often damage

transmission and distribution elements of the electric grid but can also include space weather [39]. This can also be extended to include extreme heat and cold, which impact both production and consumption. In each of these latter cases, extreme conditions lead to an increase in demand relative to nominal performance and create conditions that can limit both transmission and generation.

Human-initiated disruptions can come in multiple forms as well: Unintended accidents; physical threats on individual facilities [52]; and cyber threats against individual operators or groups of operators [11]. The last of this group has been studied, both from an offensive [69] and a defensive [74] perspective.

It is important to note the challenge in distinguishing between intentional and unintentional threats. In many cases what may be encountered in terms of direct, physical consequences to the grid can look similar from a weather event as from a high-voltage tower being toppled by removal of anchoring, and inaccurate information on system elements can come from a cyber inject or from a misinformed repair crew member reporting an incorrect outage. Therefore,

2.3.1.2. Threat Scope

The scope of the threat can take on a couple of dimensions. First is the geographic scope, reflective of customers disrupted. These can be described in the following, increasing order of magnitude:

- Individual customer
- Group of customers on an individual circuit
- Entirety of customer set on a circuit
- All circuits on a bus
- All buses in a substation
- Groups of substation service areas, within one or more utility service territories
- Entirety of a utility service area
- Groups of utility service areas within one or more North American Electric Reliability Corporation (NERC) Control Areas
- Entirety of a NERC Control Area
- Groups of NERC Control Areas within one or more Interconnections
- Entirety of an Interconnection
- Entirety of the NERC

The second element of threat scope is the duration of the disruption. Multiple industry-specific metrics exist for measuring system performance [65][70]; most of these rely on some measure of both the number of customers impacted by outages and/or the duration of those outages. Duration of an outage correlates to the geographic scope [43], but more to the level of physical damage imposed on the system (requiring replacement of elements rather than simply an ordered energization.

2.3.1.3. Systemic Visibility

A final, crucial aspect of a threat is the post-threat systemic visibility of the system by its operators. In both natural and man-made threats, knowledge of the status of components of the system can be limited due to system damage, or due to elements of a cyber-attack providing the operator with false information about operation of system elements. Each of these can limit the effectiveness of a restoration plan.

2.3.2. Application of Threats to Modeling Framework

Realizing that these threats and their aspects must be understood relative to the optimal restoration construct described in the above content, it is worth examining the impact of threat on the ways in which the restoration process can be performed. Here we'll discuss this considering each of the modeling components, as well as in the aggregate. This will aid in the identification of ways to refine the process described in Integration of Modeling Techniques above.

The optimization plan, as described in Section 2.1.1, focuses on an "optimization once" focus. That is, it aims for a singular optimal restoration. But what should an operator, or their dependent optimization, do if the restoration plan is not producing the desired results in system state? This suggests the need for an optimization loop. An optimization loop is a feedback mechanism for reflecting on information received relative to planning, to enable improved restoration reflective of additional information. This can be modification of the plan as originally developed based on irregularities or on additional information (as is often the case with restoration in natural disruptions, where systemic visibility is limited and improves over time). In this case, operators purposefully make the decision to reoptimize based on additional information, as the knowledge of the system state improves over time.

Dealing with this feedback loop has long been a staple of optimization relative to threat. Attacker-Defender [13] and Defender-Attacker-Defender [1][67] modeling layers the overall optimization with optimal decision-making by an attacker, and by a defender responding to a rational attacker, to best apply resources to protect grid operations [56][75]. For our case, we are not taking a game theoretic approach to restoration but are focusing on decision-making inside the loop.

From the perspective of the OCM, having an active restoration plan on which to operate is key. The ability of the OCM to leverage system results (as is done with the NDM) to identify variance in the restoration from the expected is the best mechanism for determining whether the nest step in the restoration plan should be attempted, or the restoration plan reassessed. That reassessment can take on one of several forms:

First, and most useful based on the restoration plan as provided, would be to begin with a decomposition of a full restoration plan into component parts. In this case, subcomponents of the restoration (such as those associated with restoration of a particular island in the overall restoration) could be executed independently while reassessment of elements of the overall system could be examined. This reassessment could begin through an iteration around the difficulties caused; in this way, examination of minor variations could help to determine the cause of irregularities, and may well identify whether an irregularity is tied to a physical difference in the system or a system response irregularity, of benefit for identification of threats having acted on the system. One can consider the development of this set of subcomponents of restoration through Machine Learning, Markov processes, or other learning techniques capturing the possible states of elements of the system. A more computationally intensive process would involve parallelization of the optimization to reprocess from the last successful step.

In either case, every pause of the OCM to change the optimization has an implementation cost associated with it, in terms of turning a restoration profile into an acted-on solution set. It is worth realizing that implementation for real-time restoration likely requires some significant computational time outside of outage conditions. Doing this in a high-performance computing environment to examine a wide array of potential outage conditions would provide a "library" of restoration plans (many of which may share restoration subcomponents). These subcomponents could serve as much more useful increments for restoration planning and operations in a wider array of circumstances.

3. DETAILS ON RESEARCH PERFORMED

Details on the integration of modeling capabilities are provided in this section. Certain foundational content is presented in [62], and the reader is directed to that reference for more information.

3.1. Power Flow Informed Restoration Model

The details on the restoration model, power flow models, and power flow-informed restoration model within the Feasibility Oracle are discussed in this section.

3.1.1. Restoration Model

Application of the restoration process to the Institute of Electrical and Electronics Engineers (IEEE) Reliability Test System (RTS-96) [34] is illustrated in Figure 3 below. Assume a power system has experienced a catastrophic insult and is fully blacked out. Additionally, assume the state of each component is known, e.g., energized or de-energized. One possible path of restoration, following the process of [10], against a portion of the RTS-96 network, consists of these steps:

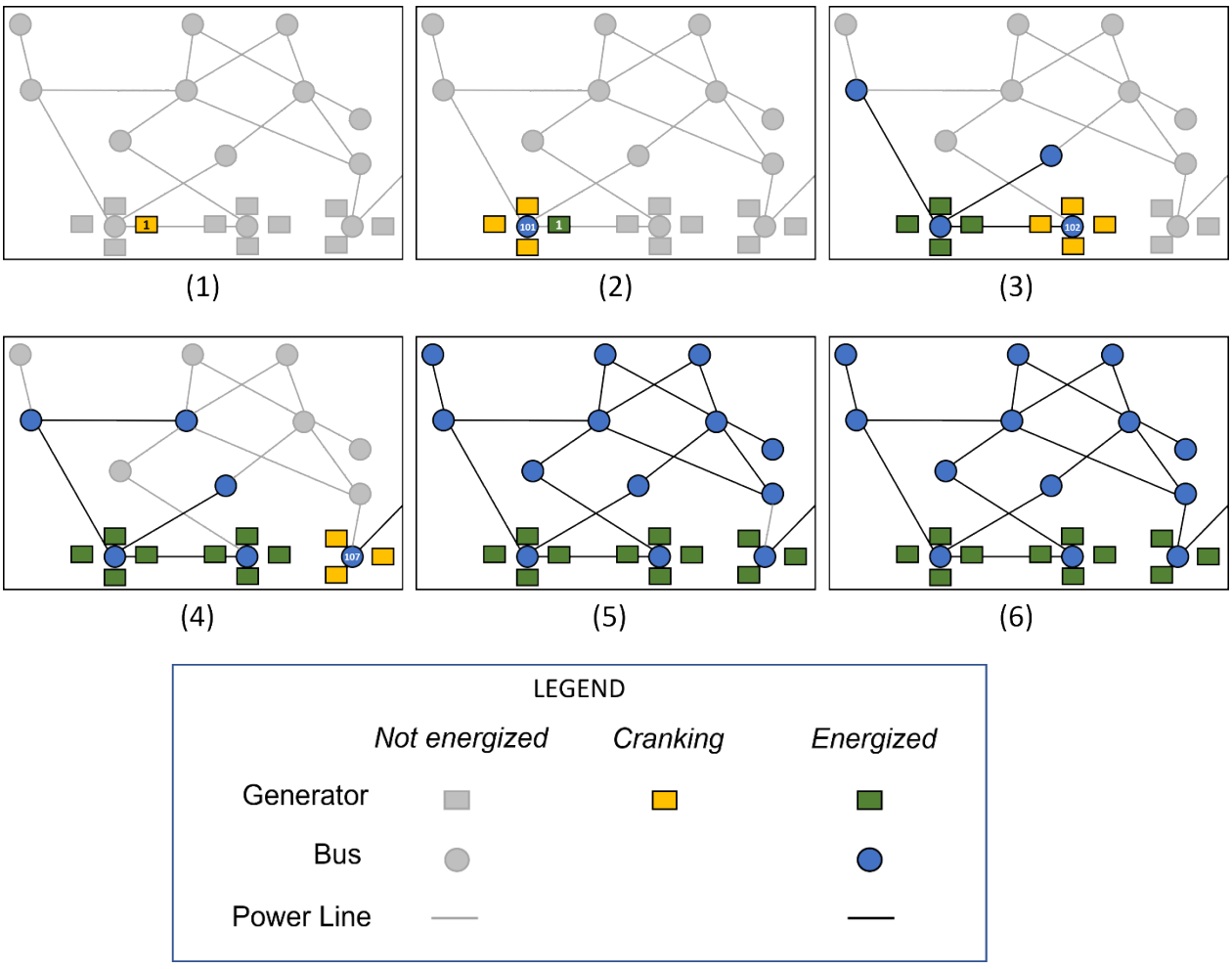

Figure 3. Example restoration sequence of a portion of the RTS-96 system. Each figure represents the energization state of components within the system at different snapshots in time.

(1) Black start generator 1 begins cranking.

(2) Generator 1 is energized and provides power to bus 101 and its other attached generators.

(3) Power reaches other buses across energized lines, and the generators at bus 102 can now crank.

(4) Power has reached the generators at bus 107, in a nearby island, and they begin cranking.

(5) The island including the generator cranked in (1) is completely energized.

(6) Finally, a line between the two islands is energized. The system is fully restored when all lines between all islands are energized (not pictured).

The authors note the objective function models how the power system "returns to a normal operational state…in terms of stability and coverage." This, of course, assumes no physical damage to elements of the system. This objective strives for power system restoration as rapidly as possible while maintaining stable dynamics through the process. For the purposes of this work, shunt- and series-compensators were not modeled, and discussion of that functionality in their work is omitted. Therefore, the restoration model discussed here consists of an objective function to drive the energization scheduling decisions for generators, buses, and lines.

3.1.2. Power Flow Implementation

The restoration model, itself a mixed-integer linear program, is designed to work with any linear continuous or mixed-integer power flow model. Case studies presented in [10] use the LPAC and MCM model from [26]. To have a collection of optimal power flow modes for use with restoration, we extended the Pyomo-based power system optimization toolkit EGRET [41] to include the LPAC and MCM models in addition to its existing DC optimal power flow model. Our restoration code is modularized so that any linear power flow can easily be used.

To easily deenergize load, generators, and transmission lines, we use binary variables in DC optimal power flow and LPAC that are fixed at zero to take a component offline and one to keep it online. These binaries are strategically placed in the power flow model so that they can deenergize components by forcing power quantities to zero and/or disable constraints. The restoration model's feasibility oracle needs this feature to generate cuts that prevent infeasible islands.

For ease of testing our implementation of the restoration model, we chose the DC optimal power flow for our use cases. However, as argued in [10], LPAC is a more appropriate choice of power flow since, under abnormal operating conditions, voltages, and reactive power need attention to ensure they remain within stable limits. The MCM model [10] is an even better power flow to use in restoration than LPAC since it approximates full power flow functions rather than individual terms within power flow functions.

To minimize model-building overhead within our restoration framework, we only create a power flow instance for use with the restoration model once. Pyomo's persistent Gurobi interface keeps our power flow in memory so power flow parameters can be modified and the model can be resolved without having to regenerate new power flows, write new model files, and restart Gurobi every time an optimal power flow needs to be solved. See the next section for more details on integration of power flow in the restoration model through its feasibility oracle.

3.1.3. *Integration with a Feasibility Oracle*

Figure 4 provides an overview of the Feasibility Oracle. The Feasibility Oracle is designed to detect any sources of infeasibility in a restoration schedule and generate constraints that will prevent these sources of infeasibility in any future schedules in the B&B solve. As the Restoration Model progresses, its set of core model constraints are appended with a pool of constraints generated by the Feasibility Oracle. In this way, the Restoration Model becomes more well-informed and finds more physically feasible restoration schedules until it terminates with an optimal restoration schedule.

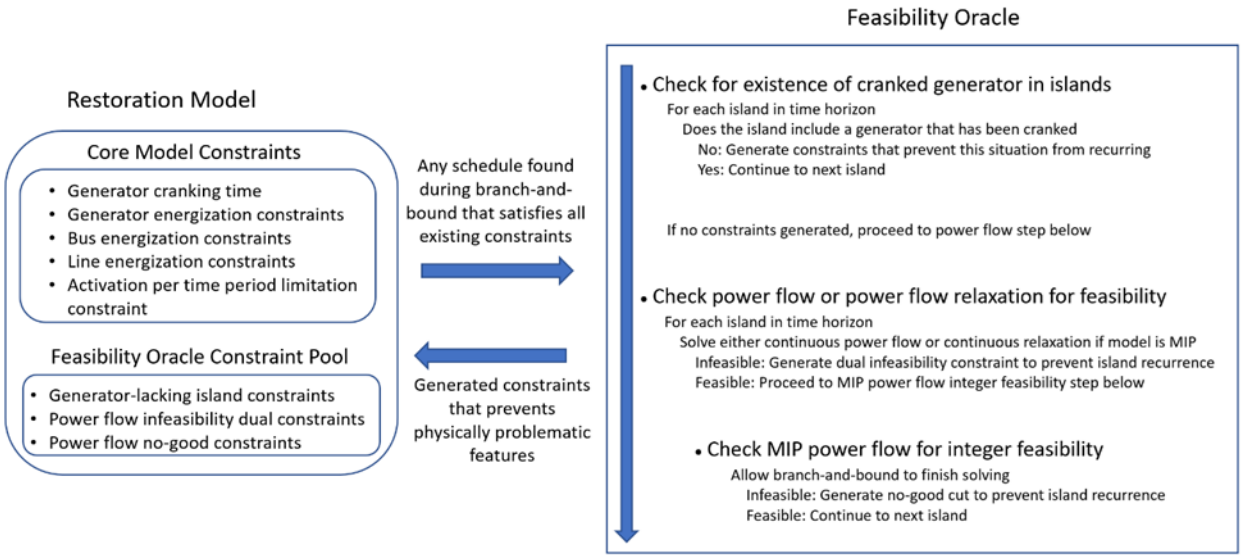

Figure 4. Overview of the Feasibility Oracle

The Feasibility Oracle proceeds in a 4-step sequence to ensure power flow feasibility within each island:

(1) Extract all islands that exist throughout the time horizon of the schedule. These islands are connected components of grid components containing transmission lines, connected buses, and generators along with the state of restoration schedule binary variables pertaining to these respective components.

(2) Check to see if any of the islands do not have fully cranked generators. If no such generators exist, the island is infeasible since there is no source of power generation in the island. In this case, one constraint per island bus as well as a single constraint for the whole island are generated to prevent this island from recurring. An additional benefit of these constraints is that no sub-island of the original island will occur with these constraints. If constraints are generated, go to step 3.

(3) If no constraints were generated in step 2, a power flow model is solved for each island. If the model is not infeasible, the restoration model B&B proceeds. Otherwise, a constraint is generated as follows:

   a. If the power flow is continuous or an infeasibility is detected at the root node where the continuous relaxation of a MIP is solved, a hybrid Benders integer constraint can be constructed using both the dual unbounded ray given by the B&B solver and the

grid component binary variables. This constraint prevents this island from recurring along with other problematic sub-islands

b. If the power flow is a MIP and the infeasibility is not detected by the continuous relaxation sub-solve, then a no-good cut is generated. This constraint prevents only this exact island from recurring.

(4) Any generated constraints are added to the Restoration Model and the B&B solve is allowed to proceed.

The Feasibility Oracle produces a restoration schedule on completion. That schedule is utilized by the NDM and OCM as described in the following sections.

3.2. Network Dynamic Model

The NDM is essentially a diffusion model, with nonlinearities introduced to impose capacity limits on flow rates through pipeline segments, as well as upper and lower limits on the amount of fluid that can be stored at nodes. Flow rates are governed by a scalar state "potential". Equilibrium entails flow balance at each node, but the transient behavior is governed by accumulation and depletion of storage at nodes.

The initial equilibrium of the system corresponds to a specified level of fluid storage at each node. Around this equilibrium, increases in storage correspond to increases in potential and decreases in storage to declines in potential. Limits on the minimum and maximum storage levels are imposed by the nonlinear sigmoid function defining the relationship between potential and storage shown in Figure 5.

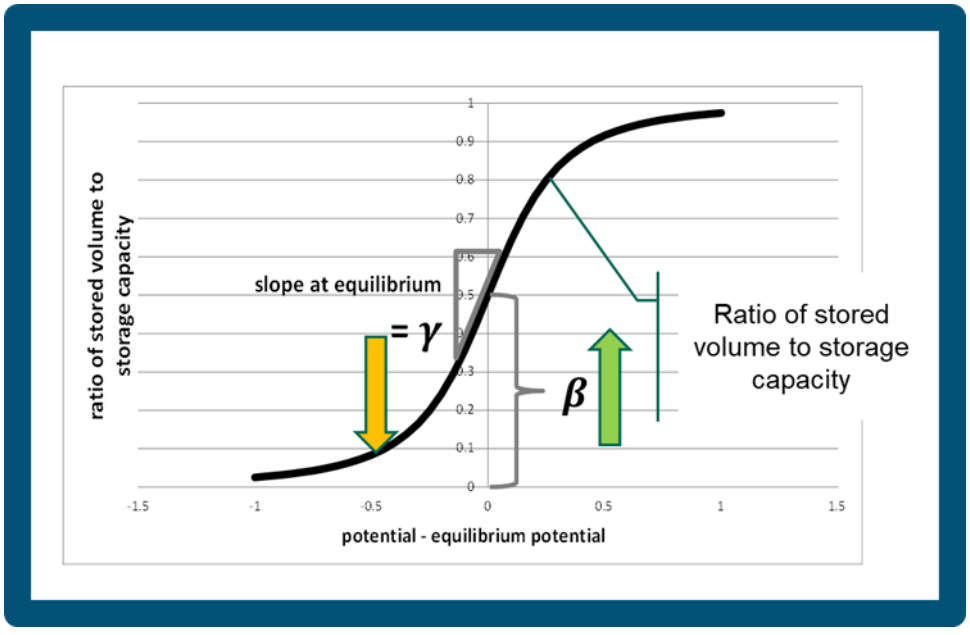

Figure 5. Function defining the relationship between nodal storage and node potential deviation in the NDM model

Parameters of the function control the responsiveness of potential to storage changes, which is a kind of inertia. Flow imbalances at the node induce accumulation or drainage of fluid, which in turn induces a change in node potential that acts to restore flow balance.

Although NDM was designed to model fluid flow over networks subject to capacity constraints, its governing equations describing mass conservation can be applied to other systems involving flow of conserved quantities on networks. Energy conservation and flow is the most appropriate analog in power systems. Although the time scales are vastly different, the process of balancing inflow to outflow at nodes is superficially analogous to the reaction of generators to power flow imbalances, in that rotational inertia acts as an energy reservoir.

A key difference is that the fluid transmission system easily functions with a post-disruption equilibrium having a permanent offset to storage levels. The power system does not. If nodal storage is interpreted as generator rotational energy, its equilibrium level corresponds to the global system frequency. To pursue the analogy between fluid and power networks it's essential to include a stabilizing process that maintains the initial equilibrium potential, analogous to prime mover regulation in a generator.

The dynamical equation for a node *i* in NDM is:

$$\sum_j q_{ji} + q_{si} - d_i = \frac{dv_i}{dt} \quad = \frac{v_i^T p}{2b} g(s_i) \frac{ds_i}{dt} \quad \forall i$$

Where:

s_i is the potential at node *i*

$q_{ij} = c_{ij}\, f\big((s_i - s_j)u_{ij}\big)$ is the flow from node *j* to node *i*

c_{ij}, u_{ij} are the capacity and utilization of the link connecting node *j* and node i

$q_{si} = c_{si}\, f\big((s_s - s_i)u_{sj}\big)$ is the flow from a source into node *i*

s_s is the source potential

c_{si}, u_{sj} are the capacity and utilization of source at node *i*

d_i is a sink rate from node *i*

v_i is the volume stored at node *i*

v_i^T is the storage capacity at node *i*

$$g(s) = \left[\frac{1}{2}\left\{1 + \frac{(\frac{s-a}{b})}{\left[1 + (\frac{s-a}{b})^2\right]^{\frac{1}{2}}}\right\}\right]^{p-1} \left[1 + (\frac{s-a}{b})^2\right]^{-3/2}$$

and $a, b,$ and p are storage parameters derived from the sigmoid function shown in Figure 5.

There are two parameters in the source equation that might be adjusted: the capacity parameter c_{si} and the utilization parameter u_{sj}. Keeping a capacity limit is fundamental, and so defining a dynamical equation for utilization is preferred. This simple expression:

$$\frac{du_{si}}{dt} = -u_{si}(\frac{s_i - y_i}{t_s})$$

causes local injection to increase (decrease) as long as the potential is lower (higher) than the equilibrium level y_i, with a reaction time governed by a time constant t_s.

This additional process can produce the kind of second-order oscillatory dynamics the characterize frequency stabilization in power systems.

Modeling black start also requires a structural elaboration that distinguishes generator nodes from the network proper. This distinction allows generators to be explicitly disconnected from and reconnected to the network. Figure 6 illustrates the added structural features and illustrates the use of those features during simulation of system shut-down and restart.

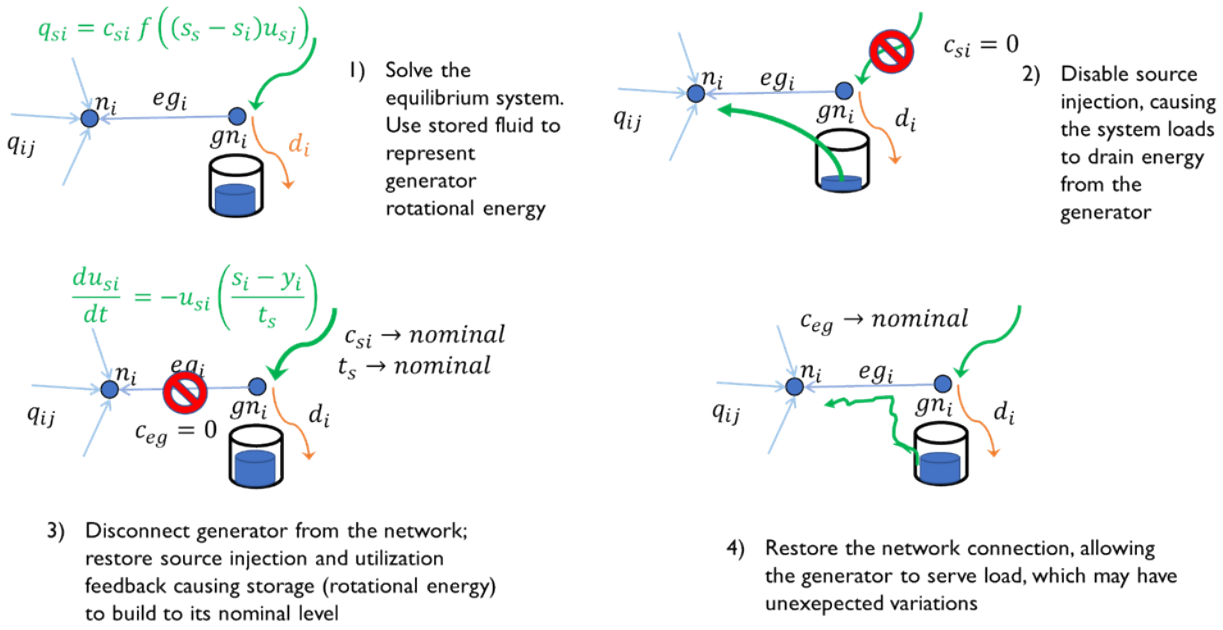

Figure 6. Representation of generator nodes in the elaborated NDM to model generator shut-down and restart

In the present application nodal storage represents rotational energy of generators, with terms added as defined above to model frequency stabilization following disruption [16]. Interpreting fluid stored at nodes as rotational energy is consistent with representing energy as fluid mass more generally. Other core NDM model parameters (i.e., supply capacity, demand rate, and link flow capacity) then correspond to power levels. The resulting model exhibits oscillatory responses to discrete events such as closure and line tripping, potentially inducing disruptive cascades. Stochastic variations in load can also activate problematic dynamics and create system balancing challenges for the operator. The overall modeling architecture allows other simulators to be used to define the ground truth, just as different models might be used to simulate operator behavior and to generate optimal plans. The only requirement for these components is that they implement the appropriate framework interfaces.

3.3. Operator Cognitive Model

For the implementation of the OCM within the Power Flow Framework, we use the CogTasks library built on top of the ACT-R base to build a cognitive agent that represents a grid operator working to bring the system back online and serves as the intermediary between the idealized model represented in the restoration schedule (built via the system optimizer) and the 'ground truth' system represented in the dynamic grid model. It is important to note that these three systems are

implemented independently, with information restricted in all directions. First, the optimizer produces a restoration schedule and provides it to the OCM at the start of the simulation. This schedule is then considered immutable, and the operator has no information on how it was created or alternate schedules that could be used. The OCM then attempts to implement the schedule on the dynamic grid model, with an intermediate 'operator console' between the two that passes information and commands. The operator does not have unrestricted access to system knowledge and must query the console for any state information they need. This is a key part of both the time estimates of the operator integrated recovery, and of the operator's decision-making process. They are entirely restricted by the information they receive when they request it, even if the information becomes obsolete, they do not receive replacement information without requesting it again later.

Prior work has outlined the decision framework operators undergo when implementing grid restoration [36], and cognitive modeling has a deep history of diagnostic [17][53] and strategic decision making [33][45][68]. Still, the two have not been integrated into a single power systems model that considers the operator ability (and speed) for recognizing, diagnosing, and adapting to deviations from expected behavior. The cognitive model presented here fills this need, working with both the optimized restoration plan and the dynamic system, monitoring the system to implement the schedule at the proper pace and adapting to deviations from planned behavior. As mentioned, we facilitate this process via the 'operator console', which provides limited control over the system to implement changes such as cranking generators, connecting energized generators, adding loads, and energizing lines. These possible actions must be done in the proper order, on the proper system assets, and at the proper times to ensure the system is balanced. For our implementation, the operator utilizes the pre-computed optimized schedule as well as the information gathered from the operator console on the ground truth of the system at a given time to make these decisions properly. Additionally, the cognitive architecture is highly extensible and has the capability to support further planning and strategic decision making in the future to make more detailed models as they become necessary.

The first portion of this is the simplest, and the fastest for the operator to implement. The operator takes six seconds to start a new stage and obtain a list of generators to crank, then for each generator they take two seconds to implement the cranking command and eight seconds to ensure that it is cranked before moving on to the next.

Then they must connect generators, which again begins by obtaining a list that need connection which takes three seconds. If there are no ready generators, it takes five seconds to gather this information and move on. If there are ready generators, however, it takes eight seconds to process the list and orient to a specific generator. Then the operator requests information on the generator which takes seven seconds to process, then three seconds to check the information and ensure it is appropriate, then two seconds to submit the connection requests and finally seven more seconds to ensure the connection went through and move on (or ten seconds if there are more generators the operator must orient too). This is the first step at which the operator has discretion for slowing down the system indefinitely, however, as the checking step requires ensuring that the generator is at an appropriate frequency to connect to the system. If it is not, the operator notes it, then after finishing all the other generators waits an additional thirty seconds before trying again. This can occur as many times as necessary for the generator to match its frequency, or a timeout can be implemented to connect the generator after a certain number of steps if needed.

The lines and buses are fairly simple as well, requiring just three seconds to request a list of lines to close then ten seconds per line to close each one and finally five seconds to finish this step and move on. Buses are similar, as it takes two seconds to obtain the list of buses and ten seconds per

bus to energize each, then six seconds to close out the task. In more sensitive simulations there is an optional stability check after each bus is connected, where the operator checks the overall stability of the system before moving on to the next bus. This, similar to generator connection, can take indefinite time or timeout as desired for the particular simulation. The actual process of the stability check is the same as that implemented at the end of each stage, outlined below.

Finally, after buses are connected, the operator takes two seconds to orient themselves to wrap-up activities, then seven seconds to decide if a stability monitor is needed. If no generators have been connected, the operator does not perform a stability monitor, and moves to stage wrap-up and requests the next stage, which takes nine seconds. If a stability monitor is needed, however, the operator takes six seconds to orient to stability checking, then the seconds to begin the process. This process consists of marking the start and end of a five second period, during which the operator console records the frequencies of every connected generator. The operator console then reports back to the operator the maximum volatility of any generator (given a percentage of the frequency change over the five second period), and the operator decides if system volatility is low enough to continue. This process takes seven seconds to trigger the end of the stability monitor and move on, four seconds to read and understand the reported value, and another four seconds to compare it to a volatility threshold. If the volatility is deemed acceptable, then it takes nine seconds to wrap up the stage and move to the new stage. If it is not acceptable, the operator waits ten seconds and begins the stability monitor process again. This, as before, can occur indefinitely or on a timeout as the simulation demands.

4. ACCOMPLISHMENTS

This chapter focuses on summarizing the results of a case study applying the integration of modeling techniques described in Section 2.2, leveraging the implementation of the Restoration Model, Power Flow Model, Feasibility Oracle, NDM, and OCM described in Section 3, against the RTS-96 network [34].

This section includes comparative analysis for the Western System Coordinating Council (WSCC) 9-Bus System [5] and the IEEE Reliability Test System (RTS-96) [34]. For both systems, the restoration optimization model objective maximized the number of components restored per time period.

In previous efforts associated with optimal restoration and optimal power flow, computation time is of significant interest, and so our case studies reflect capturing hardware specifications and run time. Tests on the WSCC 9-Bus System were performed using Gurobi 9.1 on an Intel Xeon W-2225 (4 cores, 8 threads) system with 32 GB memory running Windows 10. The RTS-96 system test was performed using Gurobi 9.1 on a 64-core optimization server with 3.17 TB memory running Red Hat Enterprise Linux v. 8.5.

4.1. Case Study: Application of the Technique to the WSCC 9-Bus System

This section provides an overview of the tests of our framework performed using the WSCC 9-Bus system. The WSCC 9-Bus System [5] contains three generators, six lines, three loads, and two winding power transformers. The system topography does not contain islands; however, its runtimes were sufficiently small to permit a variety of tests on the model input parameters. Table 1 displays the power flow data for buses that have loads and the maximum power generated by each generator.

Per the process flow in Figure 1, optimal restoration sequences were developed for the system using different criteria and constraints. The results are summarized in Section 4.1.1. These schedules were then presented to the combined operator and system model to simulate the dynamic restoration process. An example output from the system model is presented in Section 4.1.2 along with general observations about the system model behavior seen in the test. Section 4.1.3 describes the operator model's process and behavior over the suite of restoration scripts.

All tests on the WSCC 9-Bus system were run until a 0% optimality gap was obtained.

The WSCC 9-Bus system consists of three generators with a total generation of 320 MW, three loads with a total of 315 MW, and six transmission lines. Table 1 provides the details of the MW output from each generator and the MW consumption from the loads. Table 2, in turn, provides detail on each of the branches in the system.

Table 1. Generation and load detail

	Power (P.U.)	Power (MW)	MVar
Generator 1	1.04	71.6	27.9
Generator 2	1.025	163.0	4.9
Generator 3	1.025	85.0	-11.4
Total Generation	3.196	319.6	21.369
Load 1	1.25	125.0	50.0
Load 2	0.90	90.0	30.0
Load 3	1.00	100.0	35.0
Total Load	3.15	315.0	115.0

Table 2. Branch detail

Branch Type	From Bus	To Bus
Transformer 1	Bus 1	Bus 4
Transformer 2	Bus 2	Bus 7
Transformer 3	Bus 3	Bus 9
Line 1	Bus 4	Bus 5
Line 2	Bus 4	Bus 6
Line 3	Bus 5	Bus 7
Line 4	Bus 7	Bus 8
Line 5	Bus 8	Bus 9
Line 6	Bus 9	Bus 6

Sixteen tests were conducted on the WSCC 9-Bus system. The tests were selected to examine the effects from varying each of the parameter values for the model. An emphasis was placed on varying: (i) the number of black start generators; (ii) black start generator cranking times cr; (iii) the maximum number of branch lines ml that are restorable per time period. Table 3 displays the test names and their parameter values.

Table 3. Tests performed on the WSCC 9-Bus System (test names represent the combination of parameter values selected)

Test Name	Number of black start Generators	Black start Generator ID's	Cranking Time of black start Generators	Cranking Time of Non-black start Generators	Number of Branches Restorable per Time Period
Gen2_cr1_ml1	1	2	1	1	1
Gen2_cr3_ml1	1	2	3	1	1
Gen1_cr1_ml1	1	1	1	1	1
Gen1_cr3_ml1	1	1	3	1	1
Gen3_cr1_ml1	1	3	1	1	1
Gen3_cr3_ml1	1	3	3	1	1
genAll_cr1_ml1	3	1,2,3	1	1	1
genAll_cr3_ml1	3	1,2,3	3	1	1
Gen2_cr1_ml3	1	2	1	1	3
Gen2_cr3_ml3	1	2	3	1	3
Gen1_cr1_ml3	1	1	1	1	3
Gen1_cr3_ml3	1	1	3	1	3
Gen3_cr1_ml3	1	3	1	1	3
Gen3_cr3_ml3	1	3	3	1	3
genAll_cr1_ml3	3	1,2,3	1	1	3
genAll_cr3_ml3	3	1,2,3	3	1	3

4.1.1. Restoration Optimization Model Results Summary

This section provides results for the tests performed on the WSCC 9-Bus system. Table 4 provides the runtime in seconds, objective function values (highest is best), and time periods when total load was restored for each test.

The best runtime in Table 4 was test GenAll_cr3_ml3 (black start generator 3, $cr = 3$) at 0.23 seconds. The top five best runtimes were recorded for tests with a single generator and $ml = 3$ (e.g., tests Gen3_cr1_ml3, Gen3_cr3_ml3, Gen2_cr3_ml3, Gen2_cr1_ml3, and Gen1_cr3_ml3). The worst runtimes were for tests with $ml = 1$ (e.g., GenAll_cr3_ml1, Gen2_cr3_ml1, Gen3_cr1_ml1, Gen1_cr3_ml1, Gen1_cr1_ml1). There is a roughly equal mix of cranking times across the tests when sorted by runtime. This indicates runtime was impacted by *ml*, but not necessarily by generator cranking time.

Table 4. Runtimes and objective function values for each test performed on the WSCC 9-Bus System (results are sorted from largest to smallest objective function value, values are highlighted for tests with shortest runtime, best objective function value, and lowest time until total load restored)

Instance	Runtime (seconds)	Objective Function Value	Time When Total Load Restored
Gen1_cr1_ml3	0.32	233	5
Gen2_cr1_ml3	0.25	233	5
Gen3_cr1_ml3	***0.23***	233	5
Gen1_cr3_ml3	0.31	191	8
Gen2_cr3_ml3	0.24	191	8
Gen3_cr3_ml3	***0.23***	191	8
genAll_cr3_ml3	0.31	225	6
Gen1_cr1_ml1	1.33	200	9
Gen2_cr1_ml1	0.43	203	9
Gen3_cr1_ml1	0.85	203	9
genAll_cr1_ml1	0.35	228	9
genAll_cr1_ml3	0.43	***267***	***4***
Gen1_cr3_ml1	0.98	158	11
Gen2_cr3_ml1	0.72	158	11
genAll_cr3_ml1	0.5	186	11
Gen3_cr3_ml1	0.31	168	12

The best objective function value overall was test genAll_cr1_ml3 (267). Single generator tests where cr =1 and ml = 3 tied for second best (233). Two tests (Gen2_cr3_ml1, Gen1_cr3_ml1) tied for the worst objective function value (158). However, the remaining single machine test with the same parameters (Gen3_cr3_ml1) scored better (168). Additionally, all tests where every generator had black start capability scored better than any test with a single generator. Taken together, these results highlight how the choice of black start generator is significant when maximal restoration of components is the objective.

Table 4 and Figure 7 show the power restored over time for each test until the total load is met. In general, a decrease in maximum number of restorable lines is shown to increase the time until total load is restored. Additionally, the slowest time achieved when ml = 3 is better than the fastest time achieved when ml = 1. Overall, the earliest time until loads were restored was recorded for test GenAll_cr1_ml3, followed by the single machine tests where cr = 1 (time = 5 for ml = 3; time = 8

for *ml* = 1). However, when *ml* = 1, test genAll_cr1_ml1 is also tied for the earliest time. The five slowest times were recorded when *ml* = 1 (Gen1_cr1_ml1: 9, genAll_cr3_ml1: 11, Gen2_cr3_ml1: 11, Gen1_cr3_ml1: 11, Gen3_cr3_ml1: 12). This spread of times until total load is restored is asymmetrical with respect to the tests with the earliest reported times. Specifically, the test with generator 3 is slowest to restore total load. This demonstrates that black start generator cranking time *ct* was more impactful when the *ml* parameter was a lower value. These results showcase how constraining the number of restorable lines impacts the time until a network is restored. This aligns with the notion that real-world factors analogous to *ml*, such as the speed of debris removal and crew availability, can cause significant delays during restoration of real networks [18].

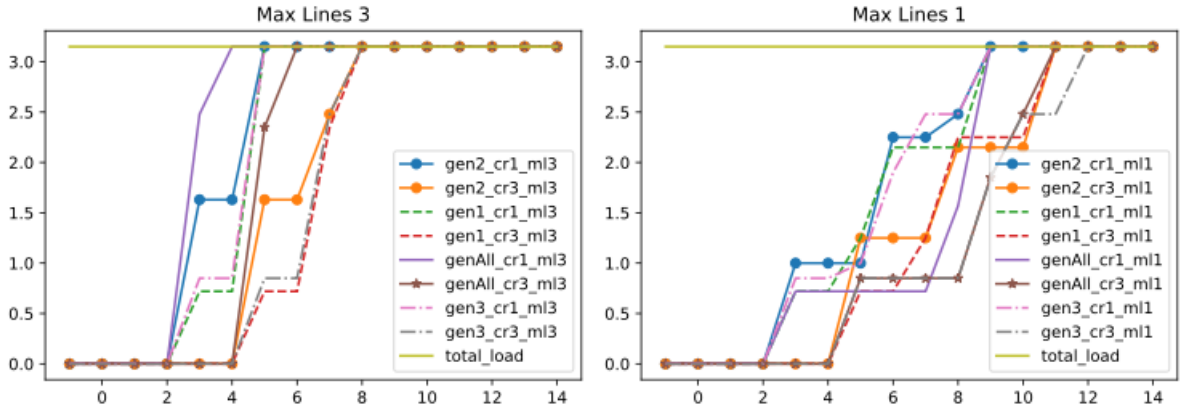

Figure 7. Power generated (in per-unit, or p.u.) over time (in time steps) until total load is restored

Figure 8 illustrates the systems for tests with the earliest time period when total load is restored, at the time of total load restoration. The test with all three black start generators (GenAll_cr1_ml3) restored total load by time = 4. Tests with a single black start generator (Gen1_cr1_ml3, Gen2_cr1_ml3, Gen2_cr1_ml3) restored the total load by time = 5. Four branches exist between each generator in the WSCC 9-Bus system, which informed the time until load is restored for each of the single generator tests. This is also the reason each of those tests didn't fully restore the system until time = 6. In a real-world system, the sequence of restored components could artificially provide the prioritization of certain loads, all else being equal. This supports the notion that the restoration of loads can present equity concerns or other issues.

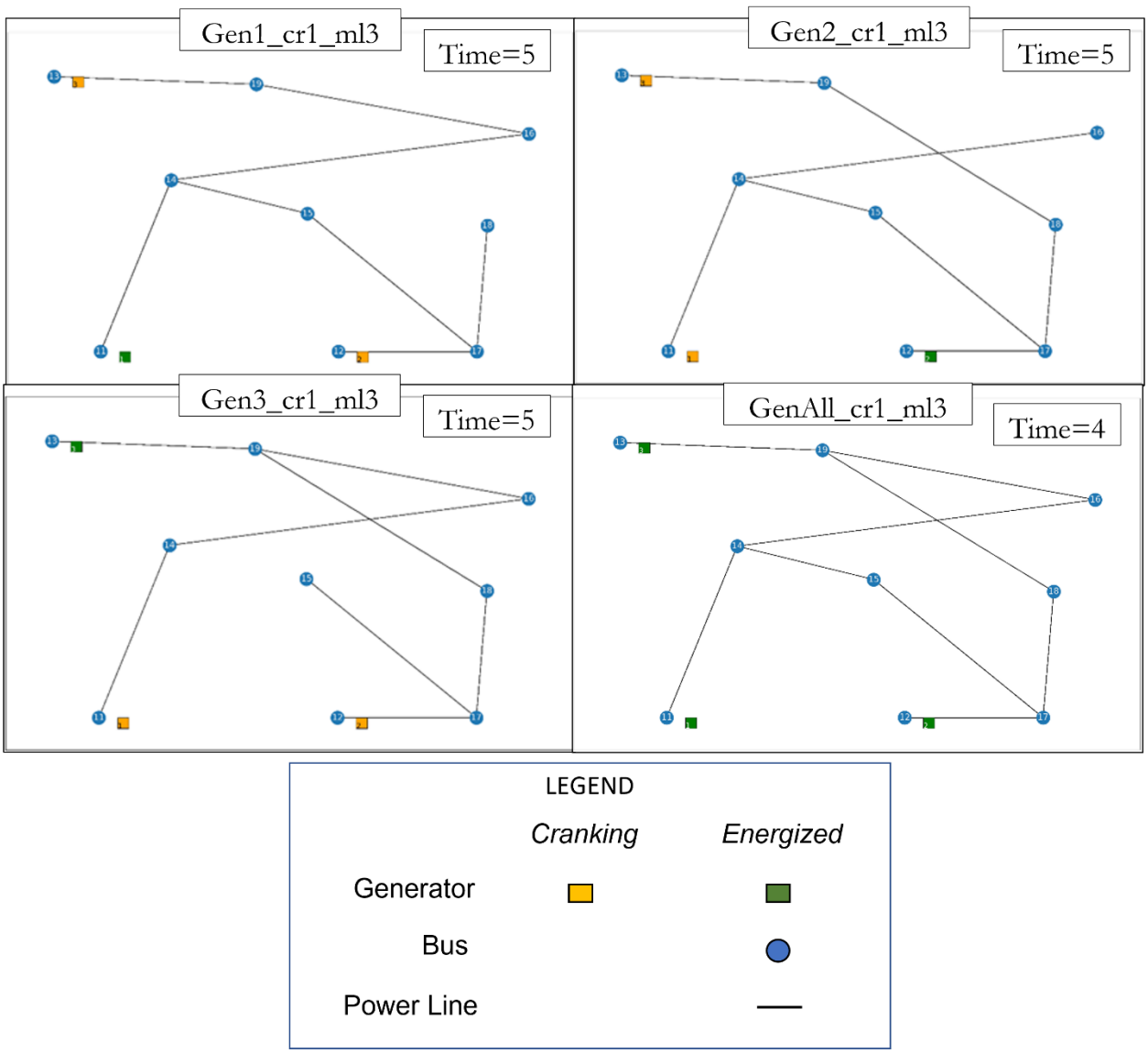

Figure 8. Systems under restoration for tests with the earliest time until total restored load

Furthermore, there exists a tradeoff between maximally restoring the network and minimizing restoration time for loads, as illustrated by the results in Table 4 and Figure 7. Results for tests where *ml* = 1 show tests with a single black start generator restored the system by the same time period as tests with all black start generators (except for test Gen3_cr3_ml1). However, the tests with all black start generators reported a better objective function value. Examining the restorations within a *ml* grouping within Table 4, the resultant restorations are essentially lumped by cranking time *cr*. Those with a *cr* = 1 are completed before those with a *cr* = 3. The *ml* = 1 cases create a significantly broader set of what appears to be "dead time" in the restoration; that is, time where we're not bringing another generator on, but doing the necessary line work necessary to enable such an excitation. In the *ml* = 3 cases, the ability to do more work simultaneously on the system reduces the effect of the *ml* constraint and increases the significance of the *ct* constraint. This also creates value in having choice among generators, as seen in the genAll_cr*_ml3 cases relative to the individual generators in the rest of the *ml* = 3 cases.

4.1.2. Network Dynamic Model Results Summary

NDM was used to define the system's response during restoration, as indicated in Figure 1. Goal-seeking dynamics added to NDM to model generator frequency stabilization are prone to instabilities. After some experimentation with the time constant parameter controlling this process, most optimal restoration schedule could be implemented successfully. Figure 9 shows an example of the state variables (analogous to frequency) of the three generators in the system during restoration using the Gen1_cr3_ml3 script. Generator activation and connection induces oscillatory dynamics which tend to decrease in frequency and amplitude, effectively disappearing after some time.

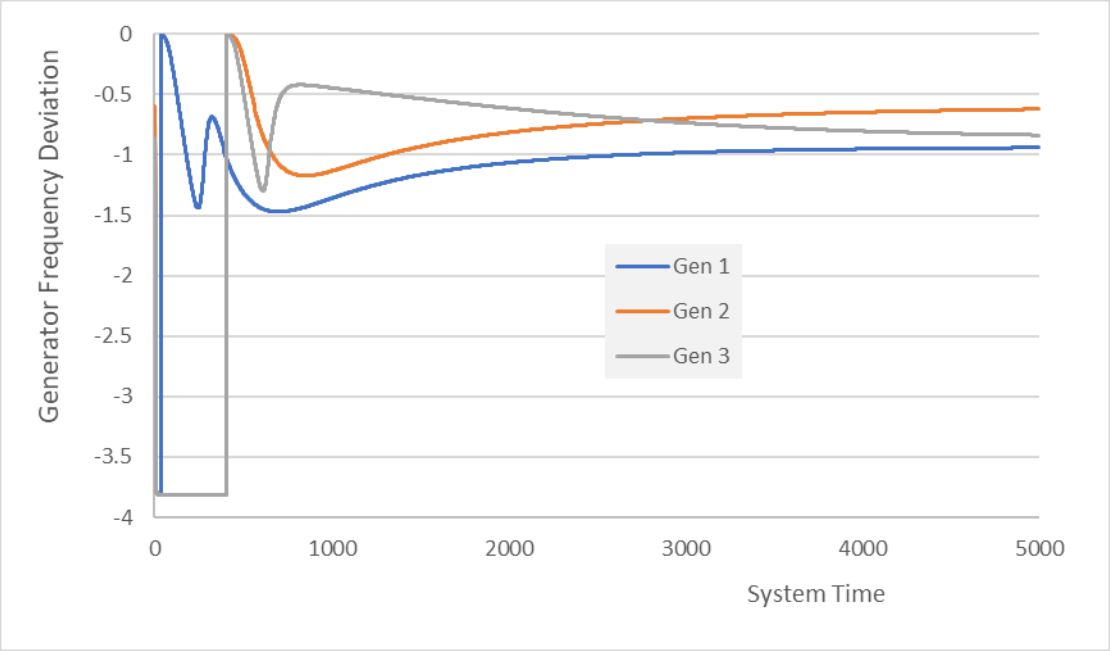

Figure 9. Frequency deviations of the three generators in the nine-bus system during restoration using script Gen1_cr3_ml3

However, the restoration process occasionally produces instabilities in the system, eventually leading to divergence. The potential for problematic system behavior during restoration is desirable in general because the overall simulation framework is intended to assess the robustness of the entire restoration process, which is an interaction between the plan, the operator, and the actual system. Real power systems deviate from expected response, and so the system simulation used in this context should has well. However, the connection between the specific sensitivities and contingencies seen in the adapted NDM and those seen in actual systems has yet to be explored. Real systems include protective mechanisms and controls that were not included in the extended NDM model, and which might dampen or eliminate excursions seen in the current model.

4.1.3. Operator Cognitive Model Results Summary

A variety of tests were simulated in the OCM. The OCM has shown success in being able to integrate the systems and identify faults within schedule plans. It can step through the plan, implementing each stage in the appropriate order while monitoring the system before continuing, the last step of which has been critical to both correctly timing the restoration activities and identifying faults where the system is unable to continue. For instance, when attempting to connect

a previously cranked generator the operator first performs a simple monitoring activity where they observe the distance between the unconnected generator frequency and the system frequency, and only connect a generator that closely matches the system. This can occasionally result in further delays on the restoration task, as the operator may have to wait for the given generator to settle out before it is ready to be connected. Similarly, the operator monitors the state of the system at the end of each stage, ensuring stability in the system before moving on to the next stage of the restoration plan.

Both of these activities not only provide insight into how the restoration plan may take shape on a real system, but also identifies flaws in incomplete schedules that prevent the system from being fully restored such as when the monitored values diverge or freeze, and the system becomes unresponsive. While a more direct approach at implementing these plans would continue implementation regardless of how the system responds, the OCM represents an adaptive element that works with the simulations and is able to raise flags, or halt the restoration, when the system response diverges from the expectation. This is a behavior we have seen in multiple cases of the RTS-96 system, where upon being given incomplete schedules or having a system with issues not covered in the restoration plan, the operator model is able to step through the plan and identify the point at which the system stops responding as expected, acting as a sort of adaptive troubleshooter in addition to its responsibilities in implementing the restoration and providing further insight into the feasibility of restoration plans.

Additionally, the OCM provides insight into the real-world timing that would be associated with each step of the plan. Even without the above adaptive properties, the OCM allows for the measurement of time within a given stage, as they are not all equal in work required. Many of the early stages require only cranking a handful of generators, a relatively quick task, while later stages require combination of cranking and connecting generators, as well as handling lines and loads elsewhere in the system. Furthermore, the OCM informs on timing for restoration steps not outlined in the original schedule that are purely a result of the system response. Time taken waiting for the system or generators to stabilize, and for the operator to be able to recognize the stability and implement connections, is produced by the model despite not being steps included in a raw restoration schedule in the first place. Finally, the need to serially perform tasks (since our implementation of the OCM uses only a single operator) adds significant time to the restoration, as that individual needs to orient themselves and accurately perform each subtask required within a given stage.

Specifically, the time added by the operator can be conceptualized by a breakdown of their action flow and the timing that requires of them. The operator has mild variation in decision and reaction time, but each discrete action they take has a reasonably consistent amount of time that it consumes (this time includes the decision-making process, the reading and processing of information, and any actual actions that need to take place). The variations combined with the sensitivity of the underlying system can make the total time to recovery vary from implementation to implementation, but by understanding the component actions it is easier to conceptualize the time taken for each stage and eventually the full recovery process. To this end, we break down the action flow and timing information for each of these smaller actions, then combine them and observe the macro effects for recovery across different schedules. A detailed description of the process is found in Section 3.3.

For each stage, the operator goes through a hierarchy of actions needed: first, they deal with generators that need cranked, then they look for previously cranked generators that need to be connected, then they work on energizing lines, then buses, then finally they do a stability check of the system before moving to the next stage.

By following these processes from action to action, it is apparent that the operator slows system restoration repeatedly, both simply by the constraints of what it is possible for the operator to accomplish as well as by the feedback of the system and whether it is ready. Since stages have varying amounts of activities to accomplish, there is no single descriptive average for any given stage, however a descriptive stage that has for instance a single generator to crank, two to connect, as well as two lines and two buses would take approximately 170 seconds, or just under three minutes to implement if there is no instability to wait for. More commonly, there are at least a few waiting periods for things to settle in making an average stage take around five minutes if it contains actions needed by the operator.

More specifically, we can observe the combined effects of these action times by studying the timeline of actions shown in Figure 10, Figure 11, and Figure 12 where we show the full recovery schedules for multiple combinations of black start generators, maximum lines per stage, and generator cranking time. Figure 10 and Figure 11 show the cases where a single generator (1 and 2 respectively) is used for the black start generators, while Figure 12 shows the case where all three generators are used for the black start. We include each combination of one or three maximum lines and one or three cranking time steps per generator for each group, to show how the different schedules are implemented in context of system stability and operator capability. These results present differences from the strict optimization model, as the optimization model considers each time period to be equal when determining the earliest possible recovery, but as can be seen in Figure 10, Figure 11, and Figure 12 this is far from the case when implemented by the operator. The variation in time to recovery is driven largely by waiting for stability when first connecting generators, then buses. This presents as decreased recovery times, even within the same number of time periods, when tasks that can be parallelized are implemented as such.

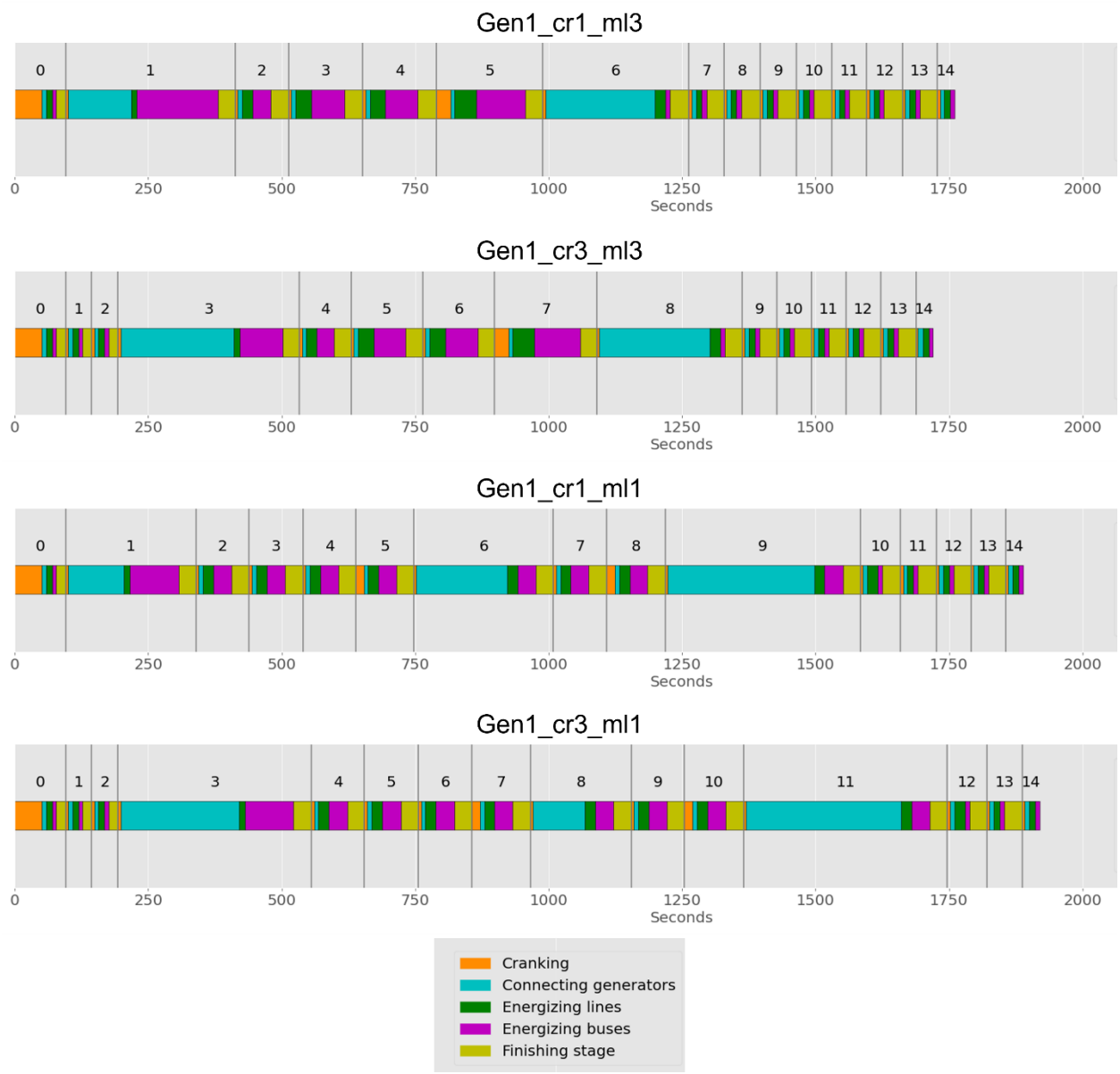

Figure 10. Timeline of operator actions for schedules based on various optimization constraints when Generator 1 is used for the black start generator, with time periods marked above each section and total time (in seconds) marked at the bottom

As can be seen, utilizing a single generator for black start presents similar restoration times for most of the other variables, but there are slight differences. When generator 1 is the black start generator, as in Figure 10, the system recovers fastest with three lines energized per step and slows down when this is constrained. This is largely due to the optimal schedules spreading the generator crank time periods out when the lines are constrained, while with three connections per time period the non-black start generators are allowed to crank simultaneously. The non-parallel cranking leads to the longest overall restoration times observed, extending to past 1900 seconds to complete the full 14 time periods and having the slowest final connection action of all as well at 1750 seconds. In general, with generator 1 as the black start generator, the fastest time to final connection of 1250 seconds corresponds with the case of higher number of line connections per time period (3) and lower

cranking times (1). Increasing the crank time has a moderate negative effect on the recovery time and constraining the links further degrades the ability to restore quickly.

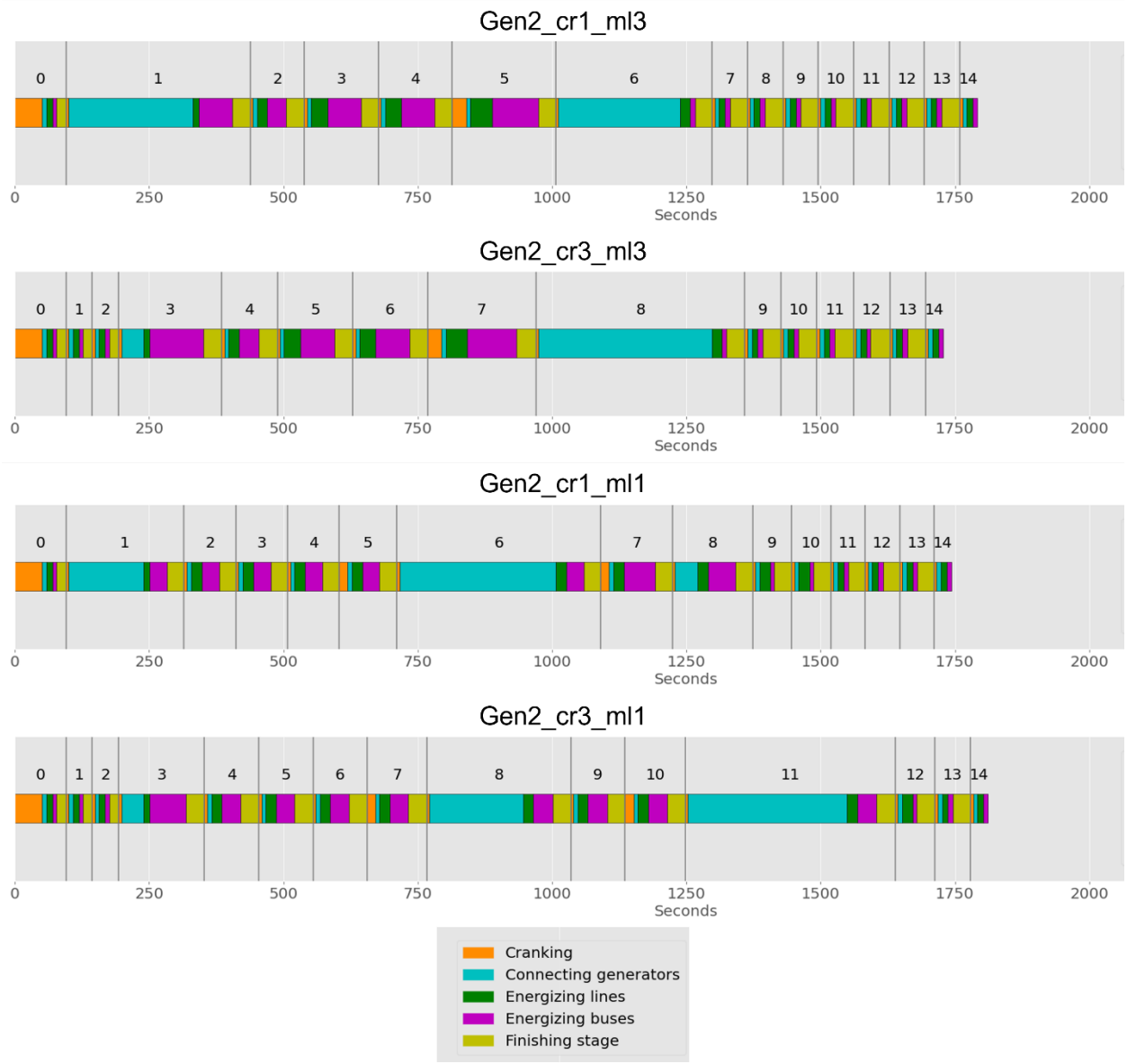

Figure 11. Timeline of operator actions for schedules based on various optimization constraints when Generator 2 is used for the black start generator, with time periods marked above each section and total time (in seconds) marked at the bottom

Utilizing generator 2 as the black start generator, as in the case in Figure 11, however, levels these times out somewhat. The same difference in schedules can be observed, where allowing a higher maximum line connections per time step leads to a schedule with generators cranked simultaneously rather than separately, but this is mitigated by this system showing greater stability and generator convergence in general. In application, generator two stabilizes and is ready to connect faster than generator one did, and the distribution of load connections allows for better system stability on the tail end of the restoration as well. Together, these shortened wait times for connection make up some of the difference in lack of parallelization and lead the system to complete all fourteen time

periods in 1700-1800 seconds with final connection times between 1300-1350 seconds. The exception to this is the case with constrained lines and long crank times, which while comparable in time to complete 14 time periods, takes a much longer 1600 seconds to final connection. In general, many of the trends seen in the generator 1 black start case hold, but the generator 2 results compress the timelines somewhat with more robust generator stability.

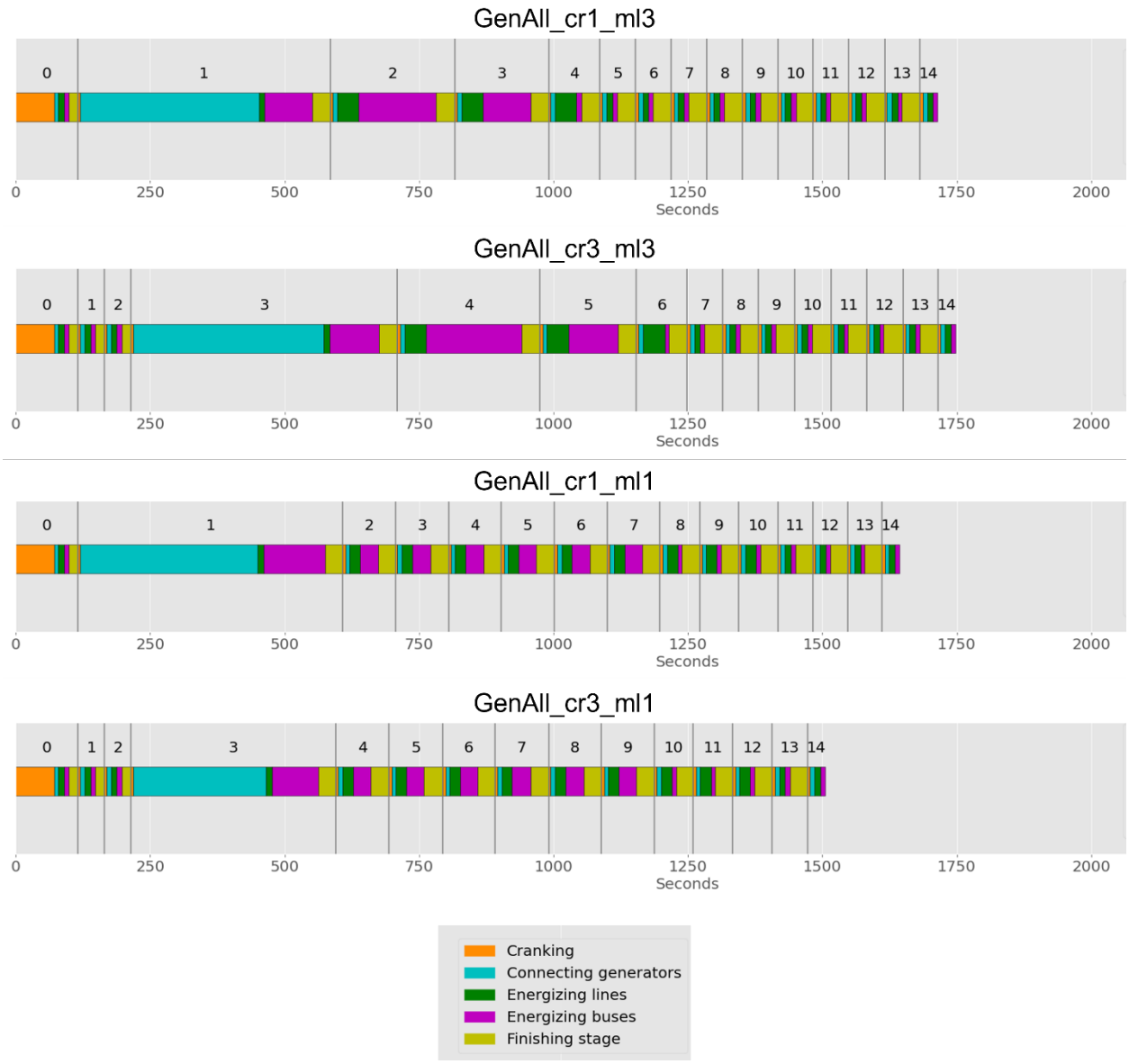

Figure 12. Timeline of operator actions for schedules based on various optimization constraints when all three generators are used for the black start generators, with time periods marked above each section and total time (in seconds) marked at the bottom

Finally, echoing the results from Section 4.1.1, utilizing all three generators as black start generators (as in Figure 12) provides the earliest possible recovery times. Utilizing all three generators as black start generators allows them to all crank at the start of the recovery process and stabilize simultaneously, where other formulations with generators cranked later often have extended wait periods in later time steps as the newly cranked generators settle into the appropriate frequency to

be connected. Similarly, increasing crank times before connection gives the generators more time to settle into their proper modes before the connection attempt is made, and thus less waiting time is incumbent on the operator who must wait for them to reach appropriate frequency even if the schedule calls for an earlier connection. The end result is a similar amount of time before the connection can feasibly be made, whether the connection is called for in time period 1 (for the crank time 1 scenario) or time period 4 (for the crank time 3 scenario).

After generator connection stability, the second biggest waiting period is the wait for stability in the connected system whenever a new bus is energized which is tied to the number of lines energized in a time period. These effects can be seen clearly in Figure 12, where the schedules with more lines connected per time period have extended bus connection times to account for stability checking. This is an interesting problem because while increasing the number of lines per stage allows for multiple bus connections within a time period and thus shortens the number of time periods needed for full recovery, it also has the problem of de-stabilizing the system by rapidly requesting bus connections and thus extending the system stability checks after each one. Additionally, even when the attached loads do not create instability, the operator must do a check for stability after each one so despite being in the same time period they are not able to be fully parallelized for the waiting period. Thus, while the optimizer shows the case of ml = 3 to be by far the most rapid recovery, this is less clear cut with the operator model in the loop. That schedule finishes its last step of the 14-stage process in approximately 1750 seconds, an average time, but completes its final connection action at around 1100 seconds, which is the fastest time shown. However, when *ml* is constrained, the final connection action happens similarly at around 1175 seconds, and the full 14-stage process can finish much faster at only around 1500 seconds for the case of three cranking time steps per generator. Of course, these differences are only a matter of minutes in this small system example, but on a larger system could represent a much more severe difference in restoration times. As such, the faster method identified as best by the optimizer may still represent a significant improvement over the others, however the unpredictability of the timescale of the stability checks and more aggressive nature of this schedule could represent issues when scaled up. Additionally, despite the final connections still coming in slightly slower, the more conservative schedules represent a significantly more competitive recovery time than the optimization time periods would indicate.

4.2. Validation of the Framework on the WSCC 9-Bus System

The performance of the restoration schedule from test Gen1_cr3_ml3 of the WSCC 9-bus System was tested in the General Electric (GE) Positive Sequence Load Flow (PSLF) software [32]. GE PSLF is a commercial dynamic power system simulator designed for utility use. The software was selected for its ability to simulate the dynamics from a restoration schedule (i) at each time period until load is restored (Section 4.2.1) and (ii) dynamically across all time periods (Section 4.2.2).

4.2.1. Base Case

The base case is modelled to be a blackout. All generators and load in the power system are offline, i.e., total generation is 0 MW and total load connected is 0 MW. All transformers and transmission lines are disconnected.

The restoration schedule can be divided into five different time periods, described here.

4.2.1.1. Time Period 1 (black start)

The following actions are taken to black start the system:

- Bus 1 is set as the slack/swing bus.
- Generator 1 is brought online. It is connected to Bus 1.
- Generator 1 power is set to 0 MW
- Transformer 1, connected to Generator 1, is also brought online

Figure 13 shows the one-line diagram of part of the system at black start.

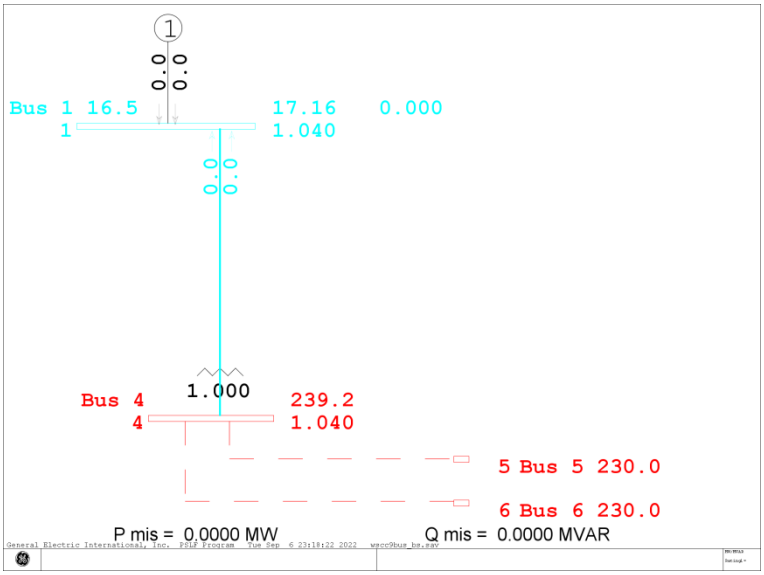

Figure 13. One-Line diagram showing the power flow after the end of Phase 1

4.2.1.2. Time Period 2

In this time period, the system achieves a complete circuit for the first time. Power generation begins and loads are brought online. Generator 1 supplies power to 42% of Load 1 in Bus 5. The power flow is solved, and a solution is reached. Figure 14 shows the one-line diagram of the solved power flow. The load is connected to Bus 5.

The summary of actions in this time period are as follows:

- Generator 1 begins to supply 72 MW
- 58% of Load 1 (connected to Bus 5) is brought online – 72 MW:
- Line 1 and Line 2 connected to Bus 4 are brought online.

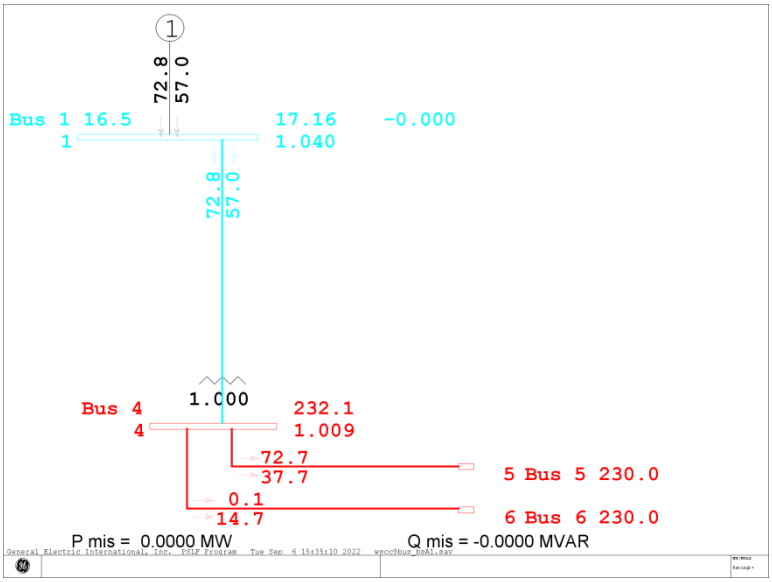

Figure 14. One-Line diagram showing the power flow after the end of Phase 2

4.2.1.3. Time Period 3

In time period 3, two more transmission lines are brought online, as Line 3 and Line 6 are energized. No changes to generation or load are made, over those seen in time period 2.

4.2.1.4. Time Period 4

In this time period, Generator 2 is brought online and Load 1 is dropped to 36%. However, Load 2 (connected to Bus 6) and Load 3 (connected to Bus 8) is brought online. Generator 2 generates 163 MW for this phase and Load 2 consumes 90 MW. At the end of this phase, all the branches (i.e. the three transformers and all six transmission lines) are all online and the total generation in the system is 235 MW and the total load connected is 135 MW. Figure 15 shows the one-line diagram of the system after a solved power flow at the end of time period 3. The summary of action in this time period is as follows:

- Generator 2 is brought online and supplies 163 MW
- Transformer 2 connected to Generator 2 is also brought online.
- Load 1 is shed from 58% to 36 %. Load 1 now consumes only 45 MW.
- Load 2 and Load 3, connected to Bus 6 and Bus 8 respectively are brought online.
- Line 4 and Line 5 are brought online.

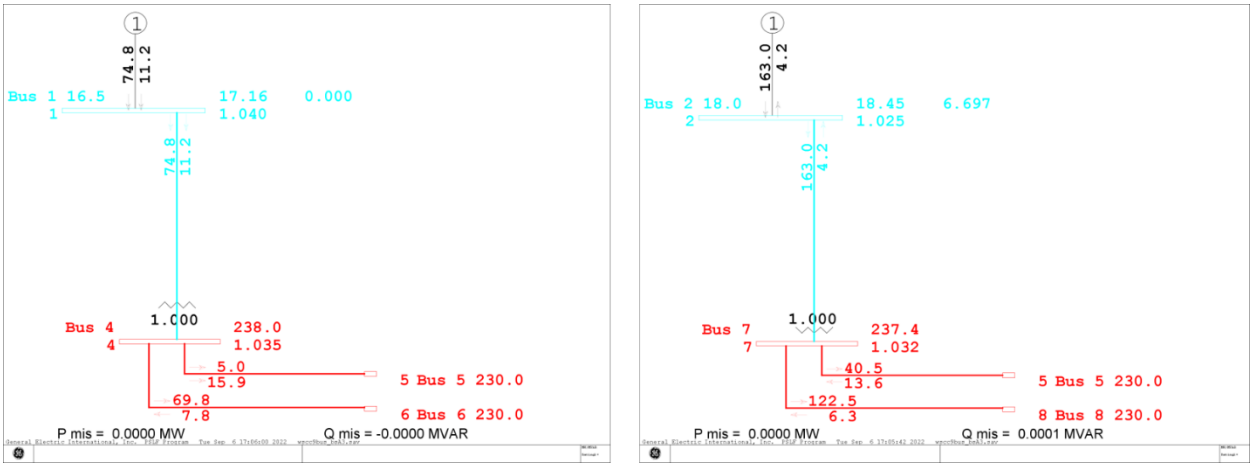

Figure 15. One-Line diagram showing the power flow after the end of Phase 4

4.2.1.5. Time Period 5

In this time period, Generator 3 is brought online to supply 85 MW, the output power from Generator 2 is dropped to 158 MW. The total generation at the end of this Phase is 315 MW. 100% of all loads are brought online. Figure 16 shows the one-line diagram and the power flow solution of system. The summary of the actions in this time period are as follows:

- Generator 2 Output is dropped to 158 MW.
- Generator 3 is brought online to supply 85 MW.
- The transformer connected to Generator 3 is brought online.
- 100 % of Load 1 is brought online.

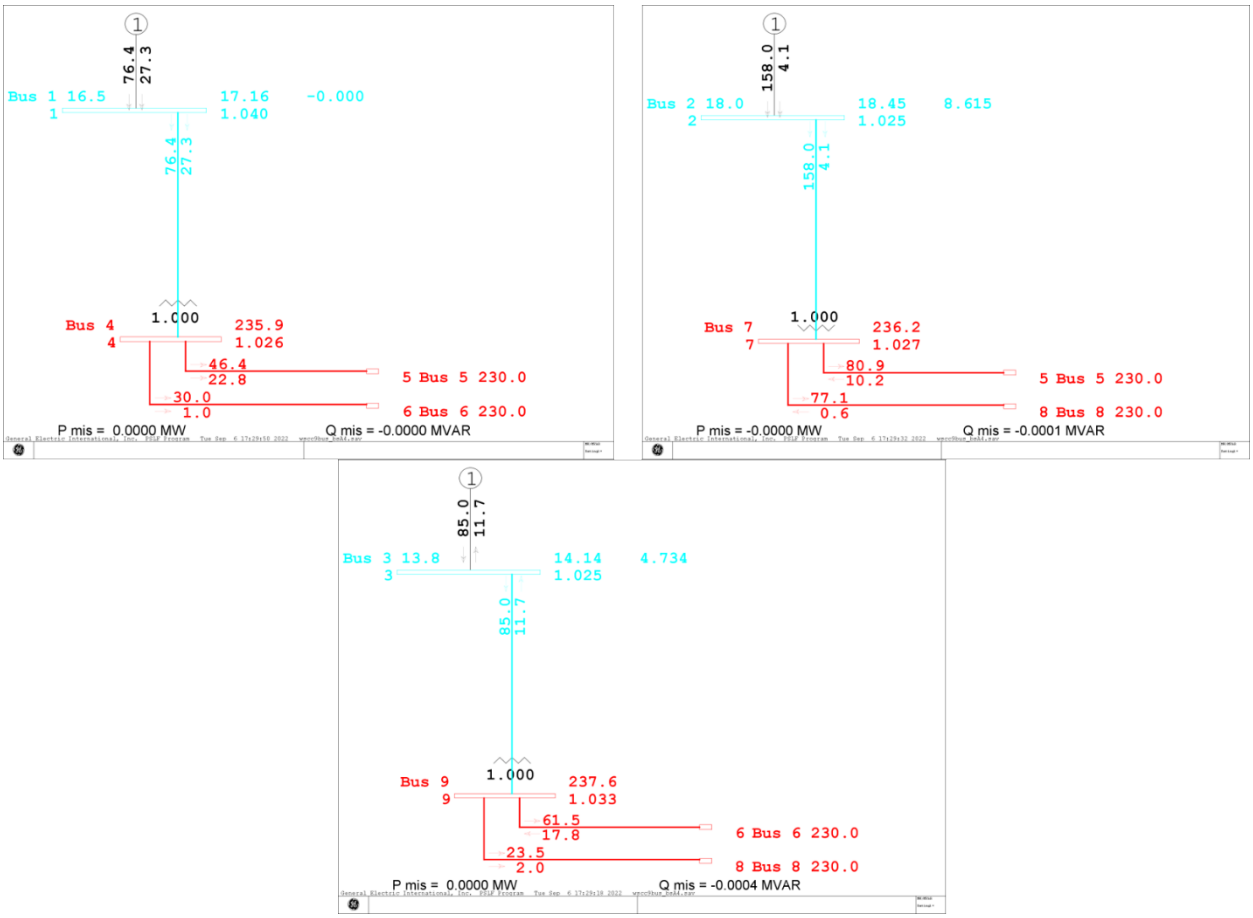

Figure 16. One-Line diagram showing the power flow after the end of Phase 5

4.2.2. Dynamic Analysis

The dynamic performance assessment underpins the design and operation of power systems. System conditions needs to be investigated to ensure adequate system behavior. For example, ensuring that stability is maintained. The proposed restoration schedule for the WSCC power system is modelled in the GE PSLF software. Each generator is modelled as a classical synchronous machine and equipped with an exciter, turbine, and governor model. Table 5 shows the details of the dynamic model parameters used for all three generators in the dynamic simulation of the WSCC system.

Table 5. Dynamic model parameters

Generator Parameter	Value		Turbine/Governor Parameter	Value		Exciter Parameter	Value
Inertia Constant (H)	3.0		Permanent droop (R)	0.05		Gain reduction ratio	0.1
Damping factor (D)	0.0		Steam bowl time constant (T1)	0.5		Gain	100
Stator resistant (Ra)	0.0		Maximum Valve Position (Vmax)	1.0		Minimum field voltage output (Emin)	-5.0
Sub transient Reactance (Lppd)	0.2		Minimum Valve Position (Vmin)	0.0		Maximum field voltage output (Emax)	5.0
			Turbine Damping coefficient (Dt)	20		Field voltage clipping limit (Efdmin)	-5.0
						Field voltage clipping limit (Efdmax)	5.0

The dynamic simulation for the system restoration is run for 300 seconds, i.e., 60 seconds each for all five time periods described above. Figure 17 shows the electric power output from the generators during the dynamic simulation. The output electrical power of the generators at each time period is approximately equal to the expected electrical power from the steady-state power flow solution. At the beginning of time period 3 and time period 5, i.e., at time = 180 and at time = 240, when Generator 2 and Generator 3 are brought online, the output electrical power of the generators oscillates. This oscillation dampens quickly within few seconds depending on the selected turbine/governor dynamics parameters.

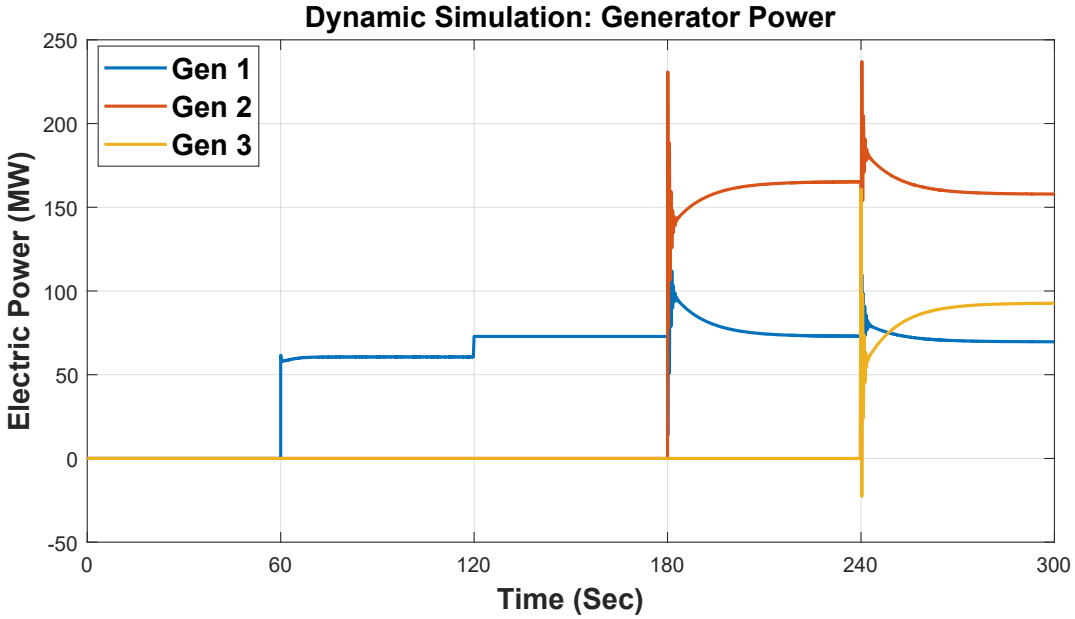

Figure 17. Electric power from all three generators across all phases

Figure 18 shows the plot of each generator speed. All three generators have an initial speed of 1 per unit. To run a dynamic power system simulation on the GE PSLF software, it is required to initialize

all dynamic models (in this case, the generator, turbine/governor and exciter models) at the start of the simulation. Hence, the initial speed of all generators is set to 1 per unit at the beginning of the simulation. This implies that each generator is running at 60 Hz before it is connected to the system. As shown in Figure 18, there is a variation in the speed at each phase transition points. However, throughout the simulation transient stability is maintained.

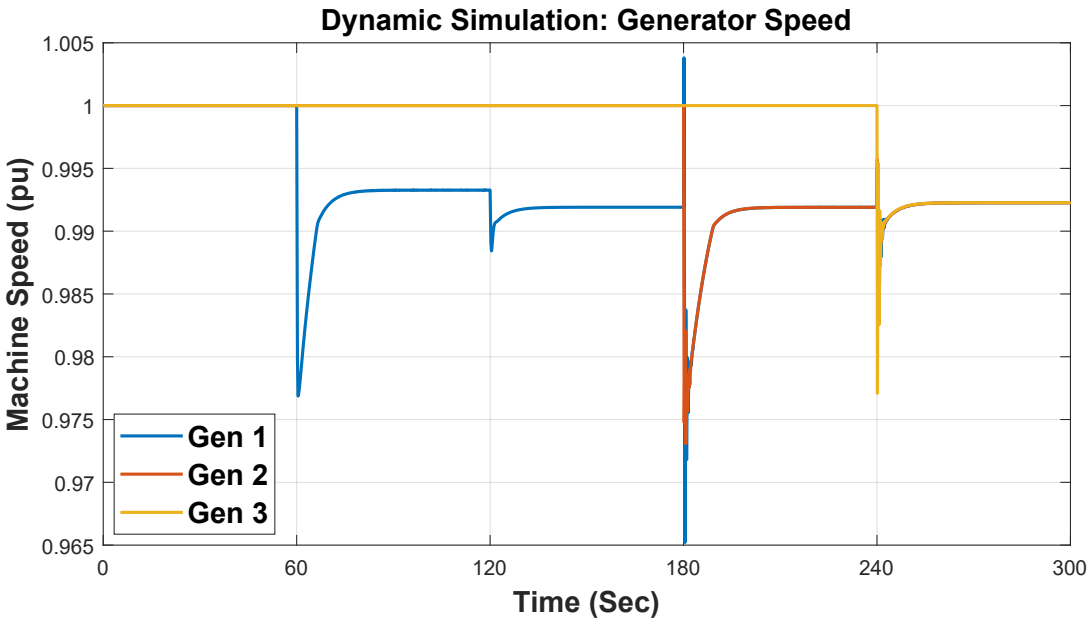

Figure 18. Generator speed across all phases

Figure 19 shows the plot of each generator bus voltage. There is a voltage violation in phase 2 (time = 60 to 120 sec) when Generator 1 begins to supply power. This is most likely due to the lack of reactive power injection into the system.

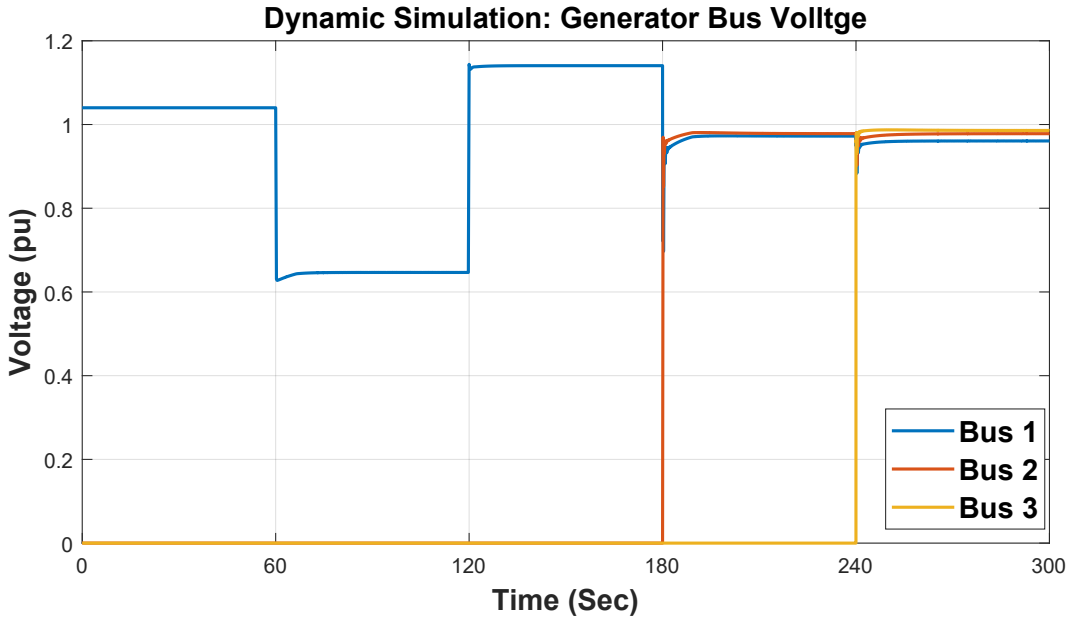

Figure 19. Generator bus voltage across all phases

The results in this section illustrate how, at each time period and across all time periods, the restoration model produced a schedule that was validated by a commercial dynamic power system simulator. In the GE PSLF case, a total of five time periods are taken to resolve the system from black start; each time period has the potential to connect more than one transmission line, and to address other tasks as necessary (so $ml > 1$). Generator 1 serves as the black start unit in this case, and in each case, generators are able to connect and satisfy load in the step after their activation (so $cr = 1$). Thus, best comparison can be made against the Gen1_cr1_ml3 case, which also presented a solution in five time periods in the optimal restoration model. It is worth noting that, with the constraints of the operator considered, this scenario does not see its' last generator energization until time period 6, suggesting that there is difference between the computationally optimal and that which can be practically executed.

The use of a commercial simulator to test this purpose is novel. Many such software packages cannot inherently simulate a power system in extreme edge cases, such as during restoration. Therefore, with additional testing and future development, the restoration model may one day be able to provide key insight to utility decision-makers who are concerned with black starting their systems. It is worth noting that translation of the restoration plan, the family of which are described in Section 4.1.1, through the OCM and NDM (in Sections 4.1.3 and 4.1.2 respectively) includes temporal delays from operator implementation and observation of system stability conditions in the NDM, the latter of which mirrors the generator and governor regulation seen in the dynamic validation of this section.

4.3. Case Study: Application of the Technique to the IEEE RTS-96 System

One test of the RTS-96 system was conducted to perform a computational "stress test" of all capabilities developed during this effort. The IEEE Reliability Test System (RTS-96) [8] [34] is a substantially larger test system than the WSCC 9-Bus system. It is comprised of three regions, each comparable to an independent utility system (or portion of a utility's system). Each of these regions is similar, with slight differences in the number of buses and lines. This system was chosen to exploit the structure of the Feasibility Oracle, which is rooted in the formation of islands as it determines the best restoration schedule. Details of the system used are printed in Appendix A.2.

Region A features 24 buses (13 of these are load buses, 10 are generator buses, and one is a swing bus with generation and load). A total of 33 generation units at the 11 generation sites have a cumulative real power capacity of 2999.3 MW. The cumulative MW load in Region A is 2850 MW. Within Region A, a total of 38 branches (lines) connect the buses. Three branches provide interconnection to Region B, while one branch provides interconnection to Region C.

Region B is similar to Region A, with 24 buses (14 of these are load buses, 11 are generator buses), 33 generators at 11 sites with a cumulative real power capacity of 2999.3 MW, cumulative MW load of 2850 MW, and a total of 38 branches connecting the buses the buses within the region. An additional branch provides interconnection to Region C.

In turn, Region C contains 25 buses (14 of these are load buses, 11 are generator buses), 33 generators at 11 sites with a cumulative real power capacity of 2999.3 MW, cumulative MW load of 2850 MW, and a total of 39 branches connecting the buses the buses within the region.

The size of the RTS-96 system allows for substantial islanding in comparison to the WECC 9-bus system, at the Region level, as well as within each of the regions, making black start restoration solution a more complicated problem.

4.3.1. Restoration Optimization Model Results Summary

Table 6 displays the input parameters used for the test of the RTS-96 system. Due to long runtimes, the test was solved until a 10% optimality gap was obtained. We work to an optimality gap rather than to optimal because, as we have discovered through this work, each of the constructs presents some degree of relaxation relative to the true optimal. A DCOPF works, as discussed in Section 2.1.1.2.1, without constraints tied to voltage angle differences and reactive power. The MCM of Aravena et al [10] follows the academic literature, and "assume[s] that dynamic phenomena and limits below the temporal resolution of our model (15 minutes to 1 hour), including ramp rate limits, electro-mechanic and electromagnetic transients, have a neglectable effect in constraining the restoration plan," thus reducing the ability of an AC approximation to factor in those transients (and the time window in which they typically occur, well under 15 minutes) to a computational solution. For this case, (a 10% optimality gap on the RTS-96 system leveraging complete RTS-96 data used for this test, found in Appendix A.2, and a DCOPF, an objective function value of 13603 is found, with a run time of 663,337 seconds. Additional details, along with snapshots of the result sequence, can be found in Appendix A.1.

Table 6. Input parameters for the test of the RTS-96 system

Parameter	Value
Number of black start generators	3
Black start Generator ID's	1, 20, 51
Number of branches restorable per time period	3
Cranking Time of Black start Generators	Gen 1: 2 time periods Gen 2: 3 time periods Gen 3: 4 time periods
Cranking Time of Non-Black start Generators	1 time period

Figure 20 shows the total load was restored by time 50 for the RTS-96 test. Figures of the restoration schedule at time = 0, 5, 42, and 55 are displayed in Appendix A.1. Figures for time = 0 and time = 5 illustrate how the islands were formed. The figure for time = 42 illustrates the time periods when all generators were restored. The system was fully restored by time = 55.

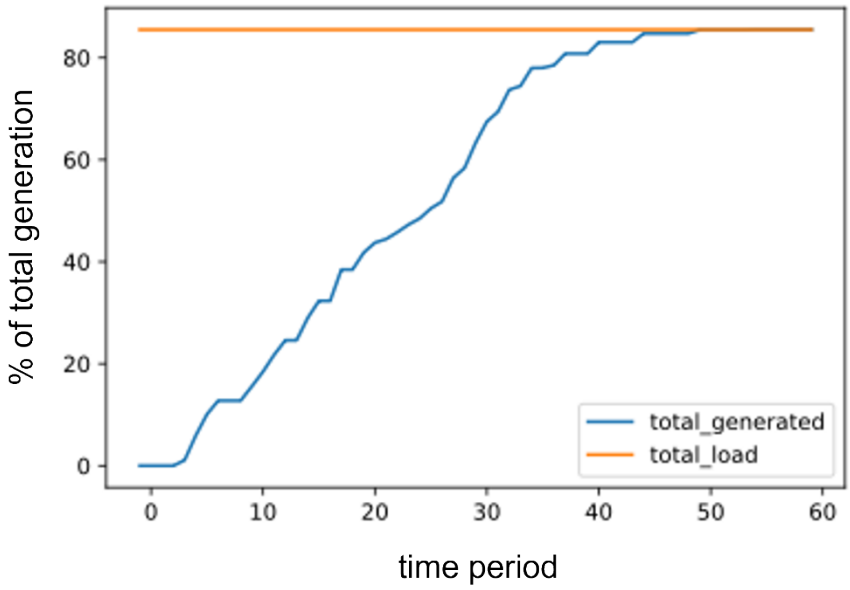

Figure 20. Time until total load is restored for the RTS-96 test

4.3.2. Network Dynamic Model Results Summary

As in the 9-bus system, recovery simulation sometimes produced instabilities and divergence rather than a successful system restart. Stable recoveries, such as that illustrated below in Figure 21 with the frequency deviations of five generators activated at different points in the schedule, exhibit oscillation around the nominal operating state followed by frequency stabilization.

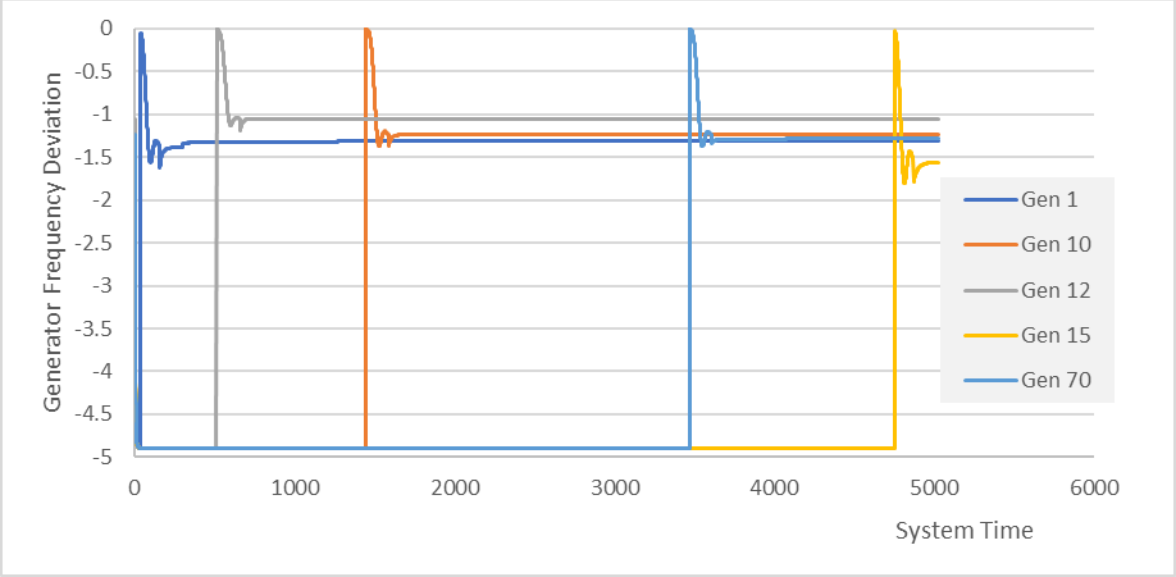

Figure 21. State of five generators brought on at different times during the simulated restoration of the RTS-96 system

This stable state is perturbed in the course of restoration as lines are closed, loads brought on, and other generation assets added. Figure 22 shows a detail from Figure 21 in which the state of the first

connected generator is displaced when it is connected to the grid, recovering quickly to its nominal state.

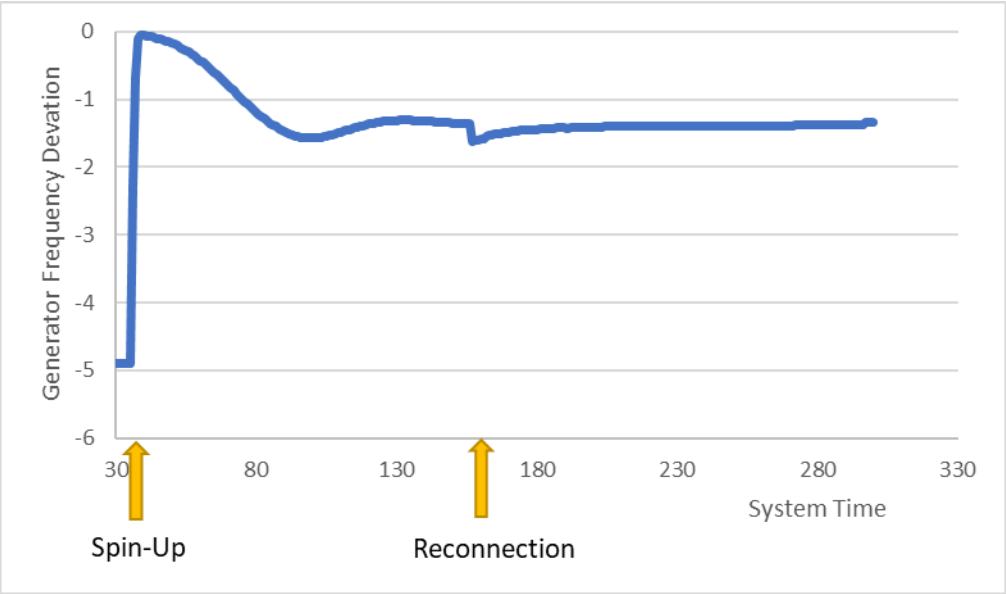

Figure 22. State of generator Gen 1: Detail of initial startup and reconnection transients

Such stable behavior is not guaranteed. As discussed above with respect to the simpler 9-bus system, the ground-truth simulator should be able to produce the kinds of instabilities and contingencies seen in real systems, in order to present effective challenges to the operator. However, it must be left for future work to establish the correspondence between the modes of instability seen in real systems and those produced in the ground-truth simulator. Furthermore, the plug-and-play nature of the modeling framework creates opportunity to replace the NDM with another representation of the system, or, if attached to a system, with actual system data to reflect systemic response. These may prove to be more efficient solutions.

4.3.3. Operator Cognitive Model Results Summary

Due to instabilities in the schedule and underlying system, the operator model was unable to complete a full restoration of the RTS-96 system, noting freezes in generator frequency in around the eighth time period of the system. This detection, however, did demonstrate the model's ability to identify system outputs that did not respond as expected indicating the fledgling utility of such a model in the space of unknown system malfunctions or in the presence of adversarial information manipulation. Additionally, through that point in the system the operator model shows a similar decoupling of optimization time period to system time, demonstrating that optimization time periods that require more actions (particularly those that trigger stability checks before moving on) represent significant increases in implementation time. As such, the results indicate that an optimal model may be tied less to minimum restoration time period and more to a balanced load of actions per timestep to leverage as much parallel action as possible for a single operator. Full implementation of the operator model on a stable larger system such as this is left to future work for testing of the scalability of conclusions from the 9-bus system detailed above.

4.4. Summary of Results

Restoration model results indicated how the choice of black start generator is significant when maximal restoration of components is the objective. Constraining the number of restorable lines impacts the time until a network is restored provided evidence for the concept that real-world factors can cause significant delays during restoration of real power networks. Equity concerns or other issues could arise if the sequence of restored components were to prioritize certain loads. Results from the restoration model tests on the WSCC 9-Bus System indicated the importance of the number of restorable lines per time period, *ml*. Additionally, it was shown that black start generator cranking time *cr* was more impactful when the value of *ml* was lower in creating discernment among similar cases. Finally, the value in having choice among generators, as seen in the genAll_cr*_ml3 cases relative to the individual generators in the rest of the *ml* = 3 cases, was also shown. Thus, there exists a tradeoff between maximally restoring the network and minimizing restoration time for total load.

A restoration schedule for the WSCC 9-Bus System was successfully validated using a commercial dynamic power system simulator. This topic could be explored more in future efforts, which would open the possibility of applying this work at an electric utility and expanded to incorporate other processes for further synchronization among capabilities and incorporation of other capabilities (e.g., Markov processes, Machine Learning) for capturing elements of the overall restoration process that can be leveraged in conjunction with restoration schedule developing software to expedite restoration.

The goal-seeking dynamics added to NDM to model generator frequency stabilization proved to be prone to instabilities. After some experimentation with the time constant parameter controlling this process, the optimal restoration schedule could be implemented successfully for the 9-bus system. Stable behavior is not guaranteed. Recovery simulation often produced instabilities and divergence rather than a successful system restart in the RTS-96. While such instabilities and contingencies seen in real systems are of value for establishing a need to reassess the restoration schedule, the NDM could not reliably producing the kinds of stable results in larger systems like the RTS-96 necessary to reinforce the operator. The plug-and-play nature of the modeling framework creates opportunity to replace the NDM with another representation of the system, or, if attached to a system, with actual system data to reflect systemic response.

The operator model implementation of the optimized schedules highlighted the decoupling of the restoration time periods from the ground truth system time, showing that schedules that took double the time periods to complete could still finish full restoration in a similar amount of system time. This is due to the inequity of the time periods in terms of work required of the operator, and the amount of stability wait time required to complete overloaded time periods. Still, as noted above, while the overall restoration time is similar, the higher time period schedules require the slower connection of buses. This allows some to get energized faster than they otherwise would, while others are slower and could lead to inequities based on load prioritization. On the other hand, parallelization of other activities such as generator cranking represented a straightforward gain for the operator as it could be done early on and lower the operator's need for separate wait times later in the schedules. We envision that a context-aware operator in the loop optimization would enable the identification of the sorts of actions that could be appropriately parallelized and those that would cause undue stress or instability on the system on which operators must wait. A good first step to this might be including average system time costs to the optimization framework such that information regarding workload per time period could be properly constrained and accounted for.

5. IMPACTS

This section outlines the impact of this research, in the form of papers and presentations made (both internally and externally), interactions with external entities to support the work, and proposals generated for future efforts leveraging this work.

5.1. Presentations and Papers

Multiple presentations have been made, and a paper published on this work. Presentations include internal and external presentations and poster sessions, on the work as a whole, as well as on components of the work. These include the following external papers and presentations:

- Two presentations were made at the 4th IEEE Systems Modelling Conference [15][16]. The first of these focused on modeling of operator behavior, with the second focused on the NDM and its application to the problem space of black start restoration.
- A paper [62] and presentation [63] were made at MODSIM World 2022. These provided an overview of the project, with summary of the analytic process.

In addition, a paper leveraging the CogTasks hierarchical tasking library to implement troubleshooting and monitoring tasks for the recovery of a complex system (e.g., the electric grid) is proposed for the Time Out of Action modeling effort. This will be submitted at the end of the calendar year to a cognitive science or computer science journal as an application of our ACT-R extension library. Additionally, a joint paper with the Dynamics-Informed Optimization effort may also be undertaken, leveraging the validation work described in Section 4.2.

Internal presentations included:

- A poster on the research, prepared and presented at the Applied Information Sciences Spring 2022 session;
- A presentation on the overall capability to the Resilient Energy Systems (RES) External Advisory Board (EAB), January 2022;
- A presentation to the Sandia Infrastructure Resilience Community of Practice, 10 December 2020; and
- A presentation on the overall capability to the RES External Advisory Board (EAB), 8 December 2020.

5.2. Interactions

Two significant external interactions were held through this effort, which supported the work. First, direct interactions with Shmuel Oren, University of California, Berkeley, led to further interactions by the project team with Ignacio Aravena, to better understand some of the elements of the MCM which were underexplained in published and unpublished work. Second, the team interacted with Bob Cummings, Senior Director of Engineering and Reliability Initiatives, North American Electric Reliability Corporation (retired), to better define the role and information load seen by operators in normal, abnormal, and black start operations.

5.3. Proposals

Several proposals were prepared suggesting extension or continuation of the work described in this document.

A DOE Advanced Grid Modeling (AGM) proposal, titled Leveraging Debris Clearance and Removal Data for Advanced Restoration Planning, was submitted for consideration in July 2021. This proposal would have leveraged and extended research from this work along with available data on debris clearance and removal for a previous event in a partner utility's area of service. Additional modeling would have been performed to identify activity prioritization in the debris clearance and removal process, with the intent of enabling an iterative loop between the power flow-informed system recovery model and the debris clearance and removal prioritization model. Leveraging this combined set of capabilities and incident data will enable development of a coordinated restoration profile that meets Federal, State, and utility requirements for restoring an electric grid under severe physical disruption. It will also identify methods of enhancing the coordination of debris clearance and removal and grid restoration in a way that reduces cumulative outage time as well as temporal outage extremes in physically isolated (and often disadvantaged) communities.

A FY23 LDRD Idea, Resilience-Focused Modeling of the Coordinated Operations of Electric Power and Natural Gas Systems Relative to Significant Acute Climate Impacts, was submitted in February 2022. The concept of this LDRD was to leverage electric grid modeling work performed under this LDRD along with natural gas network modeling built on the NetFlow Dynamics modeling framework (and previously validated against data from the New Mexico outage of 2011) for an integrated system-of-systems integration of these diverse networks, incorporating temporal synchronization of these physical models, and incorporation of market dynamics.

A DOE Renewables Advancing Community Energy Resilience (RACER) proposal, titled Expanding Grid Restoration for Underserved Communities through the Development of Model and Metric-Driven Plans Leveraging Photovoltaics, was submitted May 2022. This proposal suggested advancements on the research in this LDRD to incorporate lined, locality-based considerations sufficient for restoration planning with quantified energy justice metrics. Demonstrations, in partnership with local stakeholders (coordinated by one or more Historically Black Colleges and Universities) focused on an underserved community or communities, would advance the prototype, and explore the use of photovoltaic generation assets to support the engagement of non-traditional black start assets for more rapid restoration. The culmination of this work would be a refined capability that generates accurate restoration schedules both leveraging photovoltaics and supporting energy justice for underserved communities.

A DOE AGM proposal, titled Proactive Outage Prediction Informed Resilience Planning Considering Future Climate Change and Disadvantaged Communities, was submitted in August 2022. This proposal, led by Oak Ridge National Laboratory, would integrate work from this LDRD as a restoration model of the transmission system, in conjunction with a pre-event outage prediction system developed by researchers at the University of Connecticut and Eversource Energy along with outage observations from the Oak Ridge-managed EAGLE-I outage database, deep reinforcement learning algorithms and Bayesian techniques for distribution-level restoration, and Sandia-led efforts on the application of energy justice metrics in support of evaluation of the effectiveness of restoration plans.

6. FUTURE NEEDS

There are multiple future needs identified to enable improvement of this capability as a whole from the delivered state to one that can be more broadly implemented. This includes capability improvements from a conceptual perspective, applying to the capability at large, to specific needs applicable to elements of the above-described modeling paradigm.

In terms of overall refinements, additional thought needs to be given to pattern behavior seen in the small restoration cases, and their applicability to island behavior in larger networks. A range of techniques have yet to be adequately explored within this space (e.g., Markovian processes, Machine Learning) that could be used to explore and understand stages of restoration, identify working intermediate waypoints in a broader restoration, that can aid in the development of vectored restoration plans from that waypoint given a range of physical and informational uncertainties about the behavior or availability of the rest of the unrestored system. Moreover, as described in Section 2.3.2, having known accepted states can provide guidance as to whether elements of the restoring system are not meeting expectations and may be signs of either poor situational awareness or of threat imposed on the system, reducing situational awareness.

Improvements are possible for the optimization model. Shunt compensators and series compensators were not modeled as part of this effort. As noted by [10], these components provide functionality that could influence a restoration schedule, and therefore influence both OCM and NDM results. Future work should include these and other components that are necessary to generate more realistic schedules.

Results from the restoration model tests on the WSCC 9-Bus System indicated the importance of the number of restorable lines per time period, *ml*. Additionally, it was shown that black start generator cranking time was more impactful when the *ml* was set to a lower value. This topic should be explored further to examine how black start restoration works in tandem with overall disaster response efforts.

Significant computational complexity was experienced during the RTS-96 test. Future work on the Feasibility Oracle should address this complexity. Once addressed, the fitness of the optimization model results should be assessed for use for restoration of real electric utility systems.

In term of power flow modeling, further work on the ACOPF models could be performed. The MCM of Aravena et al [10] was implemented but not validated for correctness. Similarly, Coffrin's LPAC model [24][25][26] was developed, and partially validated, but not validated in completion. Run time issues seen with the DCOPF model, and with the integration of the optimal power flow models through the Feasibility Oracle, can be addressed through improvements to the respective ACOPF models and through improvements to the Feasibility Oracle.

Both case studies showed existent limitations for the current NDM implementation, which expanded as the system grew. Improvements to the goal-seeking dynamics developed for NDM proved prone to instabilities. Further enhancement could address these problems; in the absence of this, substitution of other modeling constructs (or system output data based on the restoration schedule) could be leveraged in the modeling construct of this effort, so as to enable performance of the OCM leveraging the restoration plans generated by the restoration model.

The operator model implementation of the optimized schedules highlighted the decoupling of the restoration time periods from the ground truth system time, showing that schedules that took double the time periods to complete could still finish full restoration in a similar amount of system time. This is due to the inequity of the time periods in terms of work required of the operator, and

the amount of stability wait time required to complete overloaded time periods. Still, as noted above, while the overall restoration time is similar, the higher time period schedules require the slower connection of buses. This allows some to get energized faster than they otherwise would., while others are slower and could lead to inequities based on load prioritization. On the other hand, parallelization of other activities such as generator cranking represented a straightforward gain for the operator as it could be done early on and lower the operator's need for separate wait times later on in the schedules. We envision that a context-aware operator in the loop optimization would enable the identification of the sorts of actions that could be appropriately parallelized and those that would cause undue stress or instability on the system that operators have to wait on. A good first step to this might be including average system time costs to the optimization framework such that information regarding workload per time period could be properly constrained and accounted for.

7. CONCLUSIONS

In line with the Summary of Proposed Work, this research effort developed, leveraging concepts described in the Approach, an alternative formulation for power-flow informed black start restoration reflecting dynamic grid restoration from extreme outages based on a hybrid agent-based and system dynamics modeling approach. The integration of these methods, described in the Details on Research Performed, enabled a number of Accomplishments. The examination of a series of Case Studies that generated restoration profiles for a series of networks given specified limitations on the respective networks' black start capabilities, the number of lines that could simultaneously be restored, and the cranking time of generators. A validation test of the restoration formulation generated by these techniques against a commercial off-the-shelf power solver was performed. While limits were identified in each of the elements of the modeling paradigm, particularly as model scale increased in size, the approach nonetheless showed the effectiveness and value of integrating these tools and techniques in addressing portions of the joint problem they face. Such an integration is, based on this research, essential for assessing actual resilience against the spectrum of problems electric grids will be subject to in restoration.

The proposed work further hypothesized that this alternative formulation would be successful at simulating the dynamics of grid restoration subject to extreme events. The ability of the NDM and OCM to identify and react to outlier behavior seen in their response to provided restoration schedules shows the value of creating an intermediary process to act upon and provide feedback on restoration schedules that violate physical constraints.

This research has made significant progress towards that goal by laying out information pathways between analysis, operations, and situational awareness, and simulating their operation. This foundation can be further tested by, among other activities, corrupting information, making sure instabilities in the ground-truth simulation correspond to possible grid events, adding variation in loading. It can also be strengthened by increasing the scope and sophistication of the models and planning tools and broadened by bringing in additional processes that constrain restoration (e.g., supplies, road conditions, crew availability) or that place other conditions on restoration (e.g., the consideration of energy justice metrics as part of restoration prioritization).

This project did result in several Impacts. Multiple publications were made as part of this research (with additional proposed publications to be discussed among the authors and in conjunction with other LDRD projects with coordinate interest. Several proposals for continuation of this effort, extending work into associated, interdependent infrastructure, as well as into integration of energy justice metrics as part of restoration, have been made.

Proposed improvements to the process, as described in Future Needs, suggest overall process refinements to reduce computational impacts (such as leveraging Markov processes or Machine Learning techniques) to allow for the retention of successful sub-elements of island restoration for use in a broader restoration schema. These techniques can also provide guidance on whether elements of the restoring system are not meeting restoration plan expectations and may as a result be signs of either poor situational awareness or of threat imposed on the system, reducing situational awareness. Additional work on each of the elements of the capability researched can and should be performed, to enhance the tools developed to date. Future work on the Feasibility Oracle should address this complexity issues experienced by the power flow and optimization models.

This approach to modeling restoration dynamics can, with improvements, improve our energy system's resilience to intentional threats.

This page left blank

REFERENCES

[1] Abbott, R., Doyle, C., & Jones, A. (2022). HIJENKS Time out of action. Albuquerque: Sandia National Laboratories, SAND Report (in progress).

[2] Albadi, M. (2019). Power Flow Analysis. In (Ed.), Computational Models in Engineering. IntechOpen. https://doi.org/10.5772/intechopen.83374.

[3] Alderson, D.L., Brown, G.G., Carlyle, W.M., & Wood, R.K. (2011). "Solving Defender-Attacker-Defender Models for Infrastructure Defense," in Operations Research, Computing, and Homeland Defense, R.K. Wood and R.F. Dell, editors, INFORMS, Hanover, MD, pp. 28-49. At http://hdl.handle.net/10945/36936, accessed August 2022.

[4] Anderson, J. R. (1996). ACT: A simple theory of complex cognition. *American Psychologist*, 51(4), 355.

[5] Anderson, P.M. & Fouad, A.A. (2003). Power System Control and Stability, 2nd Edition. New York: IEEE Press.

[6] Andersson, G., Donalek, P., Farmer, R., Hatziargyriou, N., Kamwa, I., Kundur, P., Martins, N., Paserba, J., Pourbeik, P., Sanchez-Gasca, J., Schultz, R., Stankovic, A., Taylor, C., & Vittal, V. (2005). Causes of the 2003 major grid blackouts in North America and Europe, and recommended means to improve system dynamic performance. *IEEE Transactions on Power Systems*, 20, 1922-1928.

[7] Angulo, G., Ahmed, S., & Dey, S. S. (2016). Improving the integer L-shaped method. *INFORMS Journal on Computing*, 28(3), 483-499.

[8] Application of Probability Methods Subcommittee, Reliability Test System Task Force (1979). IEEE Reliability Test System. *IEEE Transactions on Power Apparatus and Systems* 98(6), November 1979. doi: 10.1109/TPAS.1979.319398.

[9] Aravena, I., Rajan, D., & Patsakis, G. (2018). Mixed-integer linear approximations of ac power flow equations for systems under abnormal operating conditions. In *2018 IEEE Power & Energy Society General Meeting (PESGM)* (pp. 1-5). IEEE.

[10] Aravena, I., Rajan, D., Patsakis, G., Oren, S., & Rios, J. (2019). A scalable mixed-integer decomposition approach for optimal power system restoration. Proposed Journal Article, unpublished, 2019 (LLNL-JRNL-766247).

[11] Assante, M. (2016). "Confirmation of a Coordinated Attack on the Ukranian Power Grid." SANS Blog, at https://www.sans.org/blog/confirmation-of-a-coordinated-attack-on-the-ukrainian-power-grid/, accessed August 2022.

[12] Atputharajah, A., & Saha, T. K. (2009). Power system blackouts-literature review. In *2009 International Conference on Industrial and Information Systems (ICIIS)*. 460-465.

[13] Beresnev, V.L., & Melnikov, A.A. (2019). A Bilevel "Attacker-Defender" Model to Choosing the Composition of Attack Means. *J. Appl. Ind. Math.* 13, 612–622. https://doi.org/10.1134/S1990478919040045.

[14] Beyeler, W., Corbet, T., & Hobbs, J. (2012) A Demand-driven, Capacity-constrained, Adaptive Algorithm for Computing Steady-state and Transient Flows in a Petroleum Transportation Network. Sandia National Laboratories. SAND2012-9487.

[15] Beyeler, W., Abbott, R., Doyle, C., & Stamber, K. (2020). Modeling Operator Behavior During Blackstart. *4th IEEE Systems Modelling Conference, Canberra, NSW, Australia (virtual)*, 27 October

2020. Albuquerque: Sandia National Laboratories. SAND2020-11317C. At http://prod.sandia.gov/sand_doc/2020/2011317c.pdf, accessed September 2022.

[16] Beyeler, W., Stamber, K., Arguello, B., & Garrett, R. (2020). Approximating power system dynamics for black start planning. *4th IEEE Systems Modelling Conference, Canberra, NSW, Australia (virtual)*. Albuquerque: Sandia National Laboratories. 27 October 2020. Albuquerque: Sandia National Laboratories. SAND 2020-11318C. At http://prod.sandia.gov/sand_doc/2020/2011318c.pdf, accessed September 2022.

[17] Böhm, U., & Mehlhorn, K. (2009). The influence of spreading activation on memory retrieval in sequential diagnostic reasoning. In *Proceedings of the 9th International Conference on Cognitive Modeling*. Manchester, UK.

[18] J. D. Brooks and D. Mendonça, "Optimizing hauling vehicle mix for debris removal: A queueing theory approach," 2013 IEEE International Conference on Technologies for Homeland Security (HST), 2013, pp. 492-497.

[19] Cain, M.B., O'Neill, R.P., & Castillo, A. (2013). History of optimal power flow and formulations. Federal Energy Regulatory Commission, 1, 1-36. At https://www.ferc.gov/sites/default/files/2020-05/acopf-1-history-formulation-testing.pdf, accessed August 2022.

[20] Carrier, P., Alvarado, F., Bose, A., Budhraja, V., Buehring, W., Como, A., DeMarco, C., Eto, J., Griego, R., Hauer, J., Hiskens, I., Kueck, J., Overbye, T., Overholt, P., Scalingi, P., Schueler, R., Stamber, K., Thomas, R., & Zingman, F.C. (2000). Final Report of the U.S. Department of Energy's Power Outage Study Team: Findings from the summer of 1999. Department of Energy, January 2000.

[21] Castillo, A. (2014). Risk analysis and management in power outage and restoration: A literature survey. Electric Power Systems Research 107, pp. 9-15. https://doi.org/10.1016/j.epsr.2013.09.002.

[22] Cengiz, E., Yılmaz, C., Yılmaz E.N., & Tolga Kahraman, H. (2019). "Importance of Power Flow and Load Analysis in Pre-Installation Power Systems," *2019 3rd International Symposium on Multidisciplinary Studies and Innovative Technologies (ISMSIT)*. pp. 1-4, doi: 10.1109/ISMSIT.2019.8932900.

[23] Chatzivasileiadis, S. (2017). Optimal Power Flow (DC-OPF and AC-OPF). *DTU Summer School 2017*. Kongens Lyngby: Technical University of Denmark (DTU). At http://www.energy-markets-school.dk/documents/2017/Chatzivasileiadis/Optimal%20Power%20Flow%20(DC%20and%20AC%20OPF).pdf, accessed August 2022.

[24] Coffrin, C., & Van Hentenryck, P. (2014). A linear-programming approximation of AC power flows. *INFORMS Journal on Computing*, 26. 718-734.

[25] Coffrin, C., Hijazi, H.L., & Van Henterwyck, P. (2015). The QC Relaxation: Theoretical and Computational Results on Optimal Power Flow. *arXiv*. doi.org/10.48550/arxiv.1502.07847.

[26] Coffrin, C., Bent, R., Tasseff, B., Sundar, K., & Backhaus, S. (2018). Relaxations of ac maximal load delivery for severe contingency analysis. *IEEE Transactions on Power Systems*, 34(2), 1450-1458.

[27] Corbet, T.F., Beyeler, W., Wilson, M.L., & Flanagan, T.P. (2018). A model for simulating adaptive, dynamic flows on networks: Application to petroleum infrastructure. *Reliability Engineering & System Safety*, 169. 451-465.

[28] El-Zonkoly, A.M. (2015). Renewable energy sources for complete optimal power system black-start restoration. *IET Generation, Transmission & Distribution*, 9. 531-539.

[29] Farmer, R.G., & Allen, E.H. (2006). Power system dynamic performance advancement from history of North American blackouts. In *2006 IEEE PES Power Systems Conference and Exposition*. 293-300.

[30] Fazel Darbandi, A. (2021). Novel grid-forming control for black start restoration using MMC-HVdc systems. Winnipeg: University of Manitoba.

[31] Feltes, J.W., & Grande-Moran, C. (2008). Black start studies for system restoration. In *2008 IEEE Power and Energy Society General Meeting-Conversion and Delivery of Electrical Energy in the 21st Century*. 1-8.

[32] GE Energy Consulting (2022). GE PSLF (website). At https://www.geenergyconsulting.com/practice-area/software-products/pslf, accessed September 2022.

[33] Gonzalez, C., Dutt, V., Healy, A.F., Young, M.D., & Bourne Jr, L.E. (2009). Comparison of instance and strategy models in ACT-R. In *Proceedings of the 9th International Conference on Cognitive Modeling—ICCM2009*. Manchester, UK.

[34] Grigg, C., Wong, P., Albrecht, P., Allan, R., Bhavaraju, M., Billinton, R., Chen, Q., Fong, C., Haddad, S., Kuruganty, S., Li, W., Mukerji, R., Patton, D., Rau, N., Reppen, D., Schneider, A., Shahidehpour, M, & Singh, C. (1999). The IEEE reliability test system-1996. A report prepared by the reliability test system task force of the application of probability methods subcommittee. *IEEE Transactions on Power Systems*, 14(3), 1010-1020.

[35] Hines, P., Balasubramaniam, K., & Sanchez, E. C. (2009). Cascading failures in power grids. *IEEE Potentials*, 28. 24-30.

[36] Hou, M., Zhu, H., Zhou, M., & Arrabito, G. R. (2010). Optimizing operator–agent interaction in intelligent adaptive interface design: A conceptual framework. *IEEE Transactions on Systems, Man, and Cybernetics, Part C (Applications and Reviews)*, 41(2), 161-178.

[37] Huneault, M., & Galiana, F.D. (1991). A survey of the optimal power flow literature. *IEEE Transactions on Power Systems* 6(2), pp. 762-770. doi: 10.1109/59.76723.

[38] Isemonger, A. G. (2007). The viability of the competitive procurement of Black Start: Lessons from the RTOs. *The Electricity Journal*, 20. 60-67.

[39] Kappenman, J.G. (2004). Space Weather and the Vulnerability of Electric Power Grids. In: Daglis, I.A. (eds) *Effects of Space Weather on Technology Infrastructure. NATO Science Series II: Mathematics, Physics and Chemistry*, vol 176. Springer, Dordrecht. https://doi.org/10.1007/1-4020-2754-0_14.

[40] Kelic, A., DeRosa, S., Beyeler, W.E., Stamber, K.L., & Taskov, K. (2021) NetFlow Dynamics Natural Gas Model Network Development. Sandia National Laboratories. SAND2021-0723.

[41] Knueven, B. (2019). EGRET: Electrical Grid Research and Engineering Tools. Albuquerque: Sandia National Laboratories, SAND2019-12698C. At https://www.osti.gov/servlets/purl/1642890, accessed September 2022.

[42] Laporte, G., & Louveaux, F. V. (1993). The integer L-shaped method for stochastic integer programs with complete recourse. *Operations Research Le*tters, 13(3), 133-142.

[43] Larsen, P., Sanstad, A., LaCommare, K., and Eto, J. (2019). Frontiers in the Economics of Widespread, Long-Duration Power Interruptions: Proceedings from an Expert Workshop.

Lawrence Berkeley National Laboratory. At https://escholarship.org/uc/item/8c8280md, accessed August 2022.

[44] Larsson, S., & Ek, E. (2004). The black-out in southern Sweden and eastern Denmark, September 23, 2003. In *IEEE Power Engineering Society General Meeting*, 2004. 1668-1672.

[45] Lebiere, C., & Anderson, J.R. (2011). Cognitive constraints on decision making under uncertainty. *Frontiers in Psychology*, 2:305.

[46] Li, C., Sun, Y., & Chen, X. (2007, December). Analysis of the blackout in Europe on November 4, 2006. In *2007 International Power Engineering Conference (IPEC 2007)*. 939-944.

[47] Liu, D., Chen, Y., Shen, G., & Fan, Y. (2005, August). A multi-agent based approach for modeling and simulation of bulk power system restoration. In *2005 IEEE/PES Transmission & Distribution Conference & Exposition: Asia and Pacific*. 1-6.

[48] Liu, Y., Fan, R., & Terzija, V. (2016). Power system restoration: a literature review from 2006 to 2016. *Journal of Modern Power Systems and Clean Energy*, 4. 332-341.

[49] Loehr, G.C. (2017). The "Good" Blackout: The Northeast Power Failure of 9 November 1965 [History]. *IEEE Power and Energy Magazine*, 15. 84-96.

[50] Lopez-Cardalda, G., Lugo-Alvarez, M., Mendez-Santacruz, S., Rivera, E.O., & Bezares, E.A. (2018). Learnings of the Complete Power Grid Destruction in Puerto Rico by Hurricane Maria. In *2018 IEEE International Symposium on Technologies for Homeland Security (HST)*. 1-6.

[51] Mazur, H. (2019). Severe Contingency Solver: Electric Power Transmission Analysis. Los Alamos Nationakl Laboratory, LA-UR-19-29622, 17 December 2019. At https://www.lanl.gov/projects/feynman-center/techsnapshot-content/5d6594aa54e77336becd1e8f/5d6594aa54e77336becd1e8f.pdf, accessed September 2022.

[52] McGrath, J.K. (2018). Will Updated Electricity Infrastructure Security Protect the Grid? A Case Study Modeling Electrical Substation Attacks. *Infrastructures* 3(4):53. https://doi.org/10.3390/infrastructures3040053.

[53] Mehlhorn, K., Taatgen, N.A., Lebiere, C., & Krems, J.F. (2011). Memory activation and the availability of explanations in sequential diagnostic reasoning. *Journal of Experimental Psychology: Learning, Memory, and Cognition*, 37(6), 1391.

[54] Momoh, J.A., Koessler, R.J., Bond, M.S., Stott, B., Sun, D., Papalexopoulos, A., & Ristanovic, P. (1997). Challenges to optimal power flow. *IEEE Transactions on Power Systems* 12(1), pp. 444-455., doi: 10.1109/59.575768.

[55] Mones, L. (2021). A Gentle Introduction to Optimal Power Flow. *Invenia Blog* (website). At https://invenia.github.io/blog/2021/06/18/opf-intro/#mjx-eqn%3Abfm_concise, accessed August 2022.

[56] Oster, M., Chatterjee, S., Pan, F., Bakker, C., Bhattacharya, A., & Perkins, C. (2020). "Power system resilience through defender-attacker-defender models with uncertainty: an overview." *2020 Resilience Week (RWS)*, 11-17. doi: 10.1109/RWS50334.2020.9241279.

[57] Overbye, T.J., Cheng, X., & Sun, Y. (2004). "A Comparison of the AC and DC Power Flow Models for LMP Calculations." *Proceedings of the 37th Hawaii International Conference on System Sciences*. At https://ieeexplore.ieee.org/stamp/stamp.jsp?arnumber=1265164, accessed August 2022.

[58] Panteli, M., Pickering, C., Wilkinson, S., Dawson, R., and Mancarella, P. (2017). "Power System Resilience to Extreme Weather: Fragility Modeling, Probabilistic Impact Assessment,

and Adaptation Measures." *IEEE Transactions on Power Systems* 32 (5), pp. 3747-3757, Sept. 2017, doi: 10.1109/TPWRS.2016.2641463.

[59] Parrott, L.K. (2013). Iraq Crude Oil Model Summary presentation. Albuquerque: Sandia National Laboratories, SAND2013-1221C. At https://www.osti.gov/servlets/purl/1116094, accessed September 2022.

[60] Pasias, A., Schoinas, A., Drosou, A., & Tzovaras, D. (2021). A Scalable Multi-Agent System for Black Start Restoration in Low Voltage Microgrids. In 2021 IEEE International Conference on Cyber Security and Resilience (CSR). 479-484.

[61] Patsakis, G., Rajan, D., Aravena, I., Rios, J., & Oren, S. (2018). Optimal black start allocation for power system restoration. *IEEE Transactions on Power Systems*, 33. 6766-6776.

[62] Stamber, K.L., Arguello, B., Garrett, R.A., Beyeler, W.E., & Doyle, C. (2022). Optimal electric grid black start restoration subject to threats. *MODSIM World 2022*. Albuquerque: Sandia National Laboratories. SAND2022-0917C. At https://prod-ng.sandia.gov/sand_doc/2022/220917c.pdf, accessed September 2022.

[63] Stamber, K.L., Arguello, B., Garrett, R.A., Beyeler, W.E., & Doyle, C. (2022). Optimal electric grid black start restoration subject to threats. Presentation at *MODSIM World 2022*, 11 May 2022. Albuquerque: Sandia National Laboratories. SAND2022-4206C. At https://prod-ng.sandia.gov/sand_doc/2022/224206c.pdf, accessed September 2022.

[64] Sullivan, J.E., & Kamensky, D. (2017). How cyber-attacks in Ukraine show the vulnerability of the US power grid. *The Electricity Journal*, 30. 30-35.

[65] Taft, J. (2017). Electric grid resilience and reliability for grid architecture. Pacific Northwest National Laboratory (PNNL): Richland, WA, USA. At https://gridarchitecture.pnnl.gov/media/advanced/Electric_Grid_Resilience_and_Reliability.pdf, accessed August 2022.

[66] Tan, C.W., Cai, D.W., & Lou, X. (2012). DC optimal power flow: Uniqueness and algorithms. In *2012 IEEE Third International Conference on Smart Grid Communications (SmartGridComm)* (pp. 641-646). IEEE.

[67] Thompson, K.H., & Tran H. T. (2018). "Application of a Defender-Attacker-Defender Model to the U.S. Air Transportation Network," *2018 IEEE International Symposium on Technologies for Homeland Security (HST)*, pp. 1-5, doi: 10.1109/THS.2018.8574199.

[68] Thomson, R., Lebiere, C., Anderson, J.R., & Staszewski, J. (2015). A general instance-based learning framework for studying intuitive decision-making in a cognitive architecture. *Journal of Applied Research in Memory and Cognition*, 4(3), 180-190.

[69] Tu, H., Xia, Y., Tse, C.K., & Chen, X. (2020). "A Hybrid Cyber Attack Model for Cyber-Physical Power Systems." *IEEE Access* 8, pp. 114876-114883, doi: 10.1109/ACCESS.2020.3003323.

[70] Watts, C., McCarthy, C., & Levite, B. (2020). "Moving Beyond Average Reliability Metrics." S&C Electric Company. At https://www.sandc.com/globalassets/sac-electric/documents/sharepoint/documents---all-documents/technical-paper-100-t128.pdf?dt=637959445018990358, accessed August 2022.

[71] Wei, W., & Tao, Z. (2018). Occurrence and countermeasures of urban power grid accident. In *IOP Conf. Ser.: Earth Environ. Sci.* 128 012187. At https://iopscience.iop.org/article/10.1088/1755-1315/128/1/012187/pdf, accessed August 2022.

[72] Wolsey, L. A. (2007). Mixed integer programming. Wiley Encyclopedia of Computer Science and Engineering, 1-10.

[73] Wu, Y.K., Chang, S.M., & Hu, Y.L. (2017). Literature review of power system blackouts. *Energy Procedia*, 141. 428-431.

[74] Yuan, W., Zhao, L. & Zeng, B. (2014). Optimal power grid protection through a defender–attacker–defender model. *Reliability Engineering & System Safety* 121, p. 83-89. https://doi.org/10.1016/j.ress.2013.08.003

[75] Zhang, H., Ma, S., Ding, T., Lin, Y., & Shahidehpour, M. (2021). "Multi-Stage Multi-Zone Defender-Attacker-Defender Model for Optimal Resilience Strategy With Distribution Line Hardening and Energy Storage System Deployment," *IEEE Transactions on Smart Grid* 12(2), pp. 1194-1205. doi: 10.1109/TSG.2020.3027767.

[76] Zimmerman, R.D., & Murillo-Sanchez, C.E. (2020). MATPOWER User's Manual, Version 7.1, 202. [Online]. At https://matpower.org/docs/MATPOWER-manual.pdf, accessed September 2022.

[77] Zio, E., Piccinelli, R., Delfanti, M., Olivieri, V., & Pozzi, M. (2012). Application of the load flow and random flow models for the analysis of power transmission networks. *Reliability Engineering & System Safety* 103, pp. 102-109. https://doi.org/10.1016/j.ress.2012.02.005.

APPENDIX A. OPTIMIZATION MODEL DATA AND RESULTS DETAILS

A.1. Additional Results Details

Additional details for test results on the RTS-96 system are provided in this section. Figures of the restoration schedule at time=0, 5, 42, and 55 are displayed. Figures for time = 0 and time = 5 illustrate how the islands were formed. The figure for time = 42 illustrates the time periods when all generators were restored. The system was fully restored by time = 55.


Time Period 0
LEGEND
Cranking
Energized
Generator
Bus
Power Line

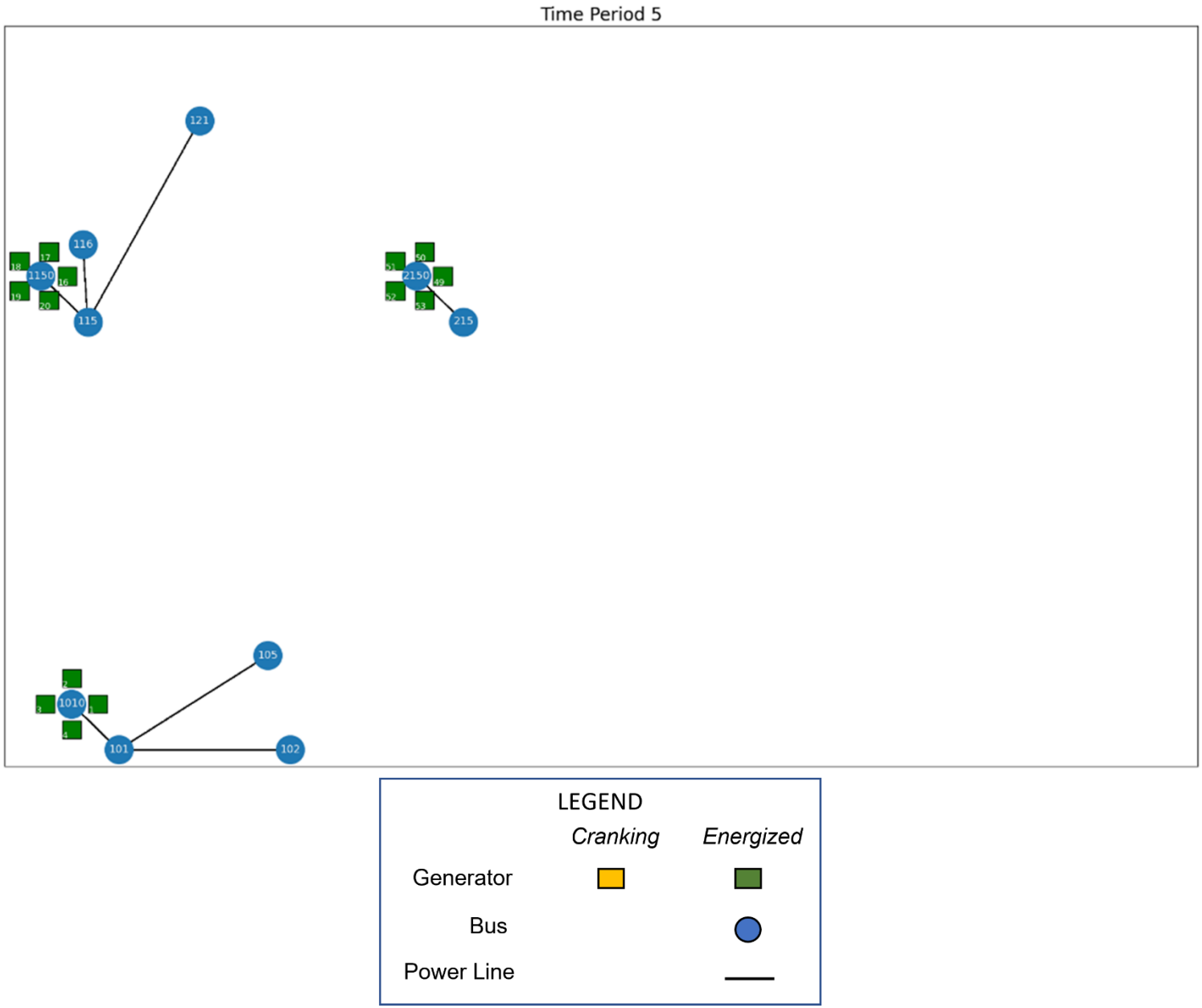
Time Period 5
121
116
115
2150
215
105
1010
101
102
LEGEND
Cranking
Energized
Generator
Bus
Power Line

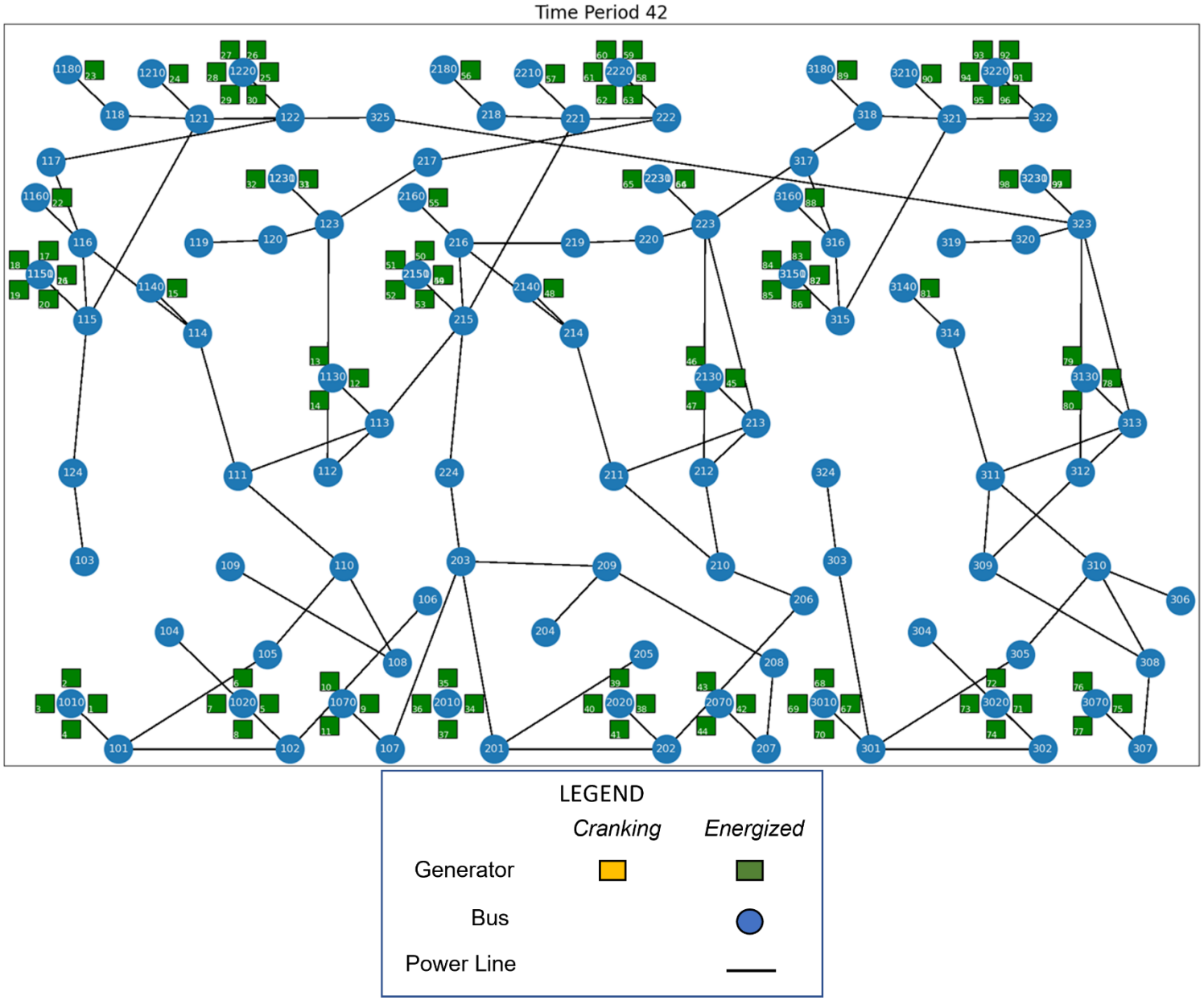
Time Period 42
LEGEND
Cranking
Energized
Generator
Bus
Power Line

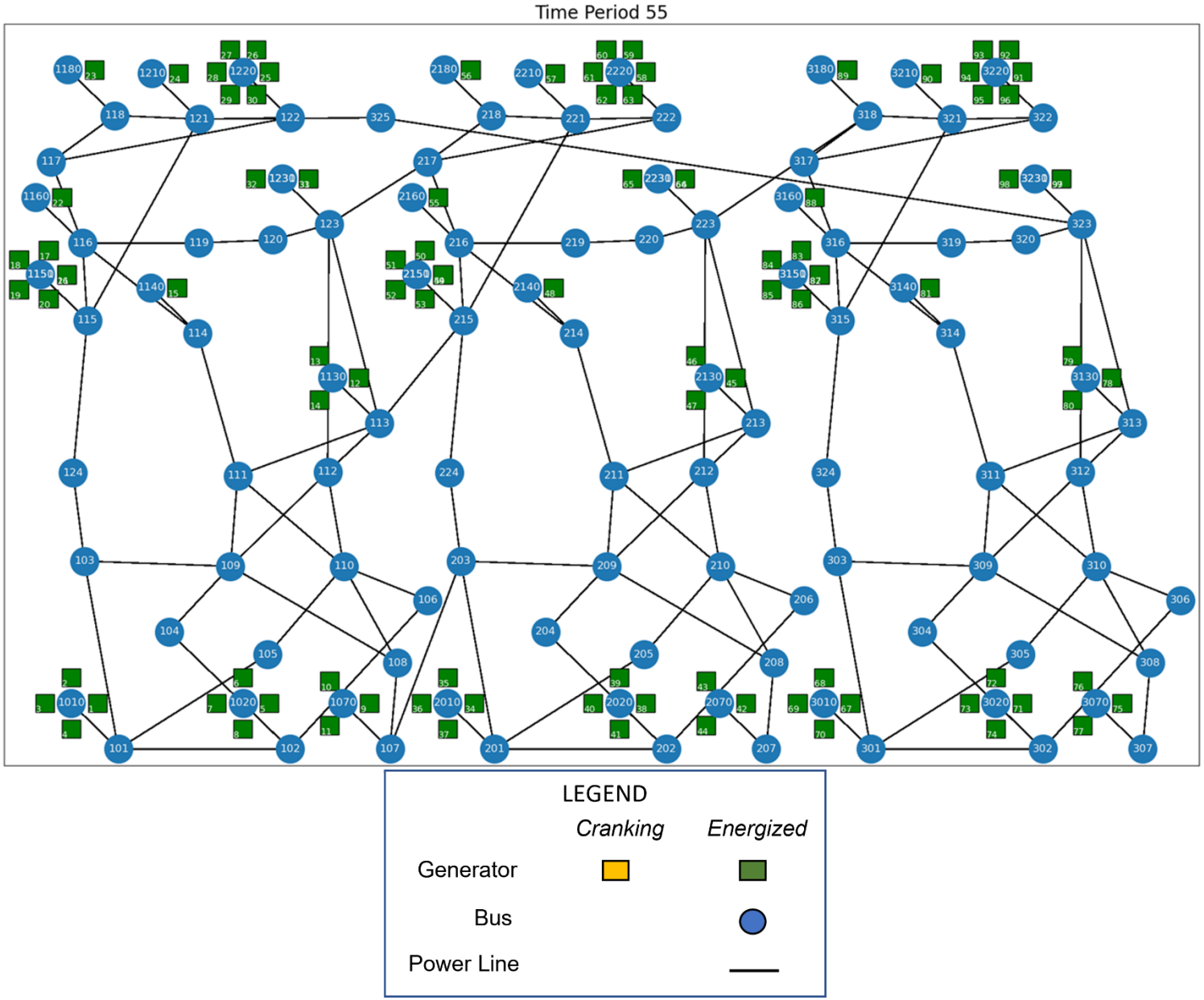
Time Period 55
LEGEND
Cranking
Energized
Generator
Bus
Power Line

A.2. RTS-96 Matpower Data

This section features MATPOWER file data for the RTS-96 test case, including files pertinent to Bus, Generator, and Branch Data [76].

A.2.1. Bus Data

Bus Data is provided as follows:

- Bus number: A positive integer, representative of the bus
- Bus Type: bus type {1: PQ bus; 2: PV bus; 3: reference bus; 4: isolated bus}
- Pd, real power demand (in MW)
- Qd, reactive power demand (in MVar)
- Gs, shunt conductance (MW demanded at V = 1.0 p.u.)
- Bs, shunt susceptance (MVar injected at V = 1.0 p.u.)
- Area number (positive integer)
- Vm, voltage magnitude (p.u.)
- Va, voltage angle (degrees)
- baseKV, base voltage (in kV)
- zone, loss zone (positive integer)
- maxVm, Kuhn-Tucker multiplier on upper voltage limit (u/p.u.)
- minVm, Kuhn-Tucker multiplier on lower voltage limit (u/p.u.)

Bus number	Bus Type	Pd	Qd	Gs	Bs	area	Vm	Va	baseKV	zone	maxVm	minVm
101	2	108	22	0	0	11	1.035	-7.17187	138	11	1.1	0.9
102	2	97	20	0	0	11	1.035	-7.27629	138	12	1.1	0.9
103	1	180	37	0	0	11	0.984563	-5.0673	138	11	1.1	0.9
104	1	74	15	0	0	11	0.998895	-9.64347	138	11	1.1	0.9
105	1	71	14	0	0	11	1.018623	-9.93017	138	11	1.1	0.9
106	1	136	130.52	0	0	11	1.012516	-12.4371	138	12	1.1	0.9

Bus number	Bus Type	Pd	Qd	Gs	Bs	area	Vm	Va	baseKV	zone	maxVm	minVm
107	2	125	25	0	0	11	1.025	-7.26006	138	12	1.1	0.9
108	1	171	35	0	0	11	0.993122	-11.017	138	12	1.1	0.9
109	1	175	36	0	0	11	1.003211	-7.42607	138	13	1.1	0.9
110	1	195	40	0	0	11	1.028822	-9.53098	138	13	1.1	0.9
111	1	0	0	0	0	11	0.995417	-2.69558	230	13	1.1	0.9
112	1	0	0	0	0	11	1.007195	-1.33035	230	13	1.1	0.9
113	2	265	54	0	0	12	1.030757	0.019388	230	14	1.1	0.9
114	2	194	39	0	0	12	0.98	0.67729	230	16	1.1	0.9
115	2	317	64	0	0	12	1.014	12.66237	230	16	1.1	0.9
116	2	100	20	0	0	12	1.017	11.76237	230	16	1.1	0.9
117	1	0	0	0	0	12	1.038284	16.07801	230	17	1.1	0.9
118	2	333	68	0	0	12	1.05	17.30574	230	17	1.1	0.9
119	1	181	37	0	0	12	1.023012	10.09739	230	15	1.1	0.9
120	1	128	26	0	0	12	1.038245	10.60009	230	15	1.1	0.9
121	2	0	0	0	0	12	1.05	18.05407	230	17	1.1	0.9
122	2	0	0	0	0	12	1.05	23.78887	230	17	1.1	0.9
123	2	0	0	0	0	12	1.05	11.59524	230	15	1.1	0.9
124	1	0	0	0	0	12	0.979766	6.130126	230	16	1.1	0.9
201	2	108	22	0	0	21	1.035	-7.44179	138	21	1.1	0.9
202	2	97	20	0	0	21	1.035	-7.51084	138	22	1.1	0.9
203	1	180	37	0	0	21	0.996921	-6.70424	138	21	1.1	0.9

Bus number	Bus Type	Pd	Qd	Gs	Bs	area	Vm	Va	baseKV	zone	maxVm	minVm
204	1	74	15	0	0	21	0.999087	-9.7613	138	21	1.1	0.9
205	1	71	14	0	0	21	1.017082	-9.95507	138	21	1.1	0.9
206	1	136	130.02	0	0	21	1.010037	-12.327	138	22	1.1	0.9
207	2	125	25	0	0	21	1.025	-7.29154	138	22	1.1	0.9
208	1	171	35	0	0	21	0.992512	-10.9914	138	22	1.1	0.9
209	1	175	36	0	0	21	1.00355	-7.44686	138	23	1.1	0.9
210	1	195	40	0	0	21	1.025573	-9.29362	138	23	1.1	0.9
211	1	0	0	0	0	21	0.991385	-2.50176	230	23	1.1	0.9
212	1	0	0	0	0	21	1.001071	-0.47877	230	23	1.1	0.9
213	2	265	54	0	0	22	1.02	1.724898	230	24	1.1	0.9
214	2	194	39	0	0	22	0.98	-0.38731	230	26	1.1	0.9
215	2	317	64	0	0	22	1.014	8.554698	230	26	1.1	0.9
216	2	100	20	0	0	22	1.017	8.943453	230	26	1.1	0.9
217	1	0	0	0	0	22	1.040377	12.67066	230	27	1.1	0.9
218	2	333	68	0	0	22	1.05	13.81692	230	27	1.1	0.9
219	1	181	37	0	0	22	1.022699	8.855437	230	25	1.1	0.9
220	1	128	26	0	0	22	1.03766	10.70196	230	25	1.1	0.9
221	2	0	0	0	0	22	1.05	14.47768	230	27	1.1	0.9
222	2	0	0	0	0	22	1.05	20.27847	230	27	1.1	0.9
223	2	0	0	0	0	22	1.05	12.41829	230	25	1.1	0.9
224	1	0	0	0	0	22	0.988318	2.870926	230	26	1.1	0.9

Bus number	Bus Type	Pd	Qd	Gs	Bs	area	Vm	Va	baseKV	zone	maxVm	minVm
301	2	108	22	0	0	31	1.035	-1.96696	138	31	1.1	0.9
302	2	97	20	0	0	31	1.035	-2.05282	138	32	1.1	0.9
303	1	180	37	0	0	31	0.984574	-0.49177	138	31	1.1	0.9
304	1	74	15	0	0	31	0.997256	-4.34113	138	31	1.1	0.9
305	1	71	14	0	0	31	1.016828	-4.57956	138	31	1.1	0.9
306	1	136	129.94	0	0	31	1.009639	-7.01172	138	32	1.1	0.9
307	2	125	25	0	0	31	1.023	-1.94933	138	32	1.1	0.9
308	1	171	35	0	0	31	0.990496	-5.6646	138	32	1.1	0.9
309	1	175	36	0	0	31	1.000298	-2.04367	138	33	1.1	0.9
310	1	195	40	0	0	31	1.025122	-4.02075	138	33	1.1	0.9
311	1	0	0	0	0	31	0.990778	2.879034	230	33	1.1	0.9
312	1	0	0	0	0	31	1.001483	4.513803	230	33	1.1	0.9
313	2	265	54	0	0	32	1.02	6.70012	230	34	1.1	0.9
314	2	194	39	0	0	32	0.98	5.389235	230	36	1.1	0.9
315	2	317	64	0	0	32	1.014	15.92216	230	36	1.1	0.9
316	2	100	20	0	0	32	1.017	15.27971	230	36	1.1	0.9
317	1	0	0	0	0	32	1.038837	18.73178	230	37	1.1	0.9
318	2	333	68	0	0	32	1.05	19.50736	230	37	1.1	0.9
319	1	181	37	0	0	32	1.023007	14.27439	230	35	1.1	0.9
320	1	128	26	0	0	32	1.038082	15.3386	230	35	1.1	0.9
321	2	0	0	0	0	32	1.05	20.72854	230	37	1.1	0.9

Bus number	Bus Type	Pd	Qd	Gs	Bs	area	Vm	Va	baseKV	zone	maxVm	minVm
322	2	0	0	0	0	32	1.05	26.45523	230	37	1.1	0.9
323	2	0	0	0	0	32	1.05	16.6352	230	35	1.1	0.9
324	1	0	0	0	0	32	0.981946	9.87527	230	36	1.1	0.9
325	1	0	0	0	0	32	1.050608	16.7535	230	35	1.1	0.9
1010	2	0	0	0	0	11	1.035395	-7.08118	13.8	11	1.1	0.9
1020	2	0	0	0	0	11	1.035313	-7.18514	13.8	12	1.1	0.9
1070	2	0	0	0	0	11	1.025887	-7.13295	13.8	12	1.1	0.9
1130	3	0	0	0	0	12	1.033	0	20	14	1.1	0.9
1140	2	0	0	0	0	12	0.979805	0.67843	13.8	16	1.1	0.9
1150	2	0	0	0	0	12	1.014059	12.6958	12.3	16	1.1	0.9
1151	2	0	0	0	0	12	1.01404	12.74937	20	16	1.1	0.9
1160	2	0	0	0	0	12	1.017431	11.84662	13.8	16	1.1	0.9
1180	2	0	0	0	0	12	1.051702	17.50603	22	17	1.1	0.9
1210	2	0	0	0	0	12	1.051329	18.25647	22	17	1.1	0.9
1220	2	0	0	0	0	12	1.049998	23.94633	13.8	17	1.1	0.9
1230	2	0	0	0	0	12	1.050924	11.75275	20	15	1.1	0.9
1231	2	0	0	0	0	12	1.050961	11.77351	22	15	1.1	0.9
2010	2	0	0	0	0	21	1.035347	-7.35083	13.8	21	1.1	0.9
2020	2	0	0	0	0	21	1.035323	-7.41975	13.8	22	1.1	0.9
2070	2	0	0	0	0	21	1.025744	-7.16361	13.8	22	1.1	0.9
2130	2	0	0	0	0	22	1.021523	1.874776	20	24	1.1	0.9

Bus number	Bus Type	Pd	Qd	Gs	Bs	area	Vm	Va	baseKV	zone	maxVm	minVm
2140	2	0	0	0	0	22	0.9798	-0.38614	13.8	26	1.1	0.9
2150	2	0	0	0	0	22	1.014059	8.588131	12.3	26	1.1	0.9
2151	2	0	0	0	0	22	1.013704	8.643626	20	26	1.1	0.9
2160	2	0	0	0	0	22	1.01722	9.028911	13.8	26	1.1	0.9
2180	2	0	0	0	0	22	1.051553	14.01806	22	27	1.1	0.9
2210	2	0	0	0	0	22	1.051477	14.67925	22	27	1.1	0.9
2220	2	0	0	0	0	22	1.049978	20.43604	13.8	27	1.1	0.9
2230	2	0	0	0	0	22	1.050986	12.57545	20	25	1.1	0.9
2231	2	0	0	0	0	22	1.051023	12.59621	22	25	1.1	0.9
3010	2	0	0	0	0	31	1.035412	-1.87637	13.8	31	1.1	0.9
3020	2	0	0	0	0	31	1.03534	-1.96182	13.8	32	1.1	0.9
3070	2	0	0	0	0	31	1.023745	-1.82091	13.8	32	1.1	0.9
3130	2	0	0	0	0	32	1.021488	6.850201	20	34	1.1	0.9
3140	2	0	0	0	0	32	0.979843	5.39015	13.8	36	1.1	0.9
3150	2	0	0	0	0	32	1.014059	15.95559	12.3	36	1.1	0.9
3151	2	0	0	0	0	32	1.013939	16.00974	20	36	1.1	0.9
3160	2	0	0	0	0	32	1.017287	15.36478	13.8	36	1.1	0.9
3180	2	0	0	0	0	32	1.051631	19.70805	22	37	1.1	0.9
3210	2	0	0	0	0	32	1.051418	20.93044	22	37	1.1	0.9
3220	2	0	0	0	0	32	1.049993	26.61271	13.8	37	1.1	0.9
3230	2	0	0	0	0	32	1.0509	16.79284	20	35	1.1	0.9

Bus number	Bus Type	Pd	Qd	Gs	Bs	area	Vm	Va	baseKV	zone	maxVm	minVm
3231	2	0	0	0	0	32	1.050937	16.8136	22	35	1.1	0.9

A.2.2. Generator Data

Generator Data is provided as follows:

- Bus Number (identifier of the bus to which a generator corresponds)
- Pg, real power output (MW)
- Qg, reactive power output (MVar)
- Qmax, maximum reactive power output (MVar)
- Qmin, minimum reactive power output (MVar)
- Vg, voltage magnitude setpoint (p.u.)
- mBase, total MVA base of machine
- status, status of the machine {>0, in service; <=0, out of service}
- Pmax, maximum real power output (MW)
- Pmin, minimum real power output (MW)
- Pc1, lower real power output of PQ capability curve (MW)
- Pc2, upper real power output of PQ capability curve (MW)
- Qc1min, minimum reactive power output at Pc1 (MVAr)
- Qc1max, maximum reactive power output at Pc1 (MVAr)
- Qc2min, minimum reactive power output at Pc2 (MVAr)
- Qc2max, maximum reactive power output at Pc2 (MVAr)
- Ramp_agc, ramp rate for load following/AGC (MW/min)
- Ramp_10, ramp rate for 10-minute reserves (MW)
- Ramp_30, ramp rate for 30-minute reserves (MW)
- Ramp_q, ramp rate for reactive power (2 sec timescale) (MVAr/min)
- apf, area participation factor

Bus Number	Pg	Qg	Qmax	Qmin	Vg	mBase	status	Pmax	Pmin	Pc1	Pc2	Qc1min	Qc1max	Qc2min	Qc2max	Ramp_agc	Ramp_10	Ramp_30	Ramp_q	apf
1010	10	3.04	10	0	1.0354	24	1	1000	0	0	0	0	0	0	0	0	0	0	0	1000
1010	10	3.04	10	0	1.0354	24	1	1000	0	0	0	0	0	0	0	0	0	0	0	1000
1010	76	8.87	30	-25	1.0354	89	1	1000	0	0	0	0	0	0	0	0	0	0	0	1000
1010	76	8.87	30	-25	1.0354	89	1	1000	0	0	0	0	0	0	0	0	0	0	0	1000
1020	10	1.95	10	0	1.0353	24	1	1000	0	0	0	0	0	0	0	0	0	0	0	1000
1020	10	1.95	10	0	1.0353	24	1	1000	0	0	0	0	0	0	0	0	0	0	0	1000
1020	76	5.71	30	-25	1.0353	89	1	1000	0	0	0	0	0	0	0	0	0	0	0	1000
1020	76	5.71	30	-25	1.0353	89	1	1000	0	0	0	0	0	0	0	0	0	0	0	1000
1070	80	22.43	60	0	1.0259	118	1	1000	0	0	0	0	0	0	0	0	0	0	0	1000
1070	80	22.43	60	0	1.0259	118	1	1000	0	0	0	0	0	0	0	0	0	0	0	1000
1070	80	22.43	60	0	1.0259	118	1	1000	0	0	0	0	0	0	0	0	0	0	0	1000
1130	-4.24	77.67	80	0	1.033	232	1	10000	0	0	0	0	0	0	0	0	0	0	0	10000
1130	-4.24	77.67	80	0	1.033	232	1	10000	0	0	0	0	0	0	0	0	0	0	0	10000
1130	-4.24	77.67	80	0	1.033	232	1	10000	0	0	0	0	0	0	0	0	0	0	0	10000
1140	0	-19.1	200	-50	0.9798	100	1	1000	0	0	0	0	0	0	0	0	0	0	0	1000
1150	12	0	6	0	1.0141	14	1	1000	0	0	0	0	0	0	0	0	0	0	0	1000
1150	12	0	6	0	1.0141	14	1	1000	0	0	0	0	0	0	0	0	0	0	0	1000
1150	12	0	6	0	1.0141	14	1	1000	0	0	0	0	0	0	0	0	0	0	0	1000
1150	12	0	6	0	1.0141	14	1	1000	0	0	0	0	0	0	0	0	0	0	0	1000

Bus Number	Pg	Qg	Qmax	Qmin	Vg	mBase	status	Pmax	Pmin	Pc1	Pc2	Qc1min	Qc1max	Qc2min	Qc2max	Ramp_agc	Ramp_10	Ramp_30	Ramp_q	apf
1150	12	0	6	0	1.0141	14	1	1000	0	0	0	0	0	0	0	0	0	0	0	1000
1151	155	-11.32	80	-50	1.014	182	1	1000	0	0	0	0	0	0	0	0	0	0	0	1000
1160	155	28.43	80	-50	1.0174	182	1	1000	0	0	0	0	0	0	0	0	0	0	0	1000
1180	400	139.73	200	-50	1.0517	471	1	1000	0	0	0	0	0	0	0	0	0	0	0	1000
1210	400	100.43	200	-5	1.0513	471	1	1000	0	0	0	0	0	0	0	0	0	0	0	1000
1220	50	-4.97	16	-10	1.05	53	1	1000	0	0	0	0	0	0	0	0	0	0	0	1000
1220	50	-4.97	16	-10	1.05	53	1	1000	0	0	0	0	0	0	0	0	0	0	0	1000
1220	50	-4.97	16	-10	1.05	53	1	1000	0	0	0	0	0	0	0	0	0	0	0	1000
1220	50	-4.97	16	-10	1.05	53	1	1000	0	0	0	0	0	0	0	0	0	0	0	1000
1220	50	-4.97	16	-10	1.05	53	1	1000	0	0	0	0	0	0	0	0	0	0	0	1000
1220	50	-4.97	16	-10	1.05	53	1	1000	0	0	0	0	0	0	0	0	0	0	0	1000
1230	155	33.24	80	-50	1.0509	182	1	1000	0	0	0	0	0	0	0	0	0	0	0	1000
1230	155	33.24	80	-50	1.0509	182	1	1000	0	0	0	0	0	0	0	0	0	0	0	1000
1231	350	66.49	150	-25	1.051	412	1	1000	0	0	0	0	0	0	0	0	0	0	0	1000
2010	10	2.41	10	0	1.0353	24	1	1000	0	0	0	0	0	0	0	0	0	0	0	1000
2010	10	2.41	10	0	1.0353	24	1	1000	0	0	0	0	0	0	0	0	0	0	0	1000
2010	76	7.03	30	-25	1.0353	89	1	1000	0	0	0	0	0	0	0	0	0	0	0	1000
2010	76	7.03	30	-25	1.0353	89	1	1000	0	0	0	0	0	0	0	0	0	0	0	1000
2020	10	2.08	10	0	1.0353	24	1	1000	0	0	0	0	0	0	0	0	0	0	0	1000

Bus Number	Pg	Qg	Qmax	Qmin	Vg	mBase	status	Pmax	Pmin	Pc1	Pc2	Qc1min	Qc1max	Qc2min	Qc2max	Ramp_agc	Ramp_10	Ramp_30	Ramp_q	apf
2020	10	2.08	10	0	1.0353	24	1	1000	0	0	0	0	0	0	0	0	0	0	0	1000
2020	76	6.09	30	-25	1.0353	89	1	1000	0	0	0	0	0	0	0	0	0	0	0	1000
2020	76	6.09	30	-25	1.0353	89	1	1000	0	0	0	0	0	0	0	0	0	0	0	1000
2070	80	17.53	60	0	1.0257	118	1	1000	0	0	0	0	0	0	0	0	0	0	0	1000
2070	80	17.53	60	0	1.0257	118	1	1000	0	0	0	0	0	0	0	0	0	0	0	1000
2070	80	17.53	60	0	1.0257	118	1	1000	0	0	0	0	0	0	0	0	0	0	0	1000
2130	95.1	42.47	80	0	1.0215	232	1	1000	0	0	0	0	0	0	0	0	0	0	0	1000
2130	95.1	42.47	80	0	1.0215	232	1	1000	0	0	0	0	0	0	0	0	0	0	0	1000
2130	95.1	42.47	80	0	1.0215	232	1	1000	0	0	0	0	0	0	0	0	0	0	0	1000
2140	0	-19.61	200	-50	0.9798	100	1	1000	0	0	0	0	0	0	0	0	0	0	0	1000
2150	12	0	6	0	1.0141	14	1	1000	0	0	0	0	0	0	0	0	0	0	0	1000
2150	12	0	6	0	1.0141	14	1	1000	0	0	0	0	0	0	0	0	0	0	0	1000
2150	12	0	6	0	1.0141	14	1	1000	0	0	0	0	0	0	0	0	0	0	0	1000
2150	12	0	6	0	1.0141	14	1	1000	0	0	0	0	0	0	0	0	0	0	0	1000
2150	12	0	6	0	1.0141	14	1	1000	0	0	0	0	0	0	0	0	0	0	0	1000
2151	155	-45.38	80	-50	1.0137	182	1	1000	0	0	0	0	0	0	0	0	0	0	0	1000
2160	155	7	80	-50	1.0172	182	1	1000	0	0	0	0	0	0	0	0	0	0	0	1000
2180	400	123.97	200	-50	1.0516	471	1	1000	0	0	0	0	0	0	0	0	0	0	0	1000
2210	400	115.97	200	-50	1.0515	471	1	1000	0	0	0	0	0	0	0	0	0	0	0	1000

Bus Number	Pg	Qg	Qmax	Qmin	Vg	mBase	status	Pmax	Pmin	Pc1	Pc2	Qc1min	Qc1max	Qc2min	Qc2max	Ramp_agc	Ramp_10	Ramp_30	Ramp_q	apf
2220	50	-5.32	16	-10	1.05	53	1	1000	0	0	0	0	0	0	0	0	0	0	0	1000
2220	50	-5.32	16	-10	1.05	53	1	1000	0	0	0	0	0	0	0	0	0	0	0	1000
2220	50	-5.32	16	-10	1.05	53	1	1000	0	0	0	0	0	0	0	0	0	0	0	1000
2220	50	-5.32	16	-10	1.05	53	1	1000	0	0	0	0	0	0	0	0	0	0	0	1000
2220	50	-5.32	16	-10	1.05	53	1	1000	0	0	0	0	0	0	0	0	0	0	0	1000
2220	50	-5.32	16	-10	1.05	53	1	1000	0	0	0	0	0	0	0	0	0	0	0	1000
2230	155	36.5	80	-50	1.051	182	1	1000	0	0	0	0	0	0	0	0	0	0	0	1000
2230	155	36.5	80	-50	1.051	182	1	1000	0	0	0	0	0	0	0	0	0	0	0	1000
2231	350	73.01	150	-25	1.051	412	1	1000	0	0	0	0	0	0	0	0	0	0	0	1000
3010	10	3.26	10	0	1.0354	24	1	1000	0	0	0	0	0	0	0	0	0	0	0	1000
3010	10	3.26	10	0	1.0354	24	1	1000	0	0	0	0	0	0	0	0	0	0	0	1000
3010	76	9.52	30	-25	1.0354	89	1	1000	0	0	0	0	0	0	0	0	0	0	0	1000
3010	76	9.52	30	-25	1.0354	89	1	1000	0	0	0	0	0	0	0	0	0	0	0	1000
3020	10	2.31	10	0	1.0353	24	1	1000	0	0	0	0	0	0	0	0	0	0	0	1000
3020	10	2.31	10	0	1.0353	24	1	1000	0	0	0	0	0	0	0	0	0	0	0	1000
3020	76	6.74	30	-25	1.0353	89	1	1000	0	0	0	0	0	0	0	0	0	0	0	1000
3020	76	6.74	30	-25	1.0353	89	1	1000	0	0	0	0	0	0	0	0	0	0	0	1000
3070	80	17.51	60	0	1.0237	118	1	1000	0	0	0	0	0	0	0	0	0	0	0	1000
3070	80	17.51	60	0	1.0237	118	1	1000	0	0	0	0	0	0	0	0	0	0	0	1000

Bus Number	Pg	Qg	Qmax	Qmin	Vg	mBase	status	Pmax	Pmin	Pc1	Pc2	Qc1min	Qc1max	Qc2min	Qc2max	Ramp_agc	Ramp_10	Ramp_30	Ramp_q	apf
3070	80	17.51	60	0	1.0237	118	1	1000	0	0	0	0	0	0	0	0	0	0	0	1000
3130	95.1	41.27	80	0	1.0215	232	1	1000	0	0	0	0	0	0	0	0	0	0	0	1000
3130	95.1	41.27	80	0	1.0215	232	1	1000	0	0	0	0	0	0	0	0	0	0	0	1000
3130	95.1	41.27	80	0	1.0215	232	1	1000	0	0	0	0	0	0	0	0	0	0	0	1000
3140	0	-15.34	200	-50	0.9798	100	1	1000	0	0	0	0	0	0	0	0	0	0	0	1000
3150	12	0	6	0	1.0141	14	1	1000	0	0	0	0	0	0	0	0	0	0	0	1000
3150	12	0	6	0	1.0141	14	1	1000	0	0	0	0	0	0	0	0	0	0	0	1000
3150	12	0	6	0	1.0141	14	1	1000	0	0	0	0	0	0	0	0	0	0	0	1000
3150	12	0	6	0	1.0141	14	1	1000	0	0	0	0	0	0	0	0	0	0	0	1000
3150	12	0	6	0	1.0141	14	1	1000	0	0	0	0	0	0	0	0	0	0	0	1000
3151	155	-21.56	80	-50	1.0139	182	1	1000	0	0	0	0	0	0	0	0	0	0	0	1000
3160	155	13.79	80	-50	1.0173	182	1	1000	0	0	0	0	0	0	0	0	0	0	0	1000
3180	400	132.21	200	-50	1.0516	471	1	1000	0	0	0	0	0	0	0	0	0	0	0	1000
3210	400	109.76	200	-50	1.0514	471	1	1000	0	0	0	0	0	0	0	0	0	0	0	1000
3220	50	-5.06	16	-10	1.05	53	1	1000	0	0	0	0	0	0	0	0	0	0	0	1000
3220	50	-5.06	16	-10	1.05	53	1	1000	0	0	0	0	0	0	0	0	0	0	0	1000
3220	50	-5.06	16	-10	1.05	53	1	1000	0	0	0	0	0	0	0	0	0	0	0	1000
3220	50	-5.06	16	-10	1.05	53	1	1000	0	0	0	0	0	0	0	0	0	0	0	1000
3220	50	-5.06	16	-10	1.05	53	1	1000	0	0	0	0	0	0	0	0	0	0	0	1000

Bus Number	Pg	Qg	Qmax	Qmin	Vg	mBase	status	Pmax	Pmin	Pc1	Pc2	Qc1min	Qc1max	Qc2min	Qc2max	Ramp_ag	Ramp_10	Ramp_30	Ramp_q	apf
3220	50	-5.06	16	-10	1.05	53	1	1000	0	0	0	0	0	0	0	0	0	0	0	1000
3230	155	32.01	80	-50	1.0509	182	1	1000	0	0	0	0	0	0	0	0	0	0	0	1000
3230	155	32.01	80	-50	1.0509	182	1	1000	0	0	0	0	0	0	0	0	0	0	0	1000
3231	350	64.01	150	-25	1.0509	412	1	1000	0	0	0	0	0	0	0	0	0	0	0	1000

A.2.3. Branch Data

Branch Data are provided as follows:

- fbus, "from" bus number
- tbus, "to" bus number
- r, resistance (p.u.)
- x, reactance (p.u.)
- b, total line charging susceptance (p.u.)
- rateA, MVA rating A (long term rating), set to 0 for unlimited
- rateB, MVA rating B (short term rating), set to 0 for unlimited
- rateC, MVA rating C (emergency rating), set to 0 for unlimited
- tap, transformer off nominal turns ratio, if non-zero (taps at 'from' bus, impedance at 'to' bus, i.e., r = x = b = 0, tap = $|V_f|/|V_t|$; tap = 0 to indicate transmission line rather than transformer, i.e. mathematically equivalent to transformer with tap = 1
- shift, transformer phase shift angle (degrees), positive => delay
- br_status, initial branch status {1: in service; 0: out of service}
- angmin, minimum angle difference, angle(Vf) - angle(Vt) (degrees)
- angmax, maximum angle difference, angle(Vf) - angle(Vt) (degrees)
- Pf, real power injected at "from" bus end (MW)
- Qf, reactive power injected at "from" bus end (MVAr)

- Pt, real power injected at "to" bus end (MW)
- Qt, reactive power injected at "to" bus end (MVAr)

fbus	tbus	r	x	b	rateA	rateB	rateC	tap	shift	br_status	angmin	angmax	Pf	Qf	Pt	Qt
101	102	0.003	0.014	0.461	175	0	0	0	0	1	0	0	13.33	-27.54	-13.33	-21.82
101	103	0.055	0.211	0.057	175	0	0	0	0	1	0	0	-10.49	24.75	10.94	-28.82
101	105	0.022	0.085	0.023	175	0	0	0	0	1	0	0	61.13	4.33	-60.35	-3.76
1010	101	0.0001	0.001	0	9999	0	0	1	0	1	0	0	172	23.84	-171.97	-23.56
102	104	0.033	0.127	0.034	175	0	0	0	0	1	0	0	38.83	18.21	-38.24	-19.46
102	106	0.05	0.192	0.052	175	0	0	0	0	1	0	0	49.47	-1.34	-48.33	0.28
1020	102	0.0001	0.001	0	9999	0	0	1	0	1	0	0	172	15.35	-171.97	-15.07
103	109	0.031	0.119	0.032	175	0	0	0	0	1	0	0	28.4	-23.67	-27.98	22.1
103	124	0.002	0.084	0	400	0	0	1.015	0	1	0	0	-219.34	15.5	220.37	27.67
104	109	0.027	0.104	0.028	175	0	0	0	0	1	0	0	-35.76	4.46	36.12	-5.9
105	110	0.023	0.088	0.024	175	0	0	0	0	1	0	0	-10.65	-10.24	10.69	7.89
106	110	0.014	0.061	2.459	175	0	0	0	0	1	0	0	-87.67	-130.8	88.72	-120.8
107	108	0.016	0.061	0.017	175	0	0	0	0	1	0	0	116.33	25.75	-114.16	-19.21
107	203	0.042	0.161	0.044	175	0	0	0	0	1	0	0	-1.39	15.96	1.53	-19.94
1070	107	0.0001	0.001	0	9999	0	0	1	0	1	0	0	240	67.26	-239.94	-66.67
108	109	0.043	0.165	0.045	175	0	0	0	0	1	0	0	-36.61	2.43	37.2	-4.64

fbus	tbus	r	x	b	rateA	rateB	rateC	tap	shift	br_status	angmin	angmax	Pf	Qf	Pt	Qt
108	110	0.043	0.165	0.045	175	0	0	0	0	1	0	0	-20.23	-18.23	20.52	14.74
109	111	0.002	0.084	0	400	0	0	1.03	0	1	0	0	-95.63	-18.63	95.83	27.04
109	112	0.002	0.084	0	400	0	0	1.03	0	1	0	0	-124.7	-28.93	125.05	43.44
110	111	0.002	0.084	0	400	0	0	1.015	0	1	0	0	-142.15	33.88	142.57	-16.43
110	112	0.002	0.084	0	400	0	0	1.015	0	1	0	0	-172.78	24.29	173.37	0.6
111	113	0.006	0.048	0.1	500	0	0	0	0	1	0	0	-108.42	-62.29	109.33	59.31
111	114	0.005	0.042	0.088	500	0	0	0	0	1	0	0	-129.98	51.68	130.99	-51.77
112	113	0.006	0.048	0.1	500	0	0	0	0	1	0	0	-56.17	-46.89	56.46	38.83
112	123	0.012	0.097	0.203	500	0	0	0	0	1	0	0	-242.25	2.85	249.21	31.94
113	123	0.011	0.087	0.182	500	0	0	0	0	1	0	0	-245.39	23.86	251.74	6.67
113	215	0.01	0.075	0.158	500	0	0	0	0	1	0	0	-198.18	56.5	202.28	-42.31
1130	113	0.0001	0.001	0	9999	0	0	1	0	1	0	0	-12.73	232.99	12.78	-232.48
114	116	0.005	0.059	0.082	500	0	0	0	0	1	0	0	-324.99	-6.34	330.49	63.05
1140	114	0.0001	0.001	0	9999	0	0	1	0	1	0	0	0	-19.11	0	19.11
115	116	0.002	0.017	0.036	500	0	0	0	0	1	0	0	91.99	-29.82	-91.81	27.63
115	121	0.006	0.049	0.103	500	0	0	0	0	1	0	0	-208.98	-44.59	211.62	55.17
115	121	0.006	0.049	0.103	500	0	0	0	0	1	0	0	-208.98	-44.59	211.62	55.17
115	124	0.007	0.052	0.109	500	0	0	0	0	1	0	0	223.95	43.41	-220.37	-27.67
1150	115	0.0001	0.001	0	9999	0	0	1	0	1	0	0	60	-0.01	-60	0.05

fbus	tbus	r	x	b	rateA	rateB	rateC	tap	shift	br_status	angmin	angmax	Pf	Qf	Pt	Qt
1151	115	0.0001	0.001	0	9999	0	0	1	0	1	0	0	155	-11.33	-154.97	11.57
116	117	0.003	0.026	0.055	500	0	0	0	0	1	0	0	-309.77	-38.84	312.59	57.48
116	119	0.003	0.023	0.049	500	0	0	0	0	1	0	0	126.07	-43.65	-125.56	42.46
1160	116	0.0001	0.001	0	9999	0	0	1	0	1	0	0	155	28.47	-154.98	-28.23
117	118	0.002	0.014	0.03	500	0	0	0	0	1	0	0	-175.43	-61.66	176.06	62.85
117	122	0.014	0.105	0.221	500	0	0	0	0	1	0	0	-137.17	4.18	139.64	-9.7
118	121	0.003	0.026	0.055	500	0	0	0	0	1	0	0	-54.61	3.63	54.69	-8.98
118	121	0.003	0.026	0.055	500	0	0	0	0	1	0	0	-54.61	3.63	54.69	-8.98
1180	118	0.0001	0.001	0	9999	0	0	1	0	1	0	0	399.99	139.68	-399.83	-138.06
119	120	0.005	0.04	0.083	500	0	0	0	0	1	0	0	-27.72	-39.73	27.82	31.69
119	120	0.005	0.04	0.083	500	0	0	0	0	1	0	0	-27.72	-39.73	27.82	31.69
120	123	0.003	0.022	0.046	500	0	0	0	0	1	0	0	-91.82	-44.69	92.1	41.76
120	123	0.003	0.022	0.046	500	0	0	0	0	1	0	0	-91.82	-44.69	92.1	41.76
121	122	0.009	0.068	0.142	500	0	0	0	0	1	0	0	-158.16	21.22	160.28	-20.93
325	121	0.012	0.097	0.203	500	0	0	0	0	1	0	0	-25.31	-7.12	25.38	-14.7
1210	121	0.0001	0.001	0	9999	0	0	1	0	1	0	0	400	100.42	-399.85	-98.88
1220	122	0.0001	0.001	0	9999	0	0	1	0	1	0	0	300	-29.78	-299.91	30.61
123	217	0.01	0.074	0.155	500	0	0	0	0	1	0	0	-25.36	8.8	25.45	-25.1
1230	123	0.0001	0.001	0	9999	0	0	1	0	1	0	0	310.01	66.52	-309.92	-65.61

fbus	tbus	r	x	b	rateA	rateB	rateC	tap	shift	br_status	angmin	angmax	Pf	Qf	Pt	Qt
1231	123	0.0001	0.001	0	9999	0	0	1	0	1	0	0	350.01	66.54	-349.89	-65.39
201	202	0.003	0.014	0.461	175	0	0	0	0	1	0	0	8.82	-26.58	-8.82	-22.8
201	203	0.055	0.211	0.057	175	0	0	0	0	1	0	0	-1.33	16.01	1.51	-21.18
201	205	0.022	0.085	0.023	175	0	0	0	0	1	0	0	56.48	7.16	-55.81	-6.99
2010	201	0.0001	0.001	0	9999	0	0	1	0	1	0	0	172	18.86	-171.97	-18.58
202	204	0.033	0.127	0.034	175	0	0	0	0	1	0	0	37.23	18.4	-36.67	-19.79
202	206	0.05	0.192	0.052	175	0	0	0	0	1	0	0	46.56	0.47	-45.54	-2
2020	202	0.0001	0.001	0	9999	0	0	1	0	1	0	0	172	16.38	-171.98	-16.1
203	209	0.031	0.119	0.032	175	0	0	0	0	1	0	0	8.87	-9.38	-8.82	6.35
203	224	0.002	0.084	0	400	0	0	1.015	0	1	0	0	-191.9	13.5	192.67	18.72
204	209	0.027	0.104	0.028	175	0	0	0	0	1	0	0	-37.33	4.79	37.71	-6.11
205	210	0.023	0.088	0.024	175	0	0	0	0	1	0	0	-15.19	-7.01	15.25	4.73
206	210	0.014	0.061	2.459	175	0	0	0	0	1	0	0	-90.46	-128.02	91.58	-121.84
207	208	0.016	0.061	0.017	175	0	0	0	0	1	0	0	114.94	27.02	-112.81	-20.63
2070	207	0.0001	0.001	0	9999	0	0	1	0	1	0	0	240	52.58	-239.94	-52
208	209	0.043	0.165	0.045	175	0	0	0	0	1	0	0	-36.29	1.76	36.87	-4.01
208	210	0.043	0.165	0.045	175	0	0	0	0	1	0	0	-21.9	-16.12	22.2	12.67
209	211	0.002	0.084	0	400	0	0	1.03	0	1	0	0	-99.44	-13.15	99.65	22.05
209	212	0.002	0.084	0	400	0	0	1.03	0	1	0	0	-141.32	-19.09	141.75	37.08

fbus	tbus	r	x	b	rateA	rateB	rateC	tap	shift	br_status	angmin	angmax	Pf	Qf	Pt	Qt
210	211	0.002	0.084	0	400	0	0	1.015	0	1	0	0	-140.21	34.6	140.62	-17.44
210	212	0.002	0.084	0	400	0	0	1.015	0	1	0	0	-183.82	29.84	184.5	-1.31
211	213	0.006	0.048	0.1	500	0	0	0	0	1	0	0	-159.45	-38.35	161.07	41.2
211	214	0.005	0.042	0.088	500	0	0	0	0	1	0	0	-80.82	33.75	81.22	-38.88
212	213	0.006	0.048	0.1	500	0	0	0	0	1	0	0	-85.2	-32.26	85.68	25.88
212	223	0.012	0.097	0.203	500	0	0	0	0	1	0	0	-241.04	-3.51	248.01	38.43
213	223	0.011	0.087	0.182	500	0	0	0	0	1	0	0	-226.54	5.38	231.99	18.22
2130	213	0.0001	0.001	0	9999	0	0	1	0	1	0	0	285.3	127.41	-285.21	-126.47
214	216	0.005	0.059	0.082	500	0	0	0	0	1	0	0	-275.22	-19.72	279.18	58.23
2140	214	0.0001	0.001	0	9999	0	0	1	0	1	0	0	0	-19.6	0	19.6
215	216	0.002	0.017	0.036	500	0	0	0	0	1	0	0	-42.66	-14.59	42.7	11.2
215	221	0.006	0.049	0.103	500	0	0	0	0	1	0	0	-228.5	-40.21	231.61	54.7
215	221	0.006	0.049	0.103	500	0	0	0	0	1	0	0	-228.5	-40.21	231.61	54.7
215	224	0.007	0.052	0.109	500	0	0	0	0	1	0	0	195.34	27.65	-192.67	-18.72
2150	215	0.0001	0.001	0	9999	0	0	1	0	1	0	0	60	-0.01	-60	0.05
2151	215	0.0001	0.001	0	9999	0	0	1	0	1	0	0	155	-45.39	-154.97	45.65
216	217	0.003	0.026	0.055	500	0	0	0	0	1	0	0	-270.5	-54.47	272.7	67.71
216	219	0.003	0.023	0.049	500	0	0	0	0	1	0	0	3.6	-28.2	-3.58	23.25
2160	216	0.0001	0.001	0	9999	0	0	1	0	1	0	0	155	7	-154.98	-6.77

fbus	tbus	r	x	b	rateA	rateB	rateC	tap	shift	br_status	angmin	angmax	Pf	Qf	Pt	Qt
217	218	0.002	0.014	0.03	500	0	0	0	0	1	0	0	-162.76	-48.32	163.29	48.75
217	222	0.014	0.105	0.221	500	0	0	0	0	1	0	0	-135.38	5.71	137.79	-11.77
218	221	0.003	0.026	0.055	500	0	0	0	0	1	0	0	-48.23	2.81	48.29	-8.32
218	221	0.003	0.026	0.055	500	0	0	0	0	1	0	0	-48.23	2.81	48.29	-8.32
2180	218	0.0001	0.001	0	9999	0	0	1	0	1	0	0	400	123.99	-399.84	-122.41
219	220	0.005	0.04	0.083	500	0	0	0	0	1	0	0	-88.71	-30.13	89.12	24.58
219	220	0.005	0.04	0.083	500	0	0	0	0	1	0	0	-88.71	-30.13	89.12	24.58
220	223	0.003	0.022	0.046	500	0	0	0	0	1	0	0	-153.12	-37.58	153.81	37.61
220	223	0.003	0.022	0.046	500	0	0	0	0	1	0	0	-153.12	-37.58	153.81	37.61
221	222	0.009	0.068	0.142	500	0	0	0	0	1	0	0	-159.97	21.65	162.13	-20.98
2210	221	0.0001	0.001	0	9999	0	0	1	0	1	0	0	400	115.99	-399.84	-114.42
2220	222	0.0001	0.001	0	9999	0	0	1	0	1	0	0	300.01	-31.89	-299.93	32.71
318	223	0.013	0.104	0.218	500	0	0	0	0	1	0	0	129.81	-20.14	-127.82	12.06
2230	223	0.0001	0.001	0	9999	0	0	1	0	1	0	0	310	73.05	-309.91	-72.13
2231	223	0.0001	0.001	0	9999	0	0	1	0	1	0	0	350	73.06	-349.89	-71.9
301	302	0.003	0.014	0.461	175	0	0	0	0	1	0	0	10.96	-27.03	-10.96	-22.33
301	303	0.055	0.211	0.057	175	0	0	0	0	1	0	0	-5.57	23.29	5.94	-27.68
301	305	0.022	0.085	0.023	175	0	0	0	0	1	0	0	58.57	7.02	-57.86	-6.67
3010	301	0.0001	0.001	0	9999	0	0	1	0	1	0	0	172	25.59	-171.97	-25.31

fbus	tbus	r	x	b	rateA	rateB	rateC	tap	shift	br_status	angmin	angmax	Pf	Qf	Pt	Qt
302	304	0.033	0.127	0.034	175	0	0	0	0	1	0	0	38.04	19.7	-37.45	-20.95
302	306	0.05	0.192	0.052	175	0	0	0	0	1	0	0	47.89	0.45	-46.81	-1.76
3020	302	0.0001	0.001	0	9999	0	0	1	0	1	0	0	172	18.13	-171.97	-17.86
303	309	0.031	0.119	0.032	175	0	0	0	0	1	0	0	17.89	-18.92	-17.69	16.53
303	324	0.002	0.084	0	400	0	0	1.015	0	1	0	0	-203.83	9.6	204.71	27.57
304	309	0.027	0.104	0.028	175	0	0	0	0	1	0	0	-36.55	5.95	36.92	-7.29
305	310	0.023	0.088	0.024	175	0	0	0	0	1	0	0	-13.14	-7.33	13.19	5.01
306	310	0.014	0.061	2.459	175	0	0	0	0	1	0	0	-89.19	-128.18	90.28	-121.59
307	308	0.016	0.061	0.017	175	0	0	0	0	1	0	0	114.94	26.96	-112.8	-20.53
3070	307	0.0001	0.001	0	9999	0	0	1	0	1	0	0	240	52.53	-239.94	-51.95
308	309	0.043	0.165	0.045	175	0	0	0	0	1	0	0	-36.65	2.66	37.25	-4.82
308	310	0.043	0.165	0.045	175	0	0	0	0	1	0	0	-21.54	-17.13	21.84	13.71
309	311	0.002	0.084	0	400	0	0	1.03	0	1	0	0	-98.68	-16.1	98.89	25.01
309	312	0.002	0.084	0	400	0	0	1.03	0	1	0	0	-132.81	-24.32	133.19	40.55
310	311	0.002	0.084	0	400	0	0	1.015	0	1	0	0	-142.27	35.09	142.7	-17.41
310	312	0.002	0.084	0	400	0	0	1.015	0	1	0	0	-178.04	27.78	178.68	-1.04
311	313	0.006	0.048	0.1	500	0	0	0	0	1	0	0	-145	-42.42	146.37	43.28
311	314	0.005	0.042	0.088	500	0	0	0	0	1	0	0	-96.59	34.82	97.14	-38.72
312	313	0.006	0.048	0.1	500	0	0	0	0	1	0	0	-84.5	-31.54	84.97	25.07

fbus	tbus	r	x	b	rateA	rateB	rateC	tap	shift	br_status	angmin	angmax	Pf	Qf	Pt	Qt
312	323	0.012	0.097	0.203	500	0	0	0	0	1	0	0	-227.37	-7.97	233.55	36.6
313	323	0.011	0.087	0.182	500	0	0	0	0	1	0	0	-211.13	0.52	215.85	17.34
3130	313	0.0001	0.001	0	9999	0	0	1	0	1	0	0	285.3	123.82	-285.21	-122.89
314	316	0.005	0.059	0.082	500	0	0	0	0	1	0	0	-291.14	-15.62	295.57	59.6
3140	314	0.0001	0.001	0	9999	0	0	1	0	1	0	0	0	-15.38	0	15.39
315	316	0.002	0.017	0.036	500	0	0	0	0	1	0	0	65.06	-27.02	-64.96	24.11
315	321	0.006	0.049	0.103	500	0	0	0	0	1	0	0	-187.44	-49.2	189.6	55.89
315	321	0.006	0.049	0.103	500	0	0	0	0	1	0	0	-187.44	-49.2	189.6	55.89
315	324	0.007	0.052	0.109	500	0	0	0	0	1	0	0	207.79	39.58	-204.71	-27.57
3150	315	0.0001	0.001	0	9999	0	0	1	0	1	0	0	60	-0.01	-59.99	0.05
3151	315	0.0001	0.001	0	9999	0	0	1	0	1	0	0	155	-21.57	-154.98	21.81
316	317	0.003	0.026	0.055	500	0	0	0	0	1	0	0	-250.35	-52	252.23	62.55
316	319	0.003	0.023	0.049	500	0	0	0	0	1	0	0	74.72	-38.15	-74.52	34.57
3160	316	0.0001	0.001	0	9999	0	0	1	0	1	0	0	155	13.82	-154.98	-13.58
317	318	0.002	0.014	0.03	500	0	0	0	0	1	0	0	-114.85	-67.33	115.18	66.33
317	322	0.014	0.105	0.221	500	0	0	0	0	1	0	0	-137.38	4.77	139.87	-10.24
318	321	0.003	0.026	0.055	500	0	0	0	0	1	0	0	-89.07	8.21	89.29	-12.37
318	321	0.003	0.026	0.055	500	0	0	0	0	1	0	0	-89.07	8.21	89.29	-12.37
3180	318	0.0001	0.001	0	9999	0	0	1	0	1	0	0	400	132.2	-399.84	-130.6

fbus	tbus	r	x	b	rateA	rateB	rateC	tap	shift	br_status	angmin	angmax	Pf	Qf	Pt	Qt
319	320	0.005	0.04	0.083	500	0	0	0	0	1	0	0	-53.24	-35.78	53.42	28.43
319	320	0.005	0.04	0.083	500	0	0	0	0	1	0	0	-53.24	-35.78	53.42	28.43
320	323	0.003	0.022	0.046	500	0	0	0	0	1	0	0	-117.42	-41.43	117.85	39.54
320	323	0.003	0.022	0.046	500	0	0	0	0	1	0	0	-117.42	-41.43	117.85	39.54
321	322	0.009	0.068	0.142	500	0	0	0	0	1	0	0	-157.94	21.17	160.05	-20.92
3210	321	0.0001	0.001	0	9999	0	0	1	0	1	0	0	400	109.78	-399.84	-108.22
3220	322	0.0001	0.001	0	9999	0	0	1	0	1	0	0	300	-30.31	-299.92	31.13
323	325	0	0.009	0	722	0	0	0	0	1	0	0	-25.31	-7.07	25.31	7.12
3230	323	0.0001	0.001	0	9999	0	0	1	0	1	0	0	310	64	-309.91	-63.09
3231	323	0.0001	0.001	0	9999	0	0	1	0	1	0	0	350	64.02	-349.89	-62.87

This page left blank

DISTRIBUTION

Email—Internal

Name	Org.	Sandia Email Address
Bryan Arguello	5521	barguel@sandia.gov
Casey L. Doyle	5522	cldoyle@sandia.gov
Richard A. Garrett	5523	ragarre@sandia.gov
Rossitza Homan	5524	rhoman@sandia.gov
Kevin L. Stamber	5524	klstamb@sandia.gov
Walter E. Beyeler	6617	webeyel@sandia.gov
Craig R. Lawton	8141	crlawto@sandia.gov
Samuel T. Ojetola	8813	sojetol@sandia.gov
David A. Schoenwald	8813	daschoe@sandia.gov
Technical Library	1911	sanddocs@sandia.gov

This page left blank

This page left blank

Sandia National Laboratories

Sandia National Laboratories is a multimission laboratory managed and operated by National Technology & Engineering Solutions of Sandia LLC, a wholly owned subsidiary of Honeywell International Inc. for the U.S. Department of Energy's National Nuclear Security Administration under contract DE-NA0003525.